PROJECT 1: MICRORNA REGULATION OF THE PROTO-ONCOGENE PBF

and

PROJECT 2: RECOGNITION OF PREVIOUSLY UNDESCRIBED RING DOMAIN RESIDUES REQUIRED FOR BRCA1:BARD1 AND RING1B:BMI1 UBIQUITIN LIGASE ACTIVITY

by

ALICE FLETCHER

This project is submitted in partial fulfilment of the requirements for the award of the MRes Biomedical Research 2013/2014.

UNIVERSITY OF BIRMINGHAM

College of Medical and Dental Sciences

University of Birmingham

May 2014

MICRORNA REGULATION OF THE PROTO-ONCOGENE PBF

by

ALICE FLETCHER

This project is submitted in partial fulfilment of the requirements for the award of the MRes Biomedical Research 2013/2014.

ABSTRACT

In thyroid cancers there have been independent observations of the overexpression of a relatively uncharacterised proto-oncogene, known as PBF, as well as the deregulation of microRNAs. However, little remains known about how PBF is regulated although, a recent investigation has identified miR-122 to have the ability to regulate PBF in hepatitis B and liver cancer.

Therefore, the aims of this investigation were to identify whether a selection of microRNAs can regulate PBF, altering its mRNA expression and protein levels. This was achieved by selecting microRNAs predicted to target PBF, transfecting SW1736 thyroid carcinoma and MCF7 breast carcinoma cell lines with microRNA mimics of these, then measuring PBF expression by qRT-PCR and Western blotting.

The most striking result indicated that hsa-miR-122-5p caused a significant decrease in PBF protein levels cells despite no change in PBF mRNA expression. Furthermore, hsa-miR-124-3p and hsa-miR-506-3p also negatively regulated PBF mRNA expression and protein levels; highlighting microRNAs do have the ability to regulate PBF. Due to the emerging importance of microRNAs as biomarkers and therapeutics the identification of specific microRNAs that play a role in thyroid cancer may bear clinical relevance although, these initial findings need to be confirmed and extended for a more stringent investigation.

ACKNOWLEDGEMENTS

Having thoroughly enjoyed my experience within the McCabe group I would firstly like to thank Professor Chris McCabe for giving me the opportunity to work on this project as well as his encouragement and support throughout, as without him this investigation would not have been possible.

I would also like to thank all the other members of the McCabe group; Dr Vicki Smith, Dr Rachel Watkins, Dr Martin Read, Bhav Modasia, Vikki Poole, Waraporn Imruetaicharoenchoke and Teresa Gagliano who have not only helped me throughout but also created a friendly working environment enhancing my lab experience.

CONTENTS

1. INTRODUCTION

1.1. Thyroid Cancer

Thyroid cancers are a rare type of cancer (http://www.cancerresearchuk.org/cancer-help/type/thyroid-cancer/about/thyroid-cancer-risks-and-causes) divided into four main groups dependent on the origin of the cancer cells within the thyroid gland, which is composed of parafollicular and follicular cells. Medullary thyroid carcinomas (MTC) are derived from parafollicular cells and are quite rare whereas tumours derived from follicular cells are more common and are divided into subtypes classified as; differentiated and undifferentiated carcinomas (Dvořáková, S., et al., 2014). Differentiated carcinomas include papillary thyroid carcinomas (PTC) and follicular thyroid carcinomas (FTC), which are slow growing and usually curable (Mazzaferri, E.L. and Kloos, R.T., 2001). The most common treatment for these is surgery followed by the use of radioiodine, which exploits the ability of the thyroid to take up iodine via the sodium iodide symporter (NIS) (Smith, V.E., et al., 2013). In comparison, undifferentiated carcinomas - known as anaplastic thyroid carcinomas (ATC) - are extremely lethal as they are aggressive and metastasise, resulting in a median patient survival of less than six months (Lim, S.M., et al., 2012).

There are multiple risk factors for thyroid cancer, including; a family history of thyroid cancer, an enlarged goitre and radiation exposure as well as being female, which results in thyroid cancer being two to three times more common in women compared to men (http://www.cancerresearchuk.org/cancer-help/type/thyroid-cancer/about/thyroid-cancer-risks-and-causes). At the molecular level, it has been described that the genetics of thyroid cancer also act as risk factors with genetic alterations described to be apparent in approximately 75% of cases (Bhaijee, F. and Nikiforov, Y.E., 2011, Read, M.L., et al., 2014).

Furthermore, the overexpression of certain proteins has also been observed in thyroid cancers, including overexpression of the proto-oncogene; pituitary tumor transforming gene 1 (PTTG1) binding factor (PBF), also known as PTTG1 interacting protein (PTTG1IP).

1.2. Pituitary Tumor Transforming Gene (PTTG) Binding Factor (PBF)

PBF is a 180 residue long protein (Read, M.L., et al., 2011) with a molecular weight of approximately 25kDa (Smith V. and McCabe, C., 2008), which was first identified due to its interaction with PTTG1 via PBF's C-terminus (Figure 1) (Chien, W. and Pei, L., 2000). This interaction between PTTG1 and PBF was described to induce the translocation of PTTG1 from the cytoplasm into the nucleus (Stratford, A.L., et al., 2005) driving tumourigenesis (Smith, V.E., et al., 2011). As PBF has no significant homology to any other human protein (Read, M.L., et al., 2011), it has been described as a 'relatively uncharacterised protein' however, since it was recognised that PBF has a transforming ability of its own both *in vitro* and *in vivo* PBF has subsequently been defined as a proto-oncogene in its own right (Smith, V.E., et al., 2011), gaining increasing interest.

Figure 1: PBF functional domains
Schematic of signals and domains on PBF, responsible for its cellular location, as well as the PTTG1 binding site, found at the C-terminus.
Smith V. and McCabe C., 2008. PTTG1IP (Pituitary Tumor-Transforming 1 Interacting Protein). Atlas of Genetics and Cytogenetics in Oncology and Haematology. (Image from: http://AtlasGeneticsOncology.org/Genes/PTTG1IPID41944ch21q22.html accessed on 27/12/13).

1.2.1. PBF Expression in Thyroid Cancer

The aforementioned overexpression of the proto-oncogene PBF within thyroid cancers, as well as breast cancers, is observed at both the mRNA expression and protein level, compared to the standard ubiquitous expression in normal thyroid tissue (Stratford, A.L., et al., 2005). This overexpression has been independently associated with a poor prognosis and lower disease-specific survival in thyroid cancers (Read, M.L., et al., 2014), likely due to the correlation with; distant metastases at diagnosis, tumour multicentricity and locoreginal recurrence (Hsueh, C., et al., 2013). Subsequently, this has resulted in PBF being described as a promising prognostic marker within thyroid cancer (Hsueh, C., et al., 2013), which is of interest due to the recent incidences of thyroid cancer increasing faster than that of any other malignancy in both genders and all ethnic backgrounds (Tuttle, R.M., 2013).

Despite the precise role of PBF not being defined, investigations have begun to characterise PBF with respect to its roles in thyroid biology and tumourigenesis. One of the first functions of PBF defined with respect to thyroid cancer was its ability to act as a regulator of NIS. By preventing NIS function and expression at the plasma membrane PBF was consequently able to result in a repressed and insufficient radioiodine uptake during the treatment of differentiated thyroid cancers leading to a poor prognosis (Boelaert, K., et al., 2007). PBF has also been observed to interact with cortactin, a cytoplasmic protein involved in actin cytoskeleton rearrangement, thus facilitating cell migration and invasion (Sharma, N., et al., 2012), making it unsurprising that PBF overexpression correlates with metastases (Hsueh, C., et al., 2013). Furthermore, in transgenic mice models where PBF is overexpressed in the thyroid gland an upregulation of Akt and the TSH receptor have been observed, which are known regulators of thyroid follicular cell proliferation (Read, M.L., et al., 2011).

Most recently, PBF has been identified to be a regulator of the tumour suppressor p53 by specifically binding to p53 in thyroid cells and repressing transactivation of responsive promoters, as well as decreasing p53 stability via ubiquitination (Read, M.L., et al., 2014). This is an important finding as it has been well-documented that a disruption to p53 is observed in numerous cancers (Read, M.L., et al., 2014), highlighting the importance of regulating PBF due to the downstream impact it may have on tumourigenesis.

Despite an overexpression of PBF being observed in thyroid and breast cancer, very little remains known about what causes PBF overexpression. Previously, it has been described that PBF has oestrogen response elements (ERE) within its promoter region, with a correlation observed between the number of EREs and PBF expression in ER-positive breast tumours, resulting in oestrogen-stimulated cell invasion (Watkins, R.J., et al., 2010). Furthermore, it has been observed that hsa-miR-122 can regulate PBF in chronic hepatitis B (CHB) and hepatocellular carcinomas (HCC) (Li, C., et al., 2012).

1.3. MicroRNAs

The observation of miR-122 regulating PBF is particularly interesting due to the increasing emergence of microRNAs being used as both biomarkers and therapeutics in cancer. Subsequently, recognition of the potential ability of microRNAs to regulate PBF contributed to the aims and hypotheses within this investigation, whereby the deregulation of specific microRNAs is hypothesised to result in PBF overexpression, as observed in thyroid cancer.

MicroRNAs are short (21-25 nucleotides in length) non-coding RNAs that negatively regulate gene expression at the post-transcriptional level by binding to the 3’ UTR of their target mRNAs and preventing protein production (Cannell, I.G., et al., 2008) (Figure 2). As microRNAs account for 1-5% of the human genome (MacFarlane, L.A. and Murphy, P.R.,

2010) and each microRNA has approximately 200 mRNA targets (Carther, R.W., 2006) they are able to target more than 60% of human protein-coding genes (Friedman, R.C., et al., 2009).

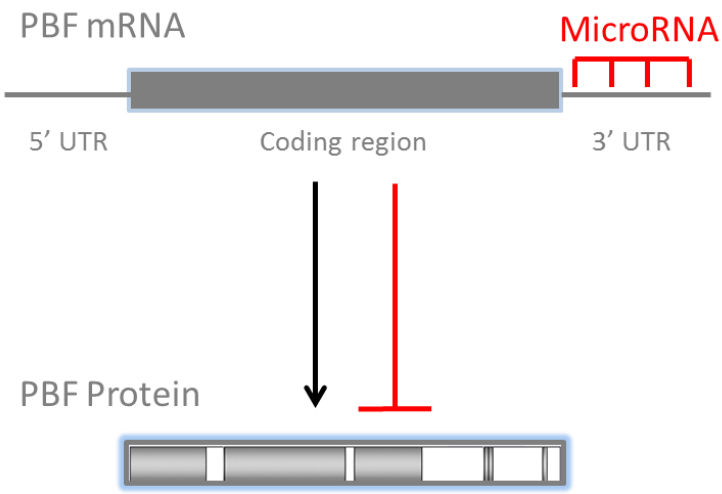

Figure 2: MicroRNA Targeting of mRNA
Schematic of a microRNA (red) targeting the 3' UTR of its mRNA target (grey), in this case PBF. This results in the prevention of translation and thus protein expression.

Before targeting their mRNA target, microRNAs must be transcribed and processed from their own genes. In animals, microRNAs are transcribed by RNA polymerase II in the nucleus as a long polycistronic primary transcript with a hairpin (Lee, Y., et al., 2004) (Figure 3). Following transcription, the upper part of the hairpin is excised by Drosha, an RNase III enzyme in the nucleus, to give a 65 nucleotide intermediate known as pre-microRNA (Figure 3). Exportin-5 then facilitates the export of pre-microRNAs from the nucleus into the cytoplasm (Yi, R. et al., 2003) where Dicer, another RNase III enzyme, removes the hairpin loop to give a RNA duplex (Cai, X., et al., 2004) (Figure 3). This duplex is then assembled into a protein complex known as the RNA-induced silencing complex (RISC), which contains Argonaute proteins (Ago (1-4)) at its centre used to separate the RNA duplex strands (Kawamata, T., et al., 2011). Subsequently, one strand of the duplex is degraded and the other strand remains as a mature microRNA guide strand (Figure 3), as determined by the internal stability of the duplex ends with a less stable 5' end resulting in strand survival (Lee, Y., et

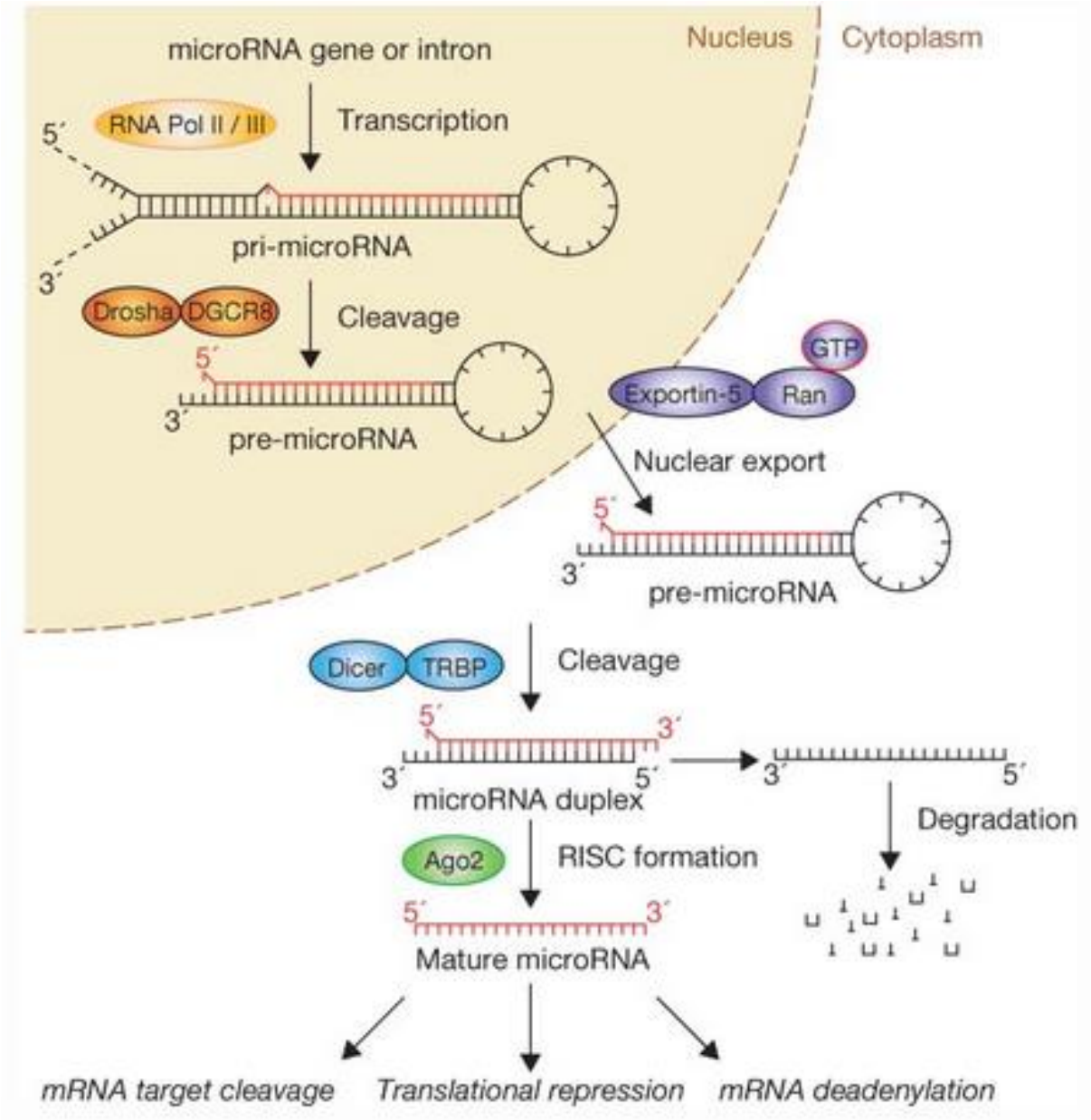

Figure 3: Pathway of microRNA processing

Pathway of microRNA processing starting from the long primary transcript (pri-microRNA) in the nucleus, which is cleaved by Drosha to give pre-microRNA. Exportin-5 along with Ran-GTP export pre-microRNA from the nucleus to the cytoplasm where Dicer cleaves the hairpin loop off to give the mature microRNA. The functional strand of the mature microRNA is then loaded onto Ago2 to form the RISC while the other strand gets degraded. RISC is then guided to its targets to cause mRNA target cleavage, translational repression or mRNA deadenylation. (Image from: Winter, J., et al., 2009. The Linear Canonical Pathway of MicroRNA Processing. Nature Cell Biology, 11, pp.228-234).

al., 2004). These processing steps ensure microRNA authenticity (Kawamata, T., et al., 2011) and guarantee the microRNA guide strand targets and binds the RISC to the correct mRNA target. This binding takes place via Watson-Crick base pairing, with a full-match base pairing between the seed region (residues 2-8 at the microRNA 5' end) and 3' UTR of the mRNA target, followed by a bulge region and then a region of partial complementarity (Ricci, E.P., et al., 2011).

Upon successful targeting of the microRNA, protein production is prevented by one of three methods; 1) slicer-dependent mRNA degradation, 2) slicer-independent translational repression or 3) mRNA degradation and translational repression in P-bodies (MacFarlane, L.A. and Murphy, P.R., 2010). Slicer-dependent mRNA degradation is where mRNA cleavage is catalysed by Ago2 in the RISC followed by the subsequent degradation of the mRNA products, which requires de-adenylation of the mRNA to remove the poly(A) tail making this an irreversible process (MacFarlane, L.A. and Murphy, P.R., 2010). In comparison, slicer-independent translational repression is due to the microRNA being bound to its mRNA target and physically preventing translation taking place. Although the exact mechanism remains unknown, it is known that Ago2 in the RISC has a cap-binding-like-motif making the 5' cap of the target mRNA important for translational repression (Cannell, I.G., et al., 2008). However, once this repression is relieved the mRNA can be translated again making this a reversible process (MacFarlane, L.A. and Murphy, P.R., 2010). Finally, the third method microRNAs use to repress protein expression of their target mRNAs is; mRNA degradation and translational repression within P-bodies (Liu, J., et al., 2005). P-bodies are cytoplasmic domains that contain enzymes and factors within specialised compartments required for mRNA decapping, deadenylation, RNA degradation and translational repression

allowing both slicer-dependent and slicer-independent silencing to take place inside (MacFarlane, L.A. and Murphy, P.R., 2010)

1.3.1. MicroRNAs in Thyroid Cancer

MicroRNAs have been observed to be downregulated *in vivo* in mouse models of thyroid cancer (Visone, R., et al., 2007); highlighting the significance of microRNAs in thyroid tumourigenesis. Furthermore, microRNA expression has been observed to differ between normal and cancerous thyroid tissue, with 32% of microRNAs being upregulated and 38% being downregulated in thyroid tumours compared to normal tissues (Nikiforova, M.N., et al., 2009) and moreover, various microRNA signatures have been associated with each of the four groups of thyroid carcinomas; MTC, FTC, PTC and ATC (Abraham, D., et al., 2011, Jacques, C., et al., 2013, Visone, R., et al., 2007). Consequently, due to the observation of microRNA deregulation in thyroid cancers this has led to recognition of the use of microRNAs in both the diagnosis and prognosis of thyroid cancers (Leonardi, G.C., et al., 2012).

1.4. Aims

The aim of this investigation was to determine whether specifically selected microRNAs can regulate PBF, due to independent observations of microRNA deregulation and PBF overexpression in thyroid cancers, as well as the recent observation of a microRNA, miR-122, targeting PBF in liver cancer. To determine the ability of microRNAs to target PBF, microRNA mimics of specifically selected microRNAs, alongside an anti-PBF siRNA as a control, were transfected into SW1736 and MCF7 cells, then PBF mRNA expression and PBF protein levels were assessed by qRT-PCR and Western blotting respectively.

It was hypothesised that PBF would be negatively regulated by the selected microRNAs and thus overexpression of these microRNAs by transfection would result in a decrease in PBF

mRNA expression and protein levels. Further investigations may determine whether there is a correlation between the downregulation of these microRNAs and PBF overexpression in thyroid cancer patient samples, which may consequently suggest clinical relevance due to the emergence of microRNAs as biomarkers and therapeutics in thyroid cancer.

2. MATERIALS & METHODS

2.1. MicroRNA Selection

Five microRNAs hypothesised to target PBF were selected by integrating results from the literature and prediction software, including; miRWalk (Dweep, H., et al., 2011), TargetScan (Friedman, R.C., et al., 2009), miRDB (Wang, X. and El Naga, I.M., 2008, Wang, X., 2008) and miRTarBase (Hsu, S.D., et al., 2010). In addition two controls were selected; a negative control siRNA, which has no homology to any known mammalian genes and anti-PBF siRNA, which directly targets PBF. These both identify thresholds for the effect of microRNA mimics, predicted to target PBF, to be measured against.

2.2. Cell Lines

The human BRAFV600E anaplastic thyroid carcinoma cell line (SW1736) and human estrogen receptor positive breast adenocarcinoma cell line (MCF7), both derived from Caucasians, were obtained from the Cell Lines Services (#300453) and European Collection of Cell Cultures (#86012803) respectively. They were maintained in RPMI 1640-L-Glutamine (Gibco) complete medium (10% FBS and 1% Penstrep) at 37^{o}C and 5% CO_2 and sub-cultured frequently to ensure 80% maximum confluency.

2.2.1. Transfection

24 hours before transfection, SW1736 and MCF7 cells were seeded at; 60,000 cells/well and 62,500 cells/well in 1ml RPMI 1640-L-Glutamine complete medium in 12-well plates for RNA analysis respectively and 150,000 cells/well and 125,000 cells/well in 2ml RPMI 1640-L-Glutamine complete medium in 6-well plates for protein analysis respectively. Transfection mixes were made by diluting the microRNA mimic (hsa-miR-1, hsa-miR-122-5p, hsa-miR-

124-3p, hsa-miR-193b-5p or hsa-miR-506-3p (Qiagen)), AllStars negative control siRNA (Qiagen) or anti-PBF siRNA (Life Technologies) in opti-MEM for a final concentration of 50nM. 12µl or 24µl HiPerfect transfection reagent (Qiagen)/well for 12-well or 6-well plates respectively was added to the transfection mixes, vortexed and incubated for 10 minutes according to the Qiagen protocol. Transfection mixes were then added in a dropwise manner to cells in a 12-well or 6-well plate. It is important to note that for RNA analysis, four replicates of each microRNA mimic and siRNA were transfected/experiment and for protein analysis one of each microRNA mimic and siRNA was transfected/experiment. Following transfection, cells were returned to 37^{o}C and 5% CO_2 for 48 or 72 hours prior to RNA isolation or protein harvesting respectively.

2.3. RNA Analysis

2.3.1. RNA Isolation

48 hours after transfection, medium was aspirated from 12-well plates and cells were washed with PBS. PBS was aspirated and cells were lysed with 250µl TRI-Reagent (Sigma)/well at room temperature for 5 minutes. Lysates were transferred into Eppendorfs and stored at -80^{o}C overnight. The next day the RNA isolation protocol was continued by adding 50µl chloroform (Sigma)/sample and incubating at room temperature for 5 minutes for phase isolation. Samples were centrifuged at 13,000x*g* and the colourless aqueous phase was transferred to a clean Eppendorf. To precipitate the RNA 125µl isopropanol (Sigma)/sample was added and incubated at room temperature for 20 minutes, followed by centrifugation at 13,000x*g* for 15 minutes. Supernatant was removed and the RNA pellet was washed with 250µl ethanol (VWR International)/sample for 5 minutes then left to air dry. Each sample was then re-suspended in 20µl nuclease free water (ProMega) and RNA concentration was determined by NanoDrop.

2.3.2. Reverse Transcription PCR (RT-PCR)

Reactions mixtures for RT-PCR for each RNA sample contained: 0.5µg RNA in 5µl nuclease free water, 2µl $MgCl_2$, 1µl RT 10x buffer, 1µl dNTP mixture (10mM), 0.25µl Recombinant RNasin, 0.25µl AMV RT and 0.5µl random primers (Reverse Transcription System, Promega)). An AMV negative control reaction was made in the same way with a randomly selected duplicate 0.5µg RNA in 5µl nuclease free water, besides substituting AMV RT with nuclease free water. The Promega RT-PCR protocol was followed and reaction mixtures underwent the following RT-PCR programme: 42^{o}C for 60 minutes, 95^{o}C for 5 minutes, then 4^{o}C for 3 minutes, following which cDNA samples were made to a total volume of 50µl with nuclease free water.

2.3.3. Quantitative Real-Time PCR (qRT-PCR)

Within a PCR hood, reaction mixtures for qRT-PCR for each cDNA sample, including the AMV RT negative control, were added to a 96-well plate in duplicate for both PBF and 18S. Reaction mixtures contained: 2µl cDNA, 10µl 2x GoldStar TaqMan PCR mastermix (Eurogentec), 7µl nuclease free water and 1µl PTTG1IP TaqMan gene expression assay labelled with FAM dye (Life Technologies) or 1µl Eukaryotic 18S rRNA endogenous control labelled with VIC dye (Life Technologies) for PBF or 18S respectively. Control reactions were also added to the 96-well plate in duplicate for PBF and 18S, made exactly the same, besides substituting 2µl cDNA with nuclease free water. Following this, plates were sealed, centrifuged and underwent the following qRT-PCR programme: 50^{o}C for 2 minutes for optimal enzyme activity, 95^{o}C for 10 minutes to activate the AmpliTaq Gold and then for the PCR; 40 cycles of 95^{o}C for 15 seconds and 60^{o}C for 1 minute to denature, anneal and extend DNA.

2.3.4. Statistics

7500 system software was used to analyse qRT-PCR data (Supplementary figures 1 and 2), with PBF mRNA expression normalised against 18S (CT values between 9 and 10) for each sample. qRT-PCR duplicates were then averaged and ΔΔCT values and power calculations were completed on duplicate averages. Following this, duplicate averages for the four replicates of each microRNA mimic and siRNA transfected/experiment were averaged for a mean power value for each microRNA and siRNA, which was presented on a bar graph. The standard error mean (SEM) for each microRNA and siRNA was calculated using average duplicate ΔCT values and the significance of results was assessed using the two-tailed student's t-test on these values, to a value of $p<0.01$, $p<0.05$ or non-significant.

When averaging qRT-PCR data from all experiments, the mean power values for each microRNA and siRNA from individual experiments were averaged and presented on a bar graph with the SEM and two-tailed student's t-test calculated using the average ΔCT values for each microRNA from each individual experiment. As before, significance was assessed to a value of $p<0.01$, $p<0.05$ or non-significant.

2.4. Protein Analysis

2.4.1. Protein Harvest

72 hours after transfection, medium was aspirated from 6-well plates and cells were washed with PBS. PBS was aspirated and cells were lysed with 150µl RIPA buffer (1.22g Trizma base, 1.8g NaCl, 160ml dH_2O – pH7.4, 2ml Igepal, 5ml sodium deoxycholate, 2ml 100mM EDTA and protease inhibitor cocktail (6:100 dilution (Sigma)))/well for 20 minutes at -20^oC. Lysates were transferred into Eppendorfs, sonicated at 4^oC for 1 minute on a medium setting using the Bioruptor Standard (Diagenode), centrifuged at 4^oC at 13,000x*g* for 5 minutes and

lysates were collected. Protein concentrations were determined using the BCA protein assay (ThermoScientific).

2.4.2. Western Blotting

Antibody	Company	Dilution
Rabbit anti-PBF	In house	1:500 (In 5% non-fat milk)
Goat anti-rabbit	Dako	1:2,000 (In 5% non-fat milk)
Mouse anti-β-actin	Sigma	1:10,000 (In 5% non-fat milk)
Rabbit anti-mouse	Dako	1:10,000 (In 5% non-fat milk)

Table 1: Antibodies
All antibodies used within this investigation listed at the dilution used and the company antibodies were purchased from.

30µg of each protein lysate in protein sample buffer (0.107g DTT (Sigma)/1ml Laemmli buffer (BioRad)) was incubated at 95^{o}C for 5 minutes before being resolved on a 12% SDS-polyacrylamide gel. Proteins were transferred onto a PVDF membrane (GE Life Sciences) and probed with a rabbit anti-PBF primary antibody in 5% non-fat milk at room temperature for 1 hour, washed in TBST (50ml 1M Tris pH7.6, 20g 5mM NaCl, 0.625ml Tween-80 and 2449.4ml dH_2O) then probed with goat anti-rabbit antibody in 5% non-fat milk at room temperature for 1 hour. Membranes were incubated with Pierce® ECL2 Western blotting substrate (ThermoScientific), placed into a light-excluding cassette and exposed to x-ray film, which was developed by the Xograph Compact X4 film processor.

Following washing in TBST, membranes were re-probed using murine anti β-actin antibody in 5% non-fat milk at room temperature for 1 hour, washed in TBST then probed with rabbit anti-murine antibody in 5% non-fat milk at room temperature for 45 minutes. Membranes

were incubated with Amersham ECL plus Western blotting substrate (GE Life Sciences) and developed as described above.

2.4.3. Statistics

Densitometry was completed on ImageJ to analyse Western blots, with PBF protein levels at 25kDa and 30kDa (as these are the main forms of PBF studied (Watkins, R.J., et al., 2010) and identified by various antibodies by Western blot) normalised against β-actin. The fold-change relative to the negative control, assigned an arbitrary value of 1.0, was calculated for each microRNA or siRNA and presented on a bar graph. When averaging Western blots from all experiments, the fold-changes relative to the negative control for each microRNA or siRNA from individual experiments were averaged and presented on a bar graph, with the SEM and two-tailed student's t-test completed using the fold-change values. Statistical significance was assessed to a value of $p<0.01$, $p<0.05$ or non-significant.

3. RESULTS

3.1. MicroRNAs Predicted to Target PBF

Five microRNAs predicted to target PBF were selected in this investigation, with the evidence and reasons for their selection based on prediction software and the literature, as shown below.

3.1.1. hsa-miR-1

MiRWalk identified hsa-miR-1 to be involved in a validated interaction with PBF (PTTG1IP) (Dweep, H., et al., 2011) (Figure 4A). Additionally, it has been described that miR-1 acts as a tumour suppressor in thyroid tumours due to a downregulation of miR-1 apparent in thyroid carcinomas compared to normal thyroid tissue (Leone, V., et al., 2011), highlighting this as a particularly interesting microRNA to investigate.

	Gene Name	EntrezID	MicroRNA Name	StemLoopName
A	PTTG1IP	754	hsa-miR-1	hsa-mir-1-2
	PTTG1IP	754	hsa-miR-1	hsa-mir-1-1
B	PTTG1IP	754	hsa-miR-124	hsa-mir-124-1
	PTTG1IP	754	hsa-miR-124	hsa-mir-124-2
	PTTG1IP	754	hsa-miR-124	hsa-mir-124-3
	PTTG1IP	754	hsa-miR-373	hsa-mir-373
	PTTG1IP	754	hsa-miR-373*	hsa-mir-373

Figure 4: Identification of PBF as a validated target of microRNA from miRWalk
A) PTTG1IP/PBF is a validated target of hsa-miR-1 (Dweep, H., et al., 2011).
B) PTTG1IP/PBF is a validated target of hsa-miR-124 (Dweep, H., et al., 2011).

3.1.2. hsa-miR-122-5p

hsa-miR-122-5p was not identified by the prediction software to target PBF however, as described previously, PBF has been shown to be regulated in CHB and HCC by miR-122. In addition, inhibition of miR-122 is described to cause an upregulation of PBF in HCC resulting in a promotion of tumour growth and invasion (Li, C. et al., 2012) making this a particularly interesting microRNA to investigate due to PBF being known to have functions in

proliferation and invasion. In addition, miR-122 has been observed to be downregulated in breast cancer and upon overexpression *in vitro* and *in vivo* inhibits breast cancer cell proliferation (Wang, B., et al., 2012), in line with the previous observations of PBF.

3.1.3. hsa-miR-124-3p

MiRWalk identified miR-124 to have a validated interaction with PBF (PTTG1IP) (Dweep, H., et al., 2011) (Figure 4B), with additional evidence from miRTarBase, in the form of a microarray, highlighting the same (Hsu, S.D., et al., 2010). Furthermore, TargetScan identified the miR-124 binding site on PBF to be conserved as well as miR-124 itself defined as broadly conserved among vertebrates (Friedman, R.C., et al., 2009) (Figure 5A), which is suggestive of an important role in regulating the genome and more specifically, PBF. In the literature, miR-124 has been described to have a role as a tumour suppressor in various cancers by modulating the proliferation and aggressiveness of tumours (Xu X., et al., 2013).

	miRNA	conserved sites				poorly conserved sites			
		Total	8mer	7mer-m8	7mer-1A	Total	8mer	7mer-m8	7mer-1A
A	miR-124/124ab/506	1	1	0	0	0	0	0	0
	miR-451	0	0	0	0	1	0	1	0
	miR-217	0	0	0	0	1	1	0	0
	miR-196abc	0	0	0	0	1	0	1	0
B	miR-193/193b/193a-3p	0	0	0	0	1	0	1	0
	miR-33a-3p/365/365-3p	1	0	1	0	0	0	0	0
	miR-143/1721/4770	0	0	0	0	1	0	1	0

Figure 5: Broadly conserved microRNA among vertebrates predicted by TargetScan to target PBF
A) miR-124 and miR-506 are ranked to be broadly conserved microRNAs in vertebrates predicted to target PBF (Friedman, R.C., et al., 2009).
B) miR-193b is also ranked to be a broadly conserved microRNA in vertebrates predicted to target PBF (Friedman, R.C., et al., 2009).

3.1.4. hsa-miR-193b-5p

The miR-193 family, including miR-193b, was predicted by TargetScan to bind to PBF at a poorly conserved site (Friedman, R.C., et al., 2009) (Figure 5B). However, despite having a

poorly conserved binding site on PBF, the miR-193 family is conserved among mammals (Friedman, R.C., et al., 2009) suggestive of an important functional role. The literature described miR-193b to target oestrogen receptor α (ER-α), resulting in an inhibition of oestrogen-induced growth of breast tissue tumours (Leivonen, S-K., et al., 2011) (Yoshimoto, N., et al., 2011), which may be pertinent given that PBF is upregulated in ER-α positive MCF7 cells (Watkins, R.J., et al., 2010).

3.1.5. hsa-miR-506-3p

hsa-miR-506 has sequence similarity with hsa-miR-124, resulting in both these microRNAs predicted to bind to the same conserved site on the 3' UTR of PBF as well as both being broadly conserved among vertebrates (Friedman, R.C., et al., 2009) (Figure 5A). Furthermore, hsa-miR-506 has been implicated in suppressing epithelial-mesenchymal transition (EMT) in breast cancer cell lines (Arora, H., et al., 2013) highlighting an importance in cell invasion and migration, which correlates with the observations of PBF playing a role in invasion (Watkins, R.J., et al., 2010).

3.2. Effect on PBF mRNA Expression Following MicroRNA Mimic Transfections

3.2.1. Effect on PBF mRNA Expression Following MicroRNA Mimic Transfections in SW1736 Cells

Following the first experiment in SW1736 cells a 94.50% decrease ($p>0.01$) in PBF mRNA expression was observed as a result of anti-PBF siRNA transfection (Figure 6). Despite this, no significant changes in PBF mRNA expression were observed following any of the microRNA mimic transfections (Figure 6). However, due to technical issues with the RNA isolation and thus RNA quality in this experiment, these results were not thought to be reliable and were not been included in any further analysis.

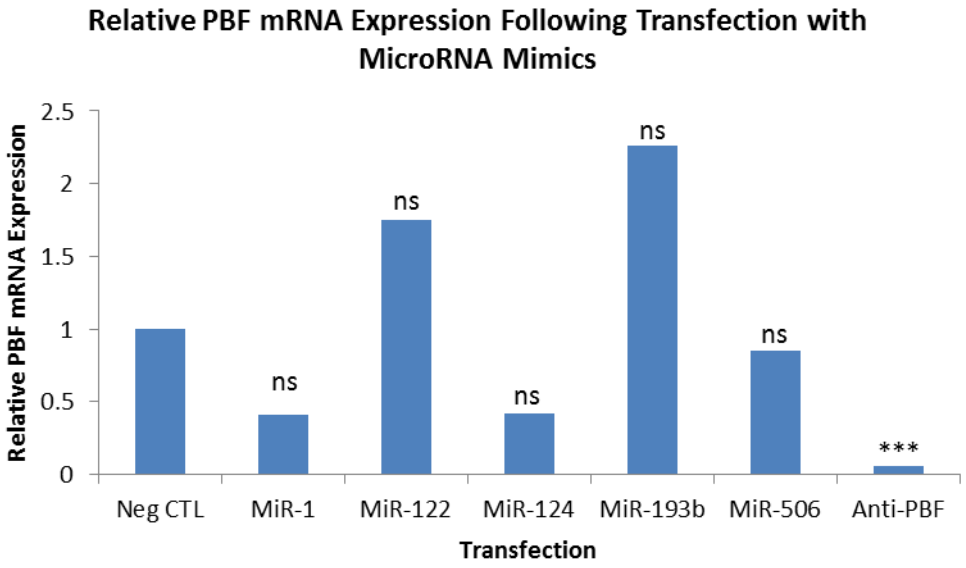

	Neg CTL	MiR-1	MiR-122	MiR-124	MiR-193b	MiR-506	Anti-PBF
ΔCT	11.58	12.95	10.80	13.09	10.45	11.84	15.88
SEM	0.42	0.46	0.30	0.45	0.27	0.14	0.32

Figure 6: PBF mRNA Expression in SW1736 cells following transfection with five microRNAs
PBF mRNA expression in SW1736 cells following the first experiment with (L-R): Negative control (Neg CTL), hsa-miR-1 (MiR-1), hsa-miR-122-5p (MiR-122), hsa-miR-124-3p (MiR-124), hsa-miR-193b-5p (MiR-193b), hsa-miR-506-3p (MiR-506) and anti-PBF siRNA (Anti-PBF) normalised to 18S. ΔCT indicates PBF CT value – 18S CT value and SEM indicates the SEM of the four replicates for each sample. Statistics were calculated using the paired t-test, where ***=$p<0.01$ and ns=non-significant.

The second experiment in SW1736 cells indicated a significant decrease in PBF mRNA expression following transfection with anti-PBF siRNA of 70.77% ($p<0.01$) as well as a significant decrease following the transfection with hsa-miR-506-3p of 55.00% ($p<0.05$). In addition, albeit non-significant, a decrease in PBF mRNA expression was observed following hsa-miR-1 and hsa-miR-124-3p transfection of 3.72% and 33.20% respectively (Figure 7).

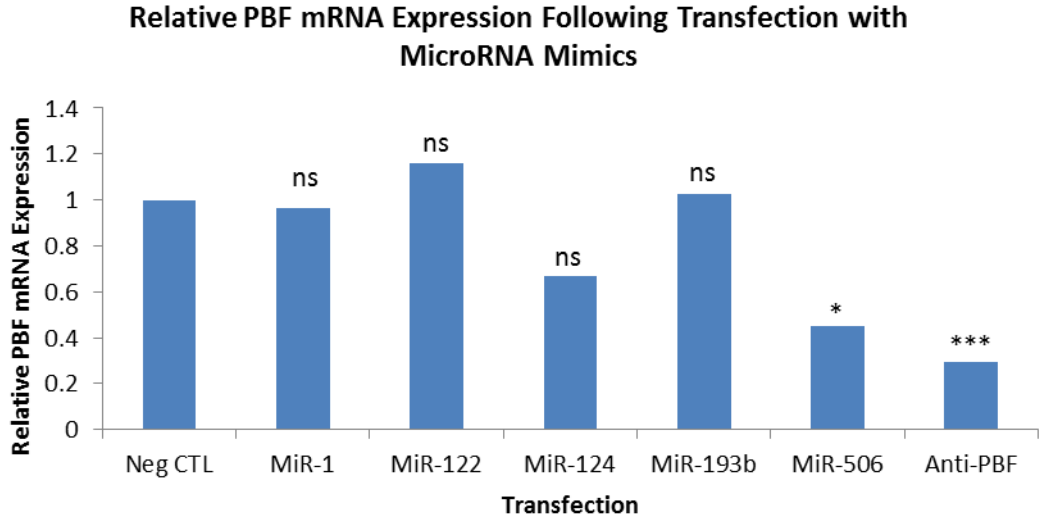

	Neg CTL	MiR-1	MiR-122	MiR-124	MiR-193b	MiR-506	Anti-PBF
ΔCT	10.22	10.64	10.51	11.22	10.05	11.26	11.87
SEM	0.31	0.28	0.46	0.38	0.08	0.15	0.10

Figure 7: PBF mRNA Expression in SW1736 cells following transfection with five microRNAs
PBF mRNA expression in SW1736 cells following the second experiment with (L-R): Negative control (Neg CTL), hsa-miR-1 (MiR-1), hsa-miR-122-5p (MiR-122), hsa-miR-124-3p (MiR-124), hsa-miR-193b-5p (MiR-193b), hsa-miR-506-3p (MiR-506) and anti-PBF siRNA (Anti-PBF) normalised to 18S. ΔCT indicates PBF CT value – 18S CT value and SEM indicates the SEM of the four replicates for each sample. Statistics were calculated using the paired t-test, where ***=$p<0.01$, *=$p>0.05$ and ns=non-significant.

In the third experiment in SW1736 cells, hsa-miR-193b-5p was not investigated as the transfection reagent was limited meaning the microRNA mimic with the least success thus far was sacrificed. The other microRNA mimics were transfected as before, with very small changes in PBF mRNA expression following transfection observed (Figure 8). However,

following anti-PBF siRNA transfection a decrease in mRNA expression of 72.72% ($p<0.05$) was observed (Figure 8).

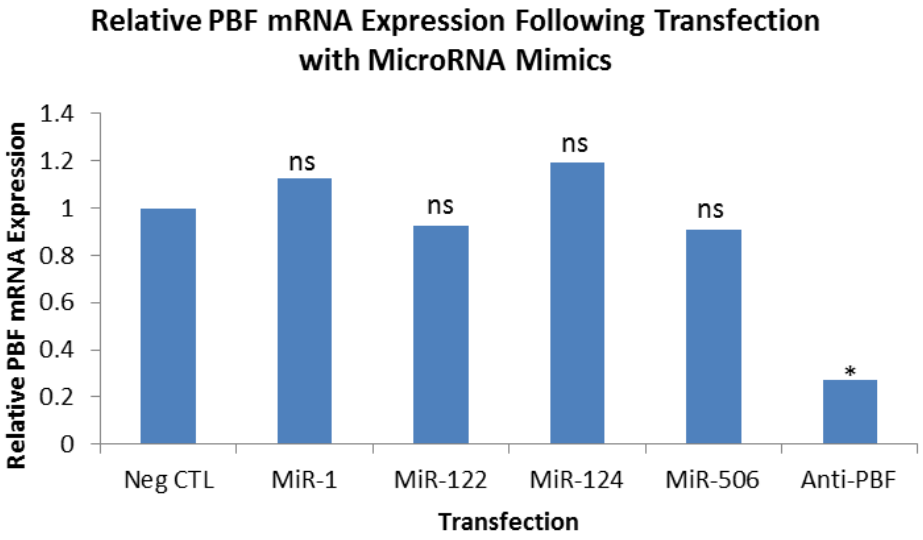

	Neg CTL	MiR-1	MiR-122	MiR-124	MiR-506	Anti-PBF
ΔCT	11.15	10.97	11.29	10.91	11.31	13.08
SEM	0.09	0.09	0.22	0.19	0.09	0.18

Figure 8: PBF mRNA Expression in SW1736 cells following transfection with four microRNAs
PBF mRNA expression in SW1736 cells following the third experiment with (L-R): Negative control (Neg CTL), hsa-miR-1 (MiR-1), hsa-miR-122-5p (MiR-122), hsa-miR-124-3p (MiR-124), hsa-miR-506-3p (MiR-506) and anti-PBF siRNA (Anti-PBF) normalised to 18S. ΔCT indicates PBF CT value – 18S CT value and SEM indicates the SEM of the four replicates for each sample. Statistics were calculated using the paired t-test, where *=$p<0.05$ and ns=non-significant.

Following the fourth experiment in SW1736 cells, where hsa-miR-193b-5p was also not investigated, anti-PBF siRNA caused a decrease in PBF mRNA expression of 61.00% ($p<0.05$). In addition, hsa-miR-122-5p, hsa-miR-124-3p and hsa-miR-506-3p caused significant decreases in PBF mRNA expression of 35.80% ($p<0.05$), 46.97% ($p<0.05$) and 42.45% ($p<0.05$) respectively (Figure 9). In addition, hsa-miR-1 also caused a decrease in PBF mRNA expression of 39.43% (non-significant) (Figure 9), however this was non-significant.

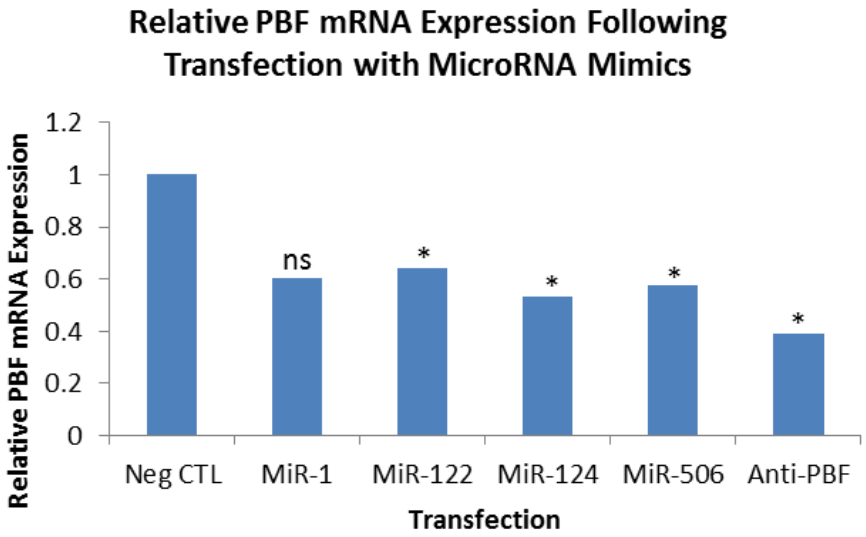

	Neg CTL	MiR-1	MiR-122	MiR-124	MiR-506	Anti-PBF
ΔCT	10.10	10.93	10.73	11.08	10.95	11.80
SEM	0.17	0.37	0.17	0.32	0.11	0.58

Figure 9: PBF mRNA Expression in SW1736 cells following transfection with four microRNAs
PBF mRNA expression in SW1736 cells following the fourth experiment with (L-R): Negative control (Neg CTL), hsa-miR-1 (MiR-1), hsa-miR-122-5p (MiR-122), hsa-miR-124-3p (MiR-124), hsa-miR-506-3p (MiR-506) and anti-PBF siRNA (Anti-PBF) normalised to 18S. ΔCT indicates PBF CT value – 18S CT value and SEM indicates the SEM of the four replicates for each sample. Statistics were calculated using the paired t-test, where *=$p<0.05$ and ns=non-significant.

Average PBF mRNA expression levels were calculated using results from the second, third and fourth experiments, due to technical issues with the RNA from the first experiment. These results can be seen in Figure 10A, with the overall averages and statistics of these in Figure 10B, indicating none of the microRNA mimics caused a significant change in PBF mRNA expression levels overall. The largest decrease in PBF mRNA expression of 35.54% (non-significant) was observed as a result of hsa-miR-506-3p transfection (Figure 10B). However, it is important to note that anti-PBF siRNA caused a significant decrease in PBF mRNA expression levels of 68.16% ($p<0.05$) (Figure 10B), around the value expected from a siRNA.

A

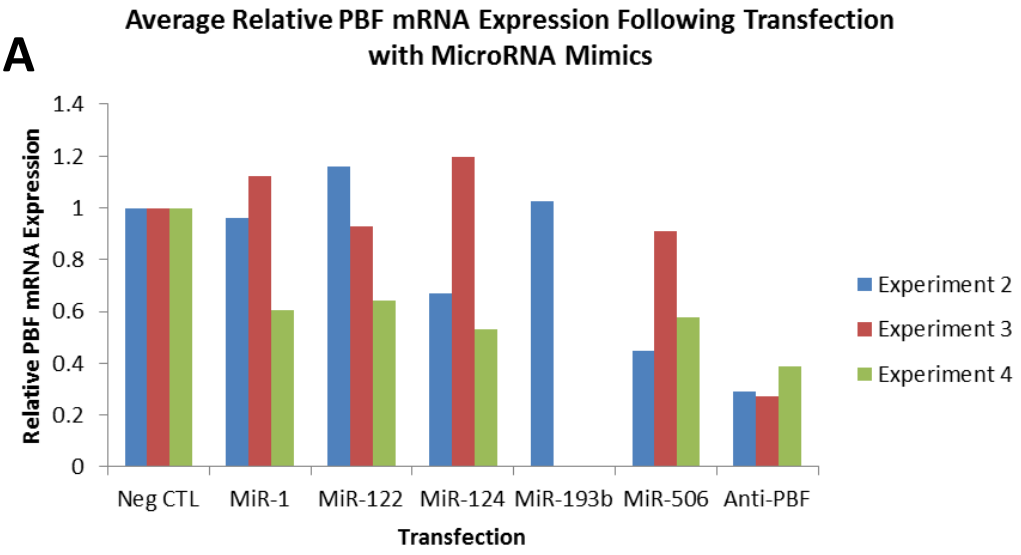

B

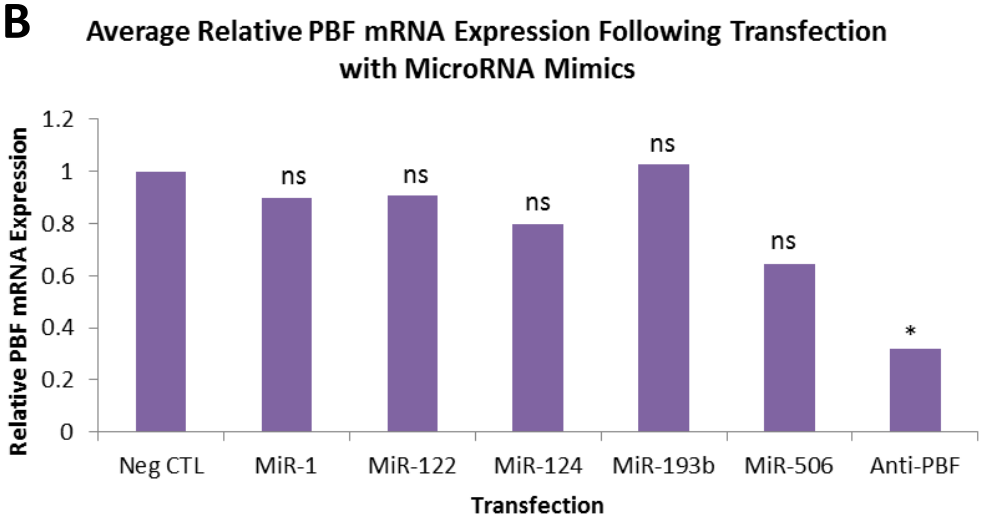

	Neg CTL	MiR-1	MiR-122	MiR-124	MiR-193b	MiR-506	Anti-PBF
ΔCT	10.48802	10.84613	10.84204	11.06813	10.054	11.17333	12.24775
SEM	0.330589	0.105105	0.23377	0.089388		0.112329	0.414503

Figure 10: Average relative PBF mRNA expression following all three transfections in SW1736 cells, with results averaged and analysed

A) Results on relative PBF protein levels following transfection with a negative control (Neg CTL), hsa-miR-1 (MiR-1), hsa-miR-122-5p (MiR-122), hsa-miR-124-3p (MiR-124), hsa-miR-193b-5p, hsa-miR-506-3p (MiR-506) and anti-PBF siRNA (Anti-PBF) (n=3 for all microRNA, except miR-193b-5p (n=1)).

B) Average PBF mRNA expression (n=3 for all microRNA, except miR-193b-5p (n=1)), calculated using results in A, with statistics calculated using the paired t-test, where *=p<0.05 and ns=non-significant. ΔCT indicates average ΔCT values from three experiments and SEM indicates the SEM from the three experiments. Statistics were calculated using the paired t-test, where *=p<0.05 and ns=non-significant.

3.2.2. Effect on PBF mRNA Expression Following MicroRNA Mimic Transfections in MCF7 Cells

Figure 11 indicates a decrease in PBF mRNA expression of 60.30% (non-significant) following anti-PBF siRNA transfection, as expected. However, none of the transfections with microRNA mimics caused a significant decrease in PBF mRNA expression, with the largest decreases in PBF mRNA expression observed following hsa-miR-124-3p and hsa-miR-506-3p transfections causing decreases in PBF mRNA expression of 18.97% (non-significant) and 59.20% (non-significant) respectively (Figure 11).

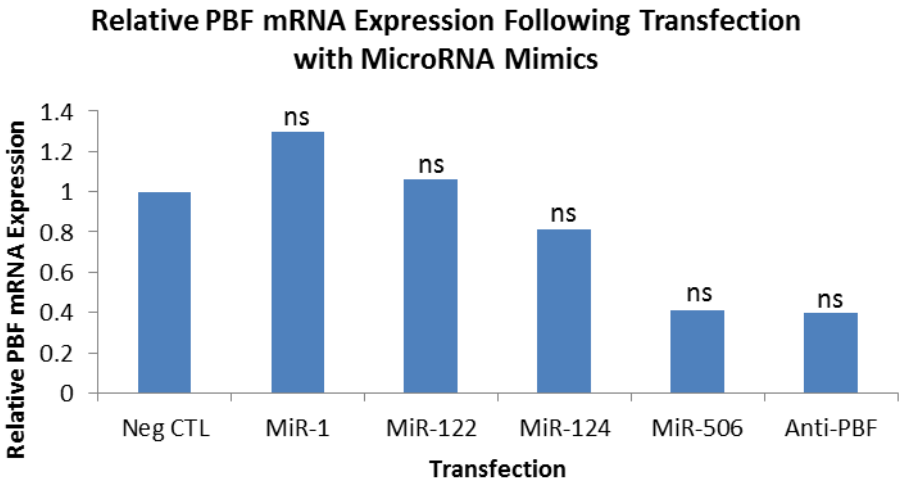

	Neg CTL	MiR-1	MiR-122	MiR-124	MiR-506	Anti-PBF
ΔCT	11.89	12.19	12.43	12.80	12.70	13.04
SEM	0.35	0.29	0.21	0.16	0.30	0.63

Figure 11: PBF mRNA Expression in MCF7 cells following transfection with four microRNAs
PBF mRNA expression in MCF7 cells following the first experiment with (L-R): Negative control (Neg CTL), hsa-miR-1 (MiR-1), hsa-miR-122-5p (MiR-122), hsa-miR-124-3p (MiR-124), hsa-miR-506-3p (MiR-506) and anti-PBF siRNA (Anti-PBF) normalised to 18S. ΔCT indicates PBF CT value – 18S CT value and SEM indicates the SEM of the four replicates for each sample. Statistics were calculated using the paired t-test, where ns=non-significant.

Following the second experiment in MCF7, despite a non-significant 16.62% decrease in PBF mRNA expression following anti-PBF siRNA transfection, a significant decrease in PBF mRNA expression of 37.75% ($p<0.05$) was observed following transfection with hsa-miR-124-3p (Figure 12). In comparison, following transfection with the other microRNA mimics; hsa-miR-1, hsa-miR-122-5p and hsa-miR-506-3p all caused an increase in PBF mRNA expression (Figure 12).

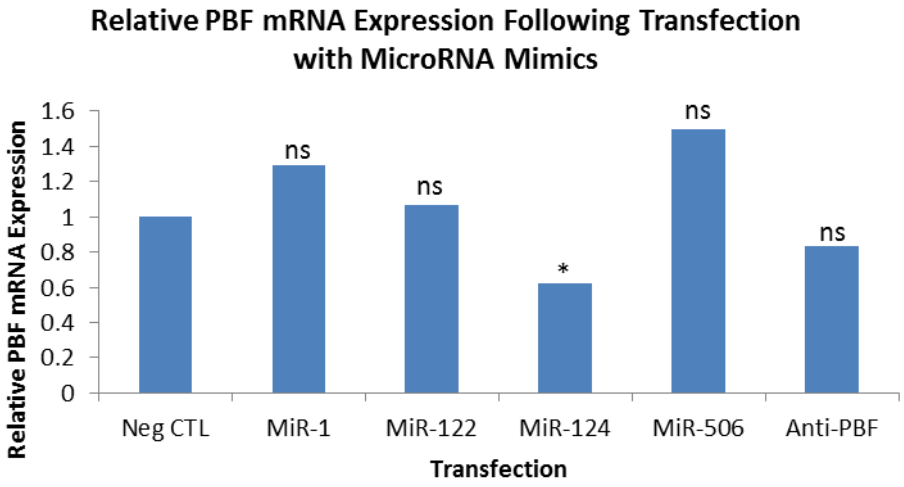

	Neg CTL	MiR-1	MiR-122	MiR-124	MiR-506	Anti-PBF
ΔCT	12.45	12.19	12.43	13.19	12.22	12.87
SEM	0.12	0.29	0.21	0.18	0.57	0.45

Figure 12: PBF mRNA Expression in MCF7 cells following transfection with four microRNAs
PBF mRNA expression in MCF7 cells following the second experiment with (L-R): Negative control (Neg CTL), hsa-miR-1 (MiR-1), hsa-miR-122-5p (MiR-122), hsa-miR-124-3p (MiR-124), hsa-miR-506-3p (MiR-506) and anti-PBF siRNA (Anti-PBF) normalised to 18S. ΔCT indicates PBF CT value – 18S CT value and SEM indicates the SEM of the four replicates for each sample. Statistics were calculated using the paired t-test, where *=p>0.05 and ns=non-significant.

Overall average results for the effect of microRNA mimic transfections on PBF mRNA expression in MCF7 cells were not completed as there were only two sets of data and thus a meaningful average could not be obtained. However, hsa-miR-124-3p was only the microRNA that decreased PBF mRNA expression in both experiments in MCF7 cells.

3.3. Effect on PBF Protein Levels Following MicroRNA Mimic Transfections

It is important to note there are multiple forms of PBF protein, which are recognised by the PBF antibody used during Western blotting - due to PBF having phosphorylation sites, five glycosylation sites as well as the ability to oligomerise (Smith V. and McCabe, C., 2008). However, the two species that were studied in this investigation were at 25kDa and 30kDa, as these are the main forms normally studied (Watkins, R.J., et al., 2010) and identified by Western blot by other commercially available antibodies.

3.3.1. Effect on PBF Protein Levels Following MicroRNA Mimic Transfections in SW1736 Cells

Figure 13A shows the Western blot following the first experiment in SW1736 cells, highlighting the 25kDa and 30kDa PBF protein bands alongside β-actin. The largest overall effect on PBF protein levels was observed following hsa-miR-122-5p and hsa-miR-124-3p transfection (Figure 13A). Densitometry indicated that at 25kDa and 30kDa, hsa-miR-122-5p caused decreases in PBF protein of 58.30% at 25kDa and 79.66% at 30kDa and hsa-miR-124-3p caused a decrease of 65.70% and 78.11% at 30kDa (Figure 13B). Furthermore, hsa-miR-506-3p also caused large decreases in PBF protein levels at 25kDa and 30kDa of 89.97% and 45.93% respectively (Figure 13B). In addition, following the anti-PBF siRNA transfection a decrease in PBF protein levels of 65.77% at 25kDa and 66.47% at 30kDa (Figure 13B) was observed, as would be expected.

Figure 13: PBF protein levels in SW1736 cells following transfection with five microRNAs

A) Western blot showing PBF protein levels (*=25kDa, *=30kDa) in SW1736 cells following the first experiment with (L-R): Negative control (Neg CTL), hsa-miR-1 (MiR-1), hsa-miR-122-5p (MiR-122), hsa-miR-124-3p (MiR-124), hsa-miR-193b-5p (MiR-193b), hsa-miR-506-3p (MiR-506) and anti-PBF siRNA (Anti-PBF). Anti-β-actin at 44kDa shows approximately equal loading.

B) Densitometry of Western blot normalised to β-actin showing PBF protein levels at 25kDa and 30kDa in SW1736 cells relative to the negative control, assigned an arbitrary value of 1.

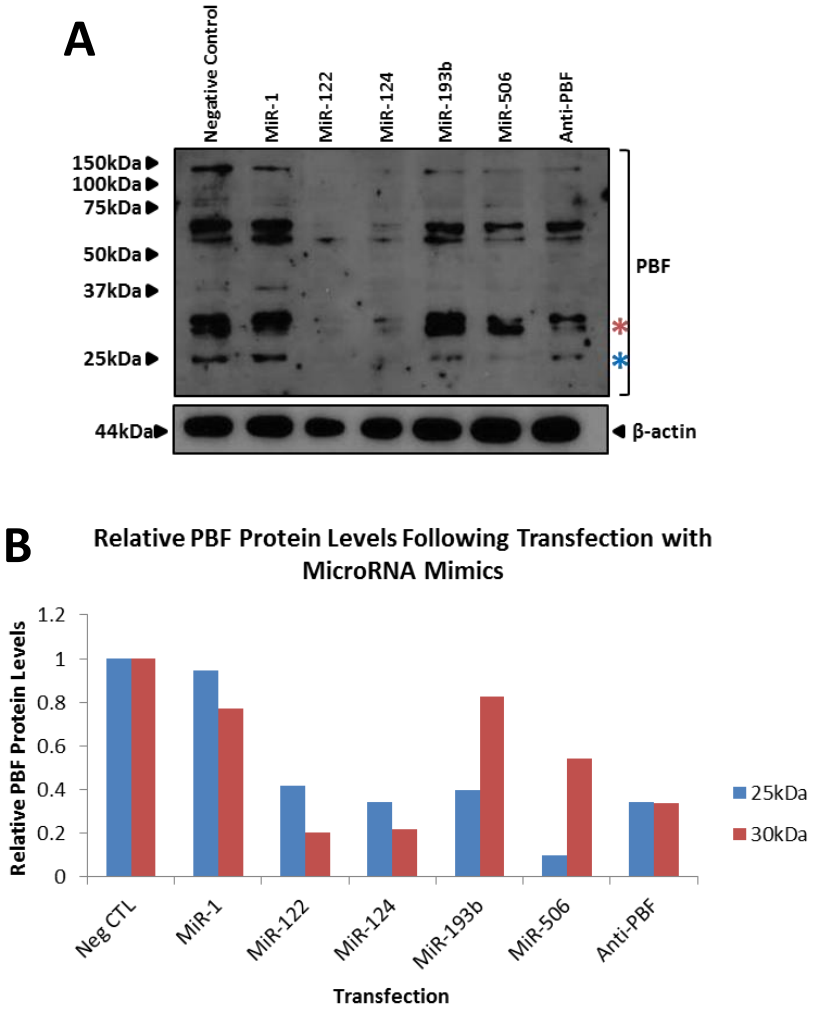

Figure 14A shows the 25kDa and 30kDa PBF protein bands on the Western blot alongside β-actin following the second experiment in SW1736 cells. Figure 14B displays the densitometry from this Western blot indicating a decrease in PBF protein levels following transfection with hsa-miR-1 of 28.42% at 25kDa and 67.27% at 30kDa and hsa-miR-122-5p of 16.34% at 25kDa and 2.31% at 30kDa (Figure 14B). However, hsa-miR-124-3p, hsa-miR-193b-5p and hsa-miR-506-3p all caused an increase in PBF protein levels at 25kDa and 30kDa. Furthermore, unexpectedly, anti-PBF siRNA resulted in an increase in PBF protein levels of 126.01% at 25kDa and 136.08% at 30kDa (Figure 14B) creating some doubt as to how reliable these results are as a decrease following anti-PBF siRNA transfection would be expected as observed for mRNA expression levels following anti-PBF transfection, which was completed at the same time (Figure 10).

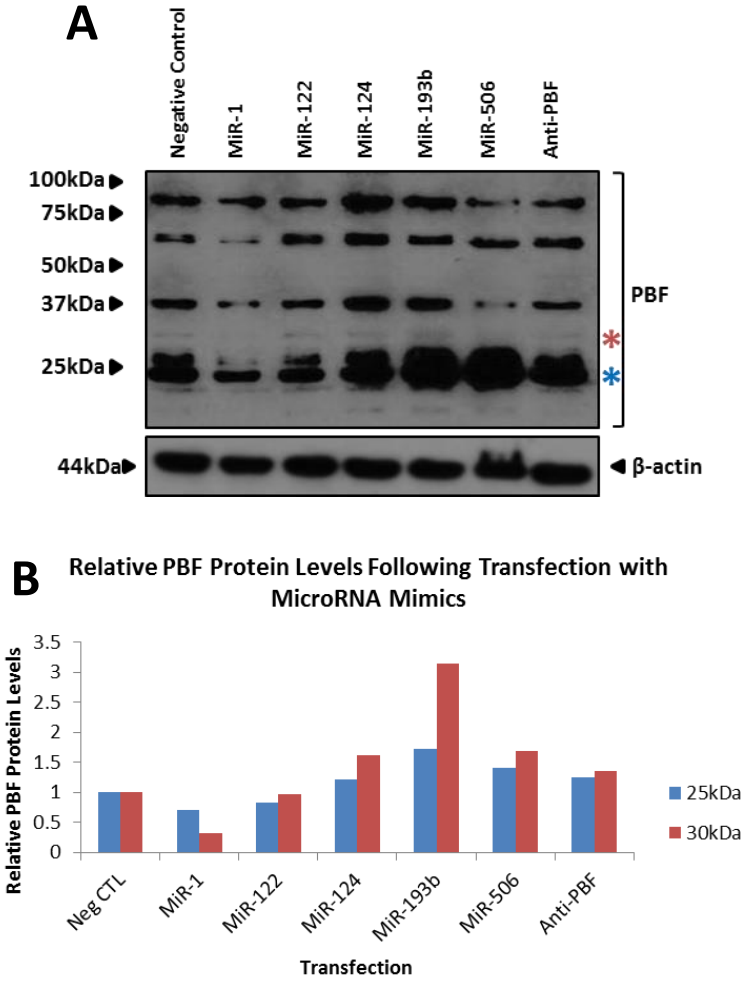

Figure 14: PBF protein levels in SW1736 cells following transfection with five microRNAs
A) Western blot showing PBF protein levels (*=25kDa, *=30kDa) in SW1736 cells following the second experiment with (L-R): Negative control (Neg CTL), hsa-miR-1 (MiR-1), hsa-miR-122-5p (MiR-122), hsa-miR-124-3p (MiR-124), hsa-miR-193b-5p (MiR-193b), hsa-miR-506-3p (MiR-506) and anti-PBF siRNA (Anti-PBF). Anti-β-actin at 44kDa shows approximately equal loading.
B) Densitometry of Western blot normalised to β-actin showing PBF protein levels at 25kDa and 30kDa in SW1736 cells relative to the negative control, assigned an arbitrary value of 1.

Figure 15A shows the Western blot following the first experiment in SW1736 cells, highlighting the 25kDa and 30kDa PBF protein bands alongside β-actin. It is important to note that hsa-miR-193b-5p was not investigated in this experiment, as transfection reagent was limited - as described previously. Densitometry indicates decreased PBF protein levels following transfection with hsa-miR-122-5p of 37.27% at 25kDa and 5.65% at 30kDa and with hsa-miR-124-3p of 34.35% at 25kDa and 39.92% at 30kDa respectively (Figure 15B). In addition, following anti-PBF siRNA transfection a 49.85% decrease at 25kDa and a 0.24% decrease at 30kDa in PBF protein levels was observed (Figure 15B).

Figure 15: PBF protein levels in SW1736 cells following transfection with four microRNAs

A) Western blot showing PBF protein levels (*=25kDa, *=30kDa) in SW1736 cells following the third experiment with (L-R): Negative control (Neg CTL), hsa-miR-1 (MiR-1), hsa-miR-122-5p (MiR-122), hsa-miR-124-3p (MiR-124), hsa-miR-506-3p (MiR-506) and anti-PBF siRNA (Anti-PBF). Anti-β-actin at 44kDa shows approximately equal loading.

B) Densitometry of Western blot normalised to β-actin showing PBF protein levels at 25kDa and 30kDa in SW1736 cells relative to the negative control, assigned an arbitrary value of 1.

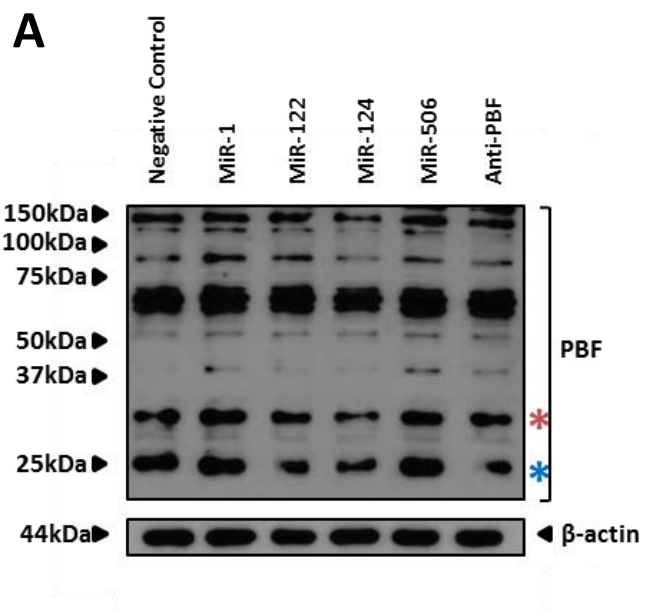

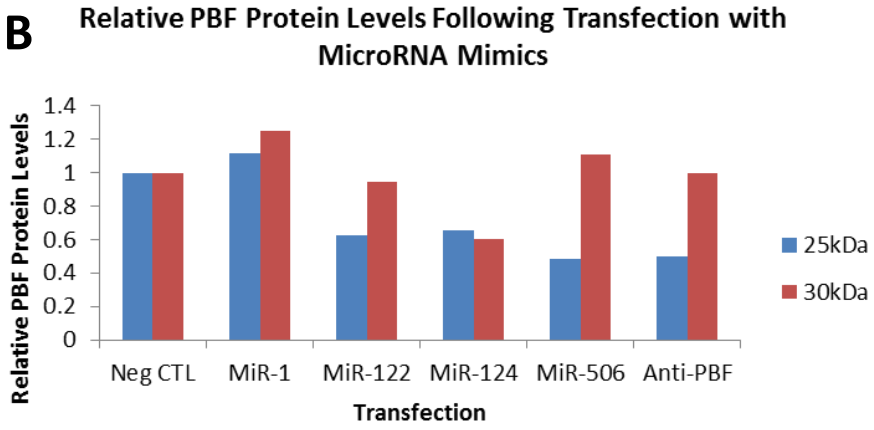

Following the fourth experiment in SW1736 cells, the 25kDa PBF protein band, which was previously identified and quantified, was not visible by Western blot. Therefore, only the 30kDa PBF protein band (Figure 16A) was quantified by densitometry (Figure 16B). Results indicated the anti-PBF siRNA transfection caused an increase in PBF protein levels of 104.51% (Figure 16B), similar to the previous unexpected observation (Figure 14B). However, despite this, a decrease in PBF protein levels at 30kDa was observed following transfection with hsa-miR-124 and hsa-miR-506-3p of 9.55% and 29.46% respectively (Figure 16B).

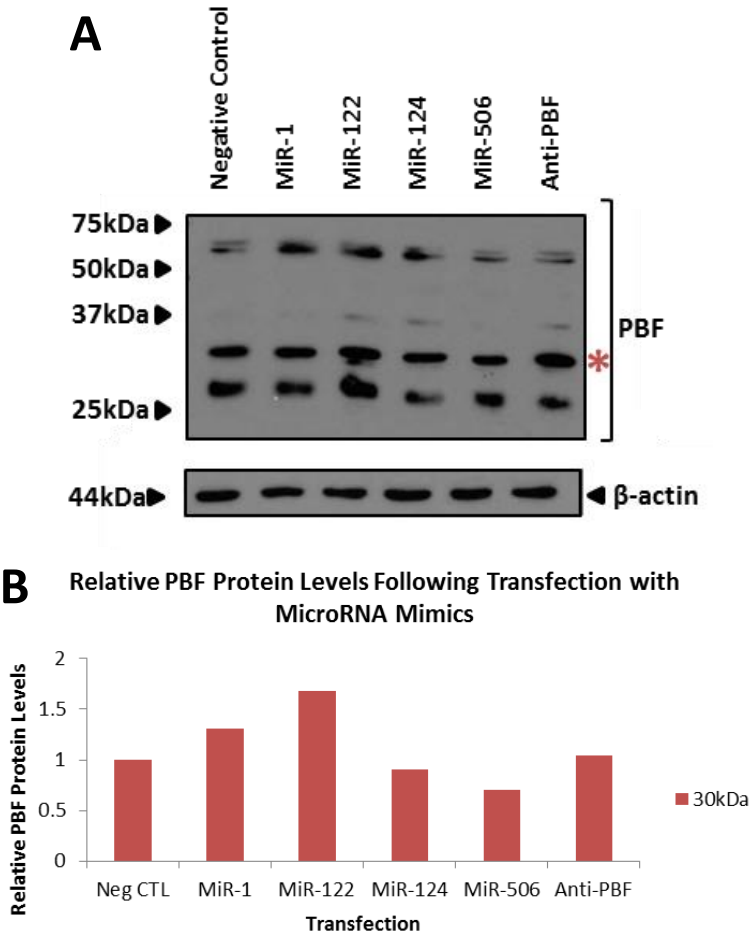

Figure 16: PBF protein levels in SW1736 cells following transfection with four microRNAs
A) Western blot showing PBF protein levels (*=30kDa) in SW1736 cells following the fourth experiment with (L-R): Negative control (Neg CTL), hsa-miR-1 (MiR-1), hsa-miR-122-5p (MiR-122), hsa-miR-124-3p (MiR-124), hsa-miR-506-3p (MiR-506) and anti-PBF siRNA (Anti-PBF). Anti-β-actin at 44kDa shows approximately equal loading.
B) Densitometry of Western blot normalised to β-actin showing PBF protein levels at 30kDa in SW1736 cells relative to the negative control, assigned an arbitrary value of 1.

The results from the four experiments above on PBF protein levels at 25kDa in SW1736 cells are shown together in Figure 17A; indicating experiment two as a potential anomaly.

However, due to small n numbers making it difficult to determine a true anomaly, results were averaged from all sets of data and statistics completed (Figure 17B), indicating a significant average decrease in PBF protein levels following transfection with hsa-miR-122-5p of 37.32±12.10 ($p>0.05$) (Figure 17B). In addition, hsa-miR-124-3p and hsa-miR-506-3p caused an average decrease of 26.21±25.48% (non-significant) and 33.66±38.85% (non-significant) (Figure 17B), albeit non-significant. The average decrease in PBF protein levels at 25kDa following transfection with anti-PBF siRNA was 29.87±28.32% (non-significant) (Figure 17B), lower than expected.

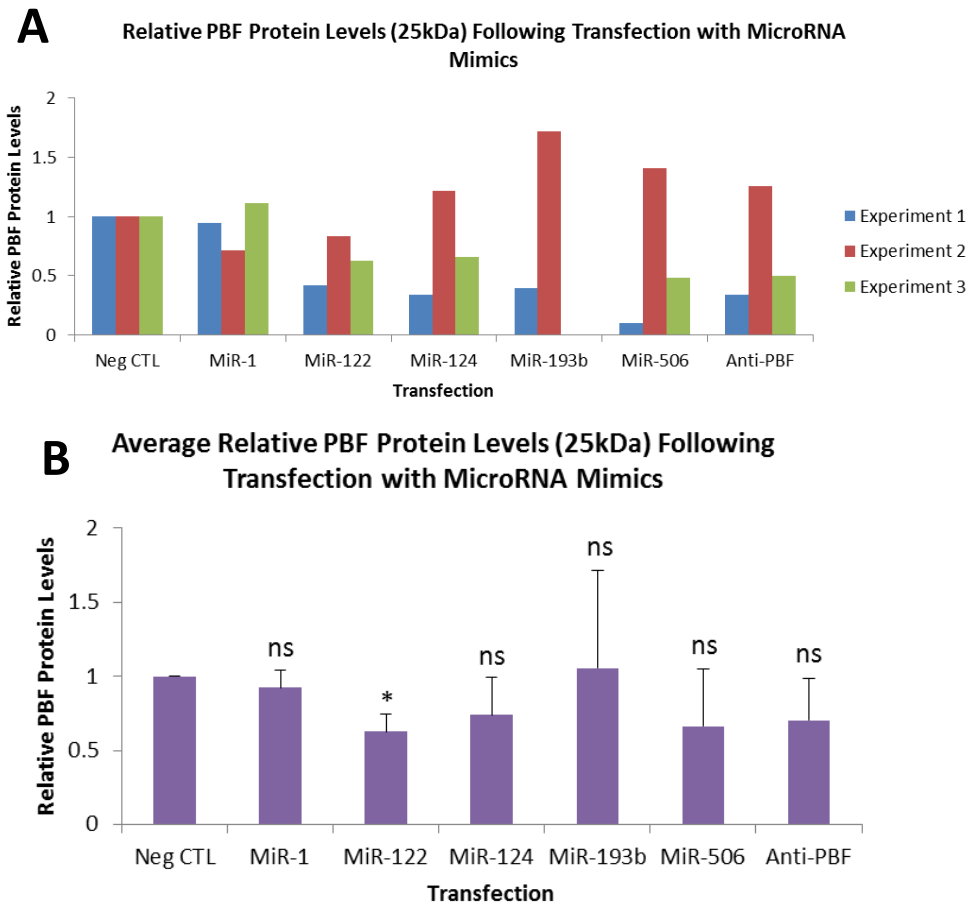

Figure 17: Average relative PBF protein levels (25kDa) following all three experiments in SW1736 cells, with results averaged and analysed

A) Results on relative PBF protein levels following transfection with a negative control (Neg CTL), hsa-miR-1 (MiR-1), hsa-miR-122-5p (MiR-122), hsa-miR-124-3p (MiR-124), hsa-miR-193b-5p, hsa-miR-506-3p (MiR-506) and anti-PBF siRNA (Anti-PBF) (n=3 for all microRNA, besides miR-193b-5p (n=2)).

B) Average PBF protein levels (n=3 for all microRNA, besides miR-193b-5p (n=2)), calculated using results in A, with statistics calculated using the paired t-test, where *=$p<0.05$ and ns=non-significant and error bars are calculated from the SEM.

The results from the four experiments above on PBF protein levels at 30kDa in SW1736 cells are shown in Figure 18A, highlighting experiment two as a potential anomaly, similarly to what was shown in Figure 17A. However, results were averaged from all sets of data and statistics completed (Figure 18B), which indicated none of the microRNA mimics or anti-PBF siRNA caused a significant average decrease in PBF protein levels at 30kDa. The largest average decrease in PBF protein levels was due to hsa-miR-124-3p, which caused a decrease of 16.35±29.70% (non-significant) at 30kDa (Figure 18B).

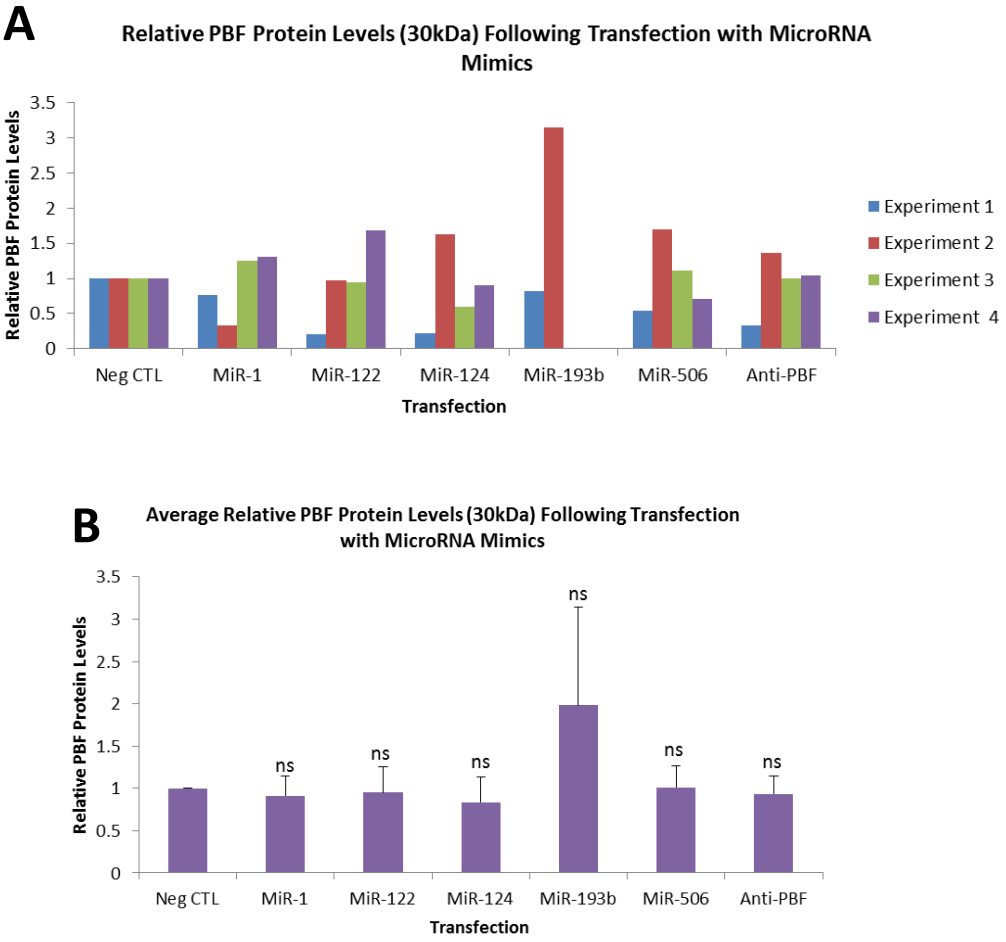

Figure 18: Average relative PBF protein levels (30kDa) following all four experiments in SW1736 cells, with results averaged and analysed

A) Results on relative PBF protein levels following transfection with a negative control (Neg CTL), hsa-miR-1 (MiR-1), hsa-miR-122-5p (MiR-122), hsa-miR-124-3p (MiR-124), hsa-miR-193b-5p, hsa-miR-506-3p (MiR-506) and anti-PBF siRNA (Anti-PBF) (n=4 for all microRNA, besides miR-193b-5p (n=2)).

B) Average PBF protein levels (n=3 for all microRNA, besides miR-193b-5p (n=2)), calculated using results in A, with statistics calculated using the paired t-test, where ns=non-significant and error bars are calculated from the SEM.

When observing the effect of microRNA mimics on PBF protein levels at both 25kDa and 30kDa, it appeared that all the selected microRNA mimics had a greater effect at 25kDa (Figure 19). Overall, hsa-miR-122-5p, hsa-miR-124-3p and hsa-miR-506-3p transfections all caused a similar degree of effect on PBF protein levels at 25kDa and 30kDa, which was comparable to the effect following anti-PBF siRNA transfection (Figure 19) suggestive of a potential of these microRNAs in regulating PBF.

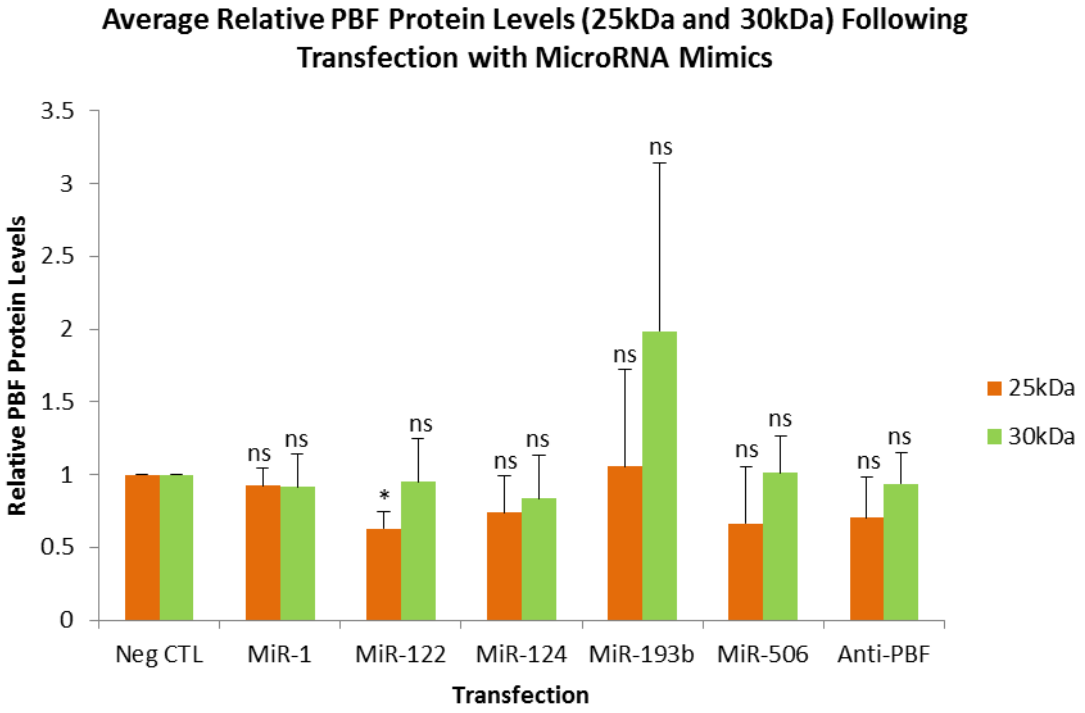

Figure 19: Comparison of average relative PBF protein levels (25kDa and 30kDa) following experiments in SW1736 cells

Average PBF protein levels (From Figure 17B and Figure 18B, with statistics calculated using the paired t-test, where *=p<0.05 and ns=non-significant and error bars are calculated from the SEM.

3.3.2. Effect on PBF Protein Levels Following MicroRNA Mimic Transfections in MCF7 Cells

The Western blot following the first experiment in MCF7 cells can be seen in Figure 20A, with the 25kDa and 30kDa PBF protein bands highlighted alongside β-actin. Densitometry indicated all transfections caused large increases in PBF protein levels at both 25kDa and 30kDa (Figure 20B), highlighting there may have been a technical issue with these transfections as even the anti-PBF siRNA caused an increase in the surplus of 700%.

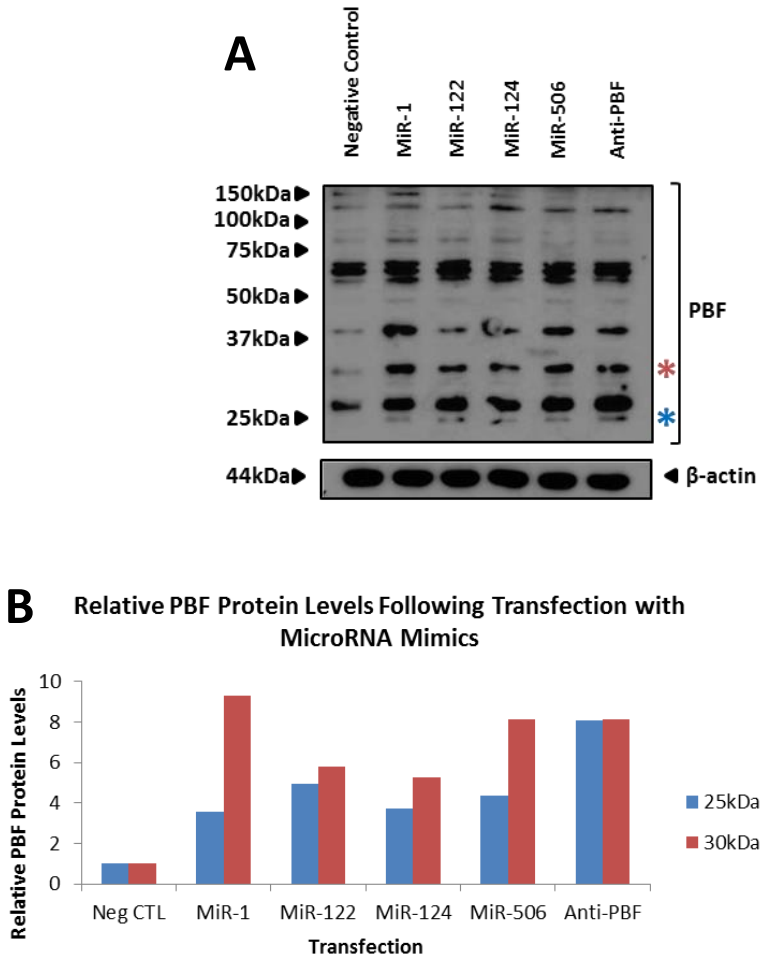

Figure 20: PBF protein levels in MCF7 cells following transfection with four microRNAs
A) Western blot showing PBF protein levels (*=25kDa, *=30kDa) in MCF7 cells following the first experiment with (L-R): Negative control (Neg CTL), hsa-miR-1 (MiR-1), hsa-miR-122-5p (MiR-122), hsa-miR-124-3p (MiR-124), hsa-miR-506-3p (MiR-506) and anti-PBF siRNA (Anti-PBF). Anti-β-actin at 44kDa shows approximately equal loading.
B) Densitometry of Western blot normalised to β-actin showing PBF protein levels at 25kDa and 30kDa in MCF7 cells relative to the negative control, assigned an arbitrary value of 1.

Following the second experiment in MCF7 cells, the Western blot indicated the 30kDa PBF protein band (Figure 21A) but the PBF antibody did not identify the 25kDa PBF protein band, as seen previously in Figure 16A. Despite this, densitometry was completed for the 30kDa

PBF protein band, which indicated only hsa-miR-1 caused a small decrease in PBF protein levels of 12.95% (Figure 21B).

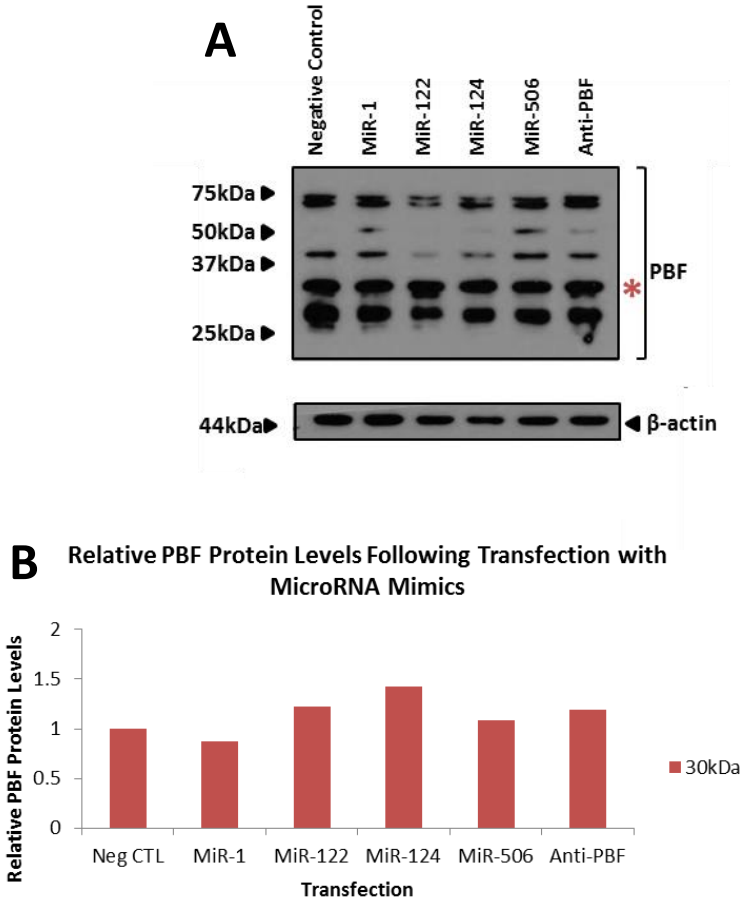

Figure 21: PBF protein levels in MCF7 cells following transfection with four microRNAs

A) Western blot showing PBF protein levels (*=30kDa) in MCF7 cells following the second experiment with (L-R): Negative control (Neg CTL), hsa-miR-1 (MiR-1), hsa-miR-122-5p (MiR-122), hsa-miR-124-3p (MiR-124), hsa-miR-506-3p (MiR-506) and anti-PBF siRNA (Anti-PBF). Anti-β-actin at 44kDa shows approximately equal loading.

B) Densitometry of Western blot normalised to β-actin showing PBF protein levels at 30kDa in MCF7 cells relative to the negative control, assigned an arbitrary value of 1.

Average results of the effect of microRNA mimic transfections on PBF protein levels in MCF7 cells was not completed due to two reasons: firstly, only one data set was available for the 25kDa PBF protein band and secondly, the 30kDa protein band gave variable results within the two sets of results making it impossible to obtain a true average result.

4. DISCUSSION

Due to the observation of PBF being overexpressed in thyroid cancers (Smith, V.E., et al., 2013) and microRNAs being described to be deregulated in thyroid cancers (Vriens, M.R., et al., 2012), it was hypothesised that there may be a correlation between microRNA deregulation and PBF overexpression. Therefore, this investigation was designed to identify microRNAs that target PBF as well as challenging the findings of Li, C., et al., who described PBF as a target of hsa-miR-122 in liver cancer (2013). Consequently, in this investigation, it was identified that hsa-miR-122-5p, hsa-miR-124-3p and hsa-miR-506-3p all targeted PBF to some degree, resulting in decreased PBF mRNA expression and/or protein levels. Subsequently, this may highlight a mechanism for the regulation of PBF, which is currently fairly elusive, whereby microRNA deregulation contributes to the overexpression of PBF, leading to thyroid cancer.

4.1. hsa-miR-122-5p Decreased PBF Protein Levels

The most striking average decrease in PBF protein levels following microRNA mimic transfection was observed following transfection with hsa-miR-122-5p in SW1736 cells, which caused a significant decrease in PBF protein levels at 25kDa of 37.32±12.10 ($p>0.05$), which was greater than the average decrease following anti-PBF siRNA transfection of 29.87±28.32% (non-significant) (Figure 17B).

However, a similar effect of hsa-miR-122-5p against PBF was not observed at 30kDa (Figure 18) in SW1736 cells or at 25kDa or 30kDa in MCF7 cells (Figures 20 and 21). Subsequently, further investigations would need to take place in both these cell lines, particularly MCF7 cells to increase the number of repeats before a full conclusion could be made on whether hsa-miR-122-5p targets PBF. In addition, it would be essential to extend the investigation to study

the other forms of PBF protein, including the larger protein bands representing dimers, as in this investigation limitations meant only the main forms of PBF at 25kDa and 30kDa (Watkins, R.J., et al., 2010) were observed.

Furthermore, despite the decrease in PBF protein levels at 25kDa, it is important to note that PBF mRNA expression levels were not significantly altered by hsa-miR-122-5p in this investigation, with an average decrease of only 9.07% (non-significant) observed following transfection in SW1736 cells (Figure 10). This may indicate that PBF is not being directly targeted by hsa-miR-122-5p, but instead is being affected by hsa-miR-122-5p targeting another protein or pathway, which subsequently alters PBF protein levels. This is possible as each microRNA has approximately 200 mRNA targets (Carther, R.W., 2006), meaning even if PBF was directly targeted by hsa-miR-122-5p other mRNAs would also be targeted. To confirm whether PBF is being targeted directly by hsa-miR-122-5p, a green fluorescent protein (GFP) reporter assay could be used, by sub-cloning PBF's WT 3'UTR microRNA target site into a GFP vector it could be observed whether hsa-miR-122-5p caused an inhibition of GFP expression.

If the observation of hsa-miR-122-5p decreasing PBF protein levels was confirmed this would be very interesting, as it complements the observations made by Li, C., et al. who described miR-122 targeted PBF in a Huh7 hepatocellular carcinoma cell line (2012). Furthermore, as Li, C., et al. also observed low miR-122 levels correlated with an upregulation of PBF in HCC (Li, C., et al., 2012) this highlights the importance of investigating hsa-miR-122 and PBF in the context of thyroid cancer. In a future investigation it would be interesting to investigate whether the targeting of PBF by hsa-miR-122-5p in SW1736 cells, an anaplastic thyroid carcinoma cell line, can be translated into cases of ATC in patients. This could be achieved by isolating RNA from ATC patient samples and completing qRT-PCR using

TaqMan assays for PBF and hsa-miR-122-5p, with a negative correlation expected between these in thyroid tumour samples compared to in normal thyroid samples. In addition, it would be interesting to observe there correlation between PBF and hsa-miR-122-5p in MTC, FTC and PTC.

4.2. hsa-miR-124-3p and hsa-miR-506-3p Decreased PBF mRNA Expression and Protein Levels

The largest average decrease in PBF mRNA expression following transfection with a microRNA mimic was observed following hsa-miR-506-3p transfection in SW1736 cells. hsa-miR-506-3p transfection caused a decrease in PBF mRNA expression relative to the negative control of 35.54% in SW1736 cells (Figure 10), although it is important to note this was non-significant. In addition, the PBF protein levels at 25kDa in SW1736 cells were also decreased, by 33.66±38.85% (non-significant) (Figure 17B) strengthening the likelihood of hsa-miR-506-3p targeting PBF directly.

As hsa-miR-506-3p shared a sequence similarity with hsa-miR-124-3p, resulting in binding at the same site on the 3' UTR of PBF (Dweep, H., et al., 2011), it was interesting to observe that despite hsa-miR-124-5p not having as great an effect as hsa-miR-506-3p on PBF, it still caused an average decrease in PBF mRNA expression levels of 20.25% in SW1736 cells (non-significant) (Figure 10 and an average decrease in PBF protein levels of 26.21±25.48% (non-significant) at 25kDa in SW1736 cells (Figure 17B). However, due to there not being enough data within this investigation to observe whether a similar effect takes place in MCF7 cells with hsa-miR-124-3p and hsa-miR-506-3p, as well as data not being significant for SW1736 cells, it would be essential to repeat these studies in both cell lines to identify

whether these microRNAs can negatively regulate PBF at both the mRNA expression and protein level.

If hsa-miR-124-3p and hsa-miR-506-3p were confirmed to cause a decrease in PBF mRNA expression and protein levels this would be an interesting observation as despite the prediction of these microRNAs binding to the 3' UTR of PBF (Dweep, H., et al., 2011) there is currently no previous evidence of these microRNAs altering PBF mRNA expression or protein levels. In addition, as both hsa-miR-124-3p and hsa-miR-506-3p are conserved microRNAs with a conserved binding site on PBF (Friedman, R.C., et al., 2009) (Figure 5A) this is suggestive of a potential important role in regulating the genome and as a result deregulation of these microRNAs may result in PBF overexpression, which may lead to the initiation of thyroid tumourigenesis. Previously, miR-124 has been shown to have a role as a tumour suppressor in bladder cancer by modulating the proliferation and aggressiveness of tumours (Xu X., et al., 2013) and hsa-miR-506 has been defined as a 'master suppressor of EMT in breast cancer' (Arora, H., et al., 2013), which is interesting due to the previous observations of PBF playing roles in both proliferation and invasion (Read, M.L., et al., 2011, Watkins, R.J., et al., 2010).

4.3. Limitations

The first limitation in this investigation was with respect to the initial stage in identifying microRNAs that target PBF. Due to both cost and time restrictions only five microRNAs were selected, which was only a handful of the potential microRNAs predicted to target PBF. Furthermore, due to the prediction software used being known to identify false positives, for example TargetScan has been described to identify false positives at a rate of 22-31% (Bentwich, I., 2005), there was potential for selected microRNAs to not actually target PBF.

Therefore, in the future it would be more useful to transfect a range of thyroid carcinoma cell lines with a large library of microRNA mimics, validate results by microarray and then select a larger group of microRNAs for qRT-PCR and Western blot analysis, as done in this investigation, to confirm whether they alter PBF mRNA expression and protein levels.

Another limitation within this investigation, as a result of time restrictions, was the conditions used within this investigation, which were based upon previous observations in the McCabe lab and were not optimised. Therefore, if this investigation was repeated, it would be essential to optimise the time points for RNA isolation and more importantly protein harvest, as the exact half-life of PBF remains unknown. In addition, as the endogenous concentration of microRNAs was not quantified in either the SW1736 or MCF7 cells this may have resulted in a skew in results due to total microRNA concentration following transfection being different not only between microRNAs but also cell lines. Therefore, in a future investigation, qRT-PCR could be used to determine endogenous expression of selected microRNAs and then the concentrations of microRNA mimics required for transfection could be optimised and then normalised with respect to this, allowing a fair comparison to be made between individual microRNAs in each cell line.

Potentially as a result of conditions not being optimised, there were some surprising inconsistencies observed between PBF mRNA expression and protein levels. For example, following the use of anti-PBF siRNA, which is designed to target PBF, there was an average decrease in PBF mRNA expression of 68.16% ($p>0.05$) in SW1736 cells (Figure 10) within the range expected from a siRNA. However, no significant decrease in PBF protein levels at either 25kDa or 30kDa were observed in SW1736 cells (Figure 19). This was unexpected as lowered mRNA levels account for >84% of the decreased protein production (Guo, H. et al., 2010), which is not in line with what was observed in this investigation. Beyond optimising

conditions, another factor to consider is the PBF antibody used; as it is potentially unreliable, indicating Western blotting may not have been a good representation of the effect of microRNAs on PBF protein levels. In a future investigation it may be beneficial to either use a commercial antibody for Western blotting, for example PBF Antibody (E-8): sc-376960 (Santa Cruz Biotechnology), which binds to the PBF C-terminus identifying PBF at between 23kDa and 34kDa. Alternatively, another option in the future, which may solve the inconsistencies between mRNA and protein as well as issues with the antibody, would be via use of the novel QuantiGene FlowRNA *in situ* hybridisation assay (Affymetrix). Despite currently having no probe sets available for PBF, this assay has the benefit of being able to compare the kinetics of RNA expression and protein levels within a single cell and has been described to be useful for measuring target expression levels when antibodies are inadequate.

4.4. Future Research

Once conditions were optimised and if hsa-miR-122-5p, hsa-miR-124-3p and hsa-miR-506-3p were each confirmed to target PBF, it would then be useful to complete functional assays to determine the impact at the cellular level following microRNA mimic transfections of these microRNAs in a range of thyroid carcinoma cell lines. It would be interesting to investigate proliferation and invasion, using a MTT proliferation assay and invasion assay respectively, as not only are these factors characteristic of cancer, but PBF has also been shown to induce both proliferation (Read, M.L., et al., 2011) and invasion (Watkins, R.J., et al., 2010). However, as mentioned previously, due to the range of mRNA targets that each microRNA has it would be important to bear in mind that any functional effects observed may not necessarily be due to the effect of microRNAs on PBF.

Following this, it would then be essential to observe whether there is a correlation between hsa-miR-122-5p, hsa-miR-124-3p or hsa-miR-506-3p and PBF in thyroid cancer patient samples using qRT-PCR, in a method similar to that described in 4.1. If microRNAs were identified to be downregulated in thyroid tumours resulting in a subsequent increase in PBF, it would be interesting to determine how the microRNAs are downregulated. One suggestion could be based on epigenetics, whereby DNA methylation causes a silencing of the genes that microRNAs are transcribed from. This phenomenon has been observed previously with respect to miR-124 gene promoters in an aggressive breast cancer cell line, where hypermethylation resulted in the decreased expression of miR-124 (Lv, X.B., et al., 2011). However, this was shown to be partially reversed by a DNA demethylating agent (Lv, X.B., et al., 2011) highlighting potential clinical relevance in restoring microRNA deregulation.

Alternatively, due to previous studies suggesting that a re-introduction of specific microRNAs underexpressed in cancer cells may benefit in reversing tumourigenesis (Trang, P., et al., 2009), another avenue of potential clinical relevance that could be investigated is the re-introduction of hsa-miR-122-5p, hsa-miR-124-3p or hsa-miR-506-3p into a system. It could then be observed whether PBF overexpression is decreased and consequently, whether there is a benefit in thyroid cancer prognosis. To assess this, an already established murine model could be used, whereby nude mice are injected with NIH-3T3 cells stably expressing PBF, which causes the subsequent growth of aggressive tumours (Stratford, A.L., et al., 2005). Following this, administration of hsa-miR-122-5p, hsa-miR-124-3p or hsa-miR-506-3p mimics respectively to the nude mice would allow determination of whether there is an improvement within these mice compared to those treated with a negative control. In addition, further investigations could be completed by isolating RNA from normal and cancerous tissue and completing qRT-PCR to determine whether there is also a reduction in PBF upon

microRNA administration. If these *in vivo* studies did show a decrease in PBF and a subsequent phenotypic benefit, the application to humans could be extended.

4.5. Conclusion

Results indicated hsa-miR-122-5p decreased PBF protein significantly at 25kDa in SW1736 cells although; this decrease was not reflected in PBF mRNA expression. Furthermore, hsa-miR-124-3p and hsa-miR-506-3p decreased PBF mRNA expression as well as PBF protein levels at 25kDa in SW1736 cells, albeit non-significantly. Due to limitations within this investigation, these preliminary findings of hsa-miR-122-5p, hsa-miR-124-3p and hsa-miR-506-3p targeting PBF would need to be confirmed by optimising conditions and repeating these experiments.

If these microRNAs were confirmed to target PBF, it would suggest a mechanism of PBF regulation whereby upon specific microRNA deregulation an overexpression of PBF is caused, resulting in thyroid tumourigenesis. Due to the emerging importance of microRNAs as biomarkers and therapeutics the identification of specific microRNAs that play a role in thyroid tumourigenesis may be clinically relevant.

5. REFERENCES

Abraham, D., et al., 2011. MicroRNA Profiling of Sporadic and Hereditary Medullary Thyroid Cancer Identifies Predictors of Nodal Metastasis, Prognosis and Potential Therapeutic Targets. Clinical Cancer Research, 17, pp.4772-4781.

Arora, H., et al., 2013. MiR-506 Regulates Epithelial Mesenchymal Transition in Breast Cancer Cell Lines. PLoS ONE, 8, pp.1-7.

Bentwich, I., 2005.Prediction and Validation of MicroRNAs and their Targets. RNAi: Mechanisms, Biology and Applications, 579, pp.5904-5910.

Bhaijee, F. and Nikiforov, Y.E., 2011. Molecular Analysis of Thyroid Tumors. Endocrine Pathology, 22, pp.126-133.

Boelaert, K., et al., 2007. PTTG and PBF Represses the Human Sodium Iodide Symporter. Oncogene, 26, pp.4344-4356.

Cai, X., et al., 2004. Human MicroRNAs are Processed from Capped, Polyadenylated Transcripts That Can Also Function as mRNAs. RNA, 10, pp.1957-1966.

Cannell, I.G., et al., 2008. How do microRNAs Regulate Gene Expression. Biochemical Society Transactions, 36, pp.1224-1231.

Carther, R.W., 2006. Gene Regulation by MicroRNAs. Current Opinion in Genetics and Development, 16, pp.203-208.

Chien, W. and Pei, L., 2000. A Novel Binding Factor Facilitates Nuclear Translocation and Transcriptional Activation Function of the Pituitary Tumor-transforming Gene Product. The Journal of Biological Chemistry, 275, pp.19422-19427.

Dvořáková, S., et al., 2014. Hereditary Thyroid Carcinoma and its Molecular Diagnostics. Cesk Patol, 50, pp.81-86.

Dweep, H., et al., 2011. MiRWalk – Database: Prediction of Possible miRNA Binding Sites by 'Walking' the Genes of Three Genomes. Journal of Biomedical Informatics, 44, pp.839-47. (MiRWalk website: http://www.umm.uni-heidelberg.de/apps/zmf/mirwalk/genetarget.html accessed on 30/10/13).

Friedman, R.C., et al., 2009. Most Mammalian mRNAs Are Conserved Targets of MicroRNAs. Genome Research, 19, pp.92-105. (TargetScan website: http://www.targetscan.org/ accessed on 30/10/13).

Guo, H., 2010. Mammalian MicroRNAs Predominantly Act to Decrease Target mRNA Levels. Nature, 466, pp.835-841.

Hsu, S.D., et al., 2010. MiRTarBase: a Database Curates Experimentally Validated MicroRNA–Target Interactions. Nucleic Acids Research, pp.1-7. (MiRTarBase website: http://mirtarbase.mbc.nctu.edu.tw/ accessed on 30/10/13).

Hsueh, C., et al., 2013. Prognostic Significance of Pituitary Tumor-Transforming Gene-Binding Factor (PBF) Expression in Papillary Thyroid Carcinoma, Clinical Endocrinology, 78, pp.303-309.

Jacques, C., et al., 2013. DNA Microarray and miRNA Analyses Reinforce the Classification of Follicular Thyroid Tumours. The Journal of Clinical Endocrinology & Metabolism, 98, pp.E981-E989.

Kawamata, T., et al., 2011. Multilayer Checkpoints for MicroRNA Authenticity During RISC Assembly. EMBO, 12, pp.944-949.

Lee, Y., et al., 2004. MicroRNA Genes are Transcribed by RNA Polymerase II. EMBO, 23, pp.4051-4060.

Leivonen, S-K., et al., 2011. Identification of miR-193b Targets in Breast Cancer Cells and Systems Biological Analysis of Their Functional Impact. Molecular and Cellular Proteomics, 10, pp.1-9.

Leone, V., et al., 2011. MiR-1 is a Tumour Suppressor in Thyroid Carcinogenesis Targeting CCND2, CXCR4, and SDF-1α. The Journal of Clinical Endocrinology & Metabolism, 96, pp.E1388-E1389.

Leonardi, G.C., et al., 2012. MicroRNAs and Thyroid Cancer: Biological and Clinical Significance (Review). International Journal of Molecular Medicine, 30, pp.991-999.

Li, C., et al., 2012. Hepatitis B Virus mRNA-Mediated miR-122 Inhibition Upregulates PTTG1-Binding Protein, Which Promotes Hepatocellular Carcinoma Tumour Growth and Cell Invasion. Journal of Virology, 87, pp.2193-2205.

Lim, S.M., et al., 2012. Treatment Outcome of Patients with Anaplastic Thyroid Cancer: A Single Center Experience. Yonsei Medical Journal, 53, pp.352-357.

Liu, J., et al., 2005. MicroRNA-Dependent Localisation of Targeted mRNAs to Mammalian P-bodies. Nature Cell Biology, 7, pp.719-723.

Lv, X.B., et al., 2011. MiR-124 Supresses Multiple Steps of Breast Cancer Metastasis by Targeting a Cohort of Pro-Metastatic Genes In Vitro. Chinese Journal of Cancer, 30, pp.821-830.

MacFarlane, L.A. and Murphy, P.R., 2010. MicroRNA: Biogenesis, Function and Role in Cancer. Current Genomics, 11, pp.537-561.

Mazzaferri, E.L. and Kloos, R.T., 2001. Current Approaches to Primary Therapy for Papillary and Follicular Thyroid Cancer. The Journal of Clinical Endocrinology & Metabolism, 86, pp.1447-1463.

Nikiforova, M.N., et al., 2009. MicroRNA Expression Profiles in Thyroid Tumors. Endocrine Pathology, 20, pp.85-91.

Read, M.L., et al., 2011. Proto-Oncogene PBF/PTTG1IP Regulates Thyroid Cell Growth and Represses Radioiodide Treatment. Cancer Research, 71, pp.6153-6164.

Read, M.L., et al., 2014. The PTTG1-Binding Factor (PBF/PTTG1IP) Regulates p53 Activity in Thyroid Cells. Endocrinology, 155, pp.1222-1234.

Ricci, E.P., et al., 2011. Activation of a MicroRNA Response in trans Reveals a New Role for Poly(A) in Translational Repression. Nucleic Acids Research, 39, pp.5215-5231.

Sharma, N., et al., 2012. PBF Interacts with Cortactin and Thyroglobulin in Thyroid Cells. Endocrine Abstracts, 28, p.338.

Smith V. and McCabe C., 2008. PTTG1IP (Pituitary Tumor-Transforming 1 Interacting Protein). Atlas of Genetics and Cytogenetics in Oncology and Haematology. (Webpage: http://AtlasGeneticsOncology.org/Genes/PTTG1IPID41944ch21q22.html Accessed on 27/12/13).

Smith, V.E., et al., 2011. Expression and Function of the Novel Proto-Oncogene PBF in Thyroid Cancer: A New Target for Augmenting Radioiodine Uptake. Journal of Endocrinology, 210, pp.157-163.

Smith, V.E., et al., 2013. Manipulation of PBF/PTTG1IP Phosphorylation Status; a Potential New Therapeutic Strategy for Improving Radioiodine Uptake in Thyroid and Other Tumors. The Journal of Clinical Endocrinology & Metabolism, 98, pp.2876-2886.

Stratford, A.L., et al., 2005. Pituitary Tumor Transforming Gene Binding Factor: A Novel Transforming Gene in Thyroid Tumorigenesis. The Journal of Clinical Endocrinology & Metabolism, 90, pp.4341–4349.

Trang, P., et al., 2009. MicroRNAs as Potential Cancer Therapeutics. Oncogene, 27, pp.S52-S57.

Tuttle, R.M., 2013. Differentiated Thyroid Cancer: Overview of Management. UpToDate. (Webpage: http://www.uptodate.com/contents/differentiated-thyroid-cancer-overview-of-management#H4610264 Accessed on 07/05/14).

Visone, R., et al., 2007. Specific MicroRNAs are Downregulated in Human Thyroid Anaplastic Carcinomas. Oncogene, 26, pp.7590-7595.

Vriens, M.R., et al., 2012. MicroRNA Expression Profiling is a Potential Diagnostic Tool for Thyroid Cancer. Cancer, 118, pp.3426-32.

Wang, B., et al., 2012. MiR-122 Inhibits Cell Proliferation and Tumourigenesis of Breast Cancer by Targeting IGF1R. PLoS ONE, 7, pp.1-9.

Wang, X., 2008. MiRDB: a MicroRNA Target Prediction and Functional Annotation Database with a Wiki Interface. RNA, 14, pp. 1012-1017. (MiRDB website: http://mirdb.org/miRDB/ accessed on 25/10/13).

Wang, X. and El Naga, I.M., 2008. Prediction of Both Conserved and Non-Conserved microRNA targets in Animals. Bioinformatics, 24, pp.325-332. (MiRDB website: http://mirdb.org/miRDB/ accessed on 25/10/13).

Watkins, R.J., et al., 2010. Pituitary Tumor Transforming Gene Binding Factor: A New Gene in Breast Cancer. Cancer Research, 70, pp.3739-3749.

Xu, X., et al., 2013. Micro-RNA-124-3p Inhibits Cell Migration and Invasion in Bladder Cancer Cells by Targeting ROCK1. Journal of Translational Medicine, 11.

Yi, R., et al., 2003. Exportin-5 Mediates the Nuclear Export of Pre-MicroRNAs and Short Hairpin RNAs. Genes & Development, 17, pp.3011-3016.

Yoshimoto, N., et al., 2011. Distinct Expressions of microRNAs that Directly Target Estrogen Receptor α in Human Breast Cancer. Breast Cancer Research and Treatment, 130, pp.331-339.

http://www.cancerresearchuk.org/cancer-help/type/thyroid-cancer/about/thyroid-cancer-risks-and-causes Accessed on 06/12/13.

6. APPENDIX

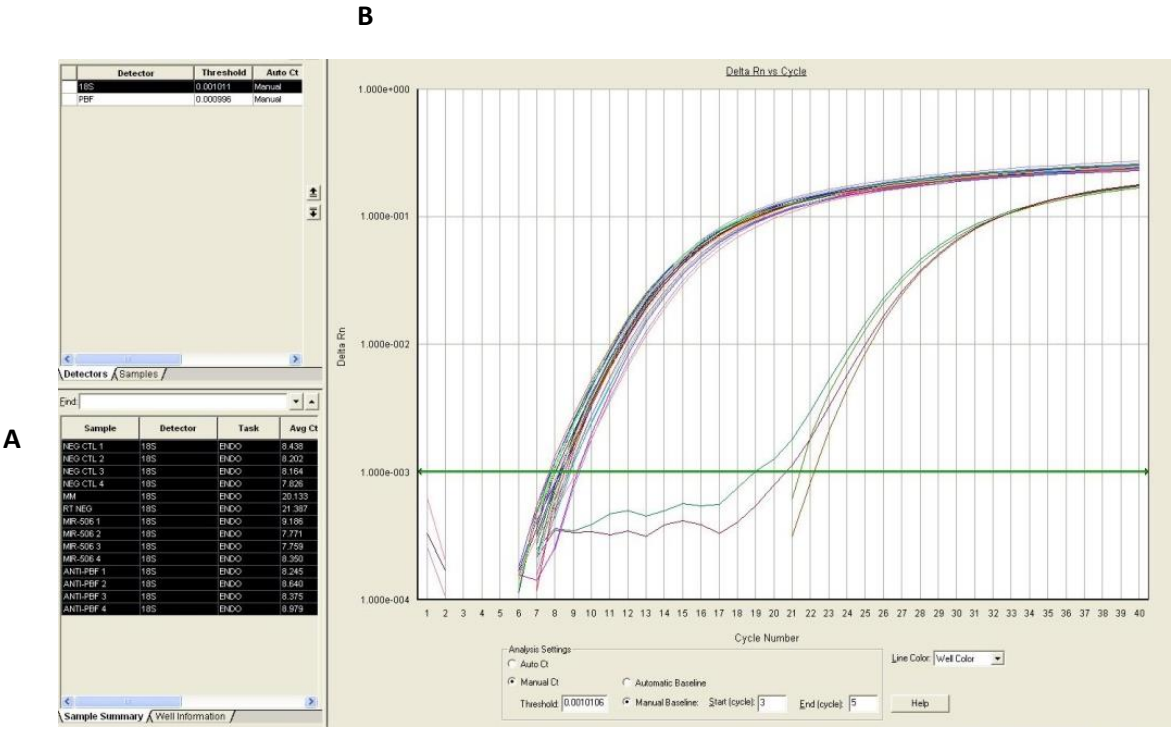

Supplementary figure 1: 18s example plot from 7500 system software

A) Raw data from 7500 system software indicating cDNA and RT negative mastermix controls were at higher average CT values compared to data from samples containing cDNA and RT positive mastermix.

B) Plots for 18s for samples containing cDNA and RT positive mastermix can be seen close together with cDNA and RT negative mastermix control plots at a higher cycle number. The threshold bar can be seen at 1.000e-003 Delta Rn.

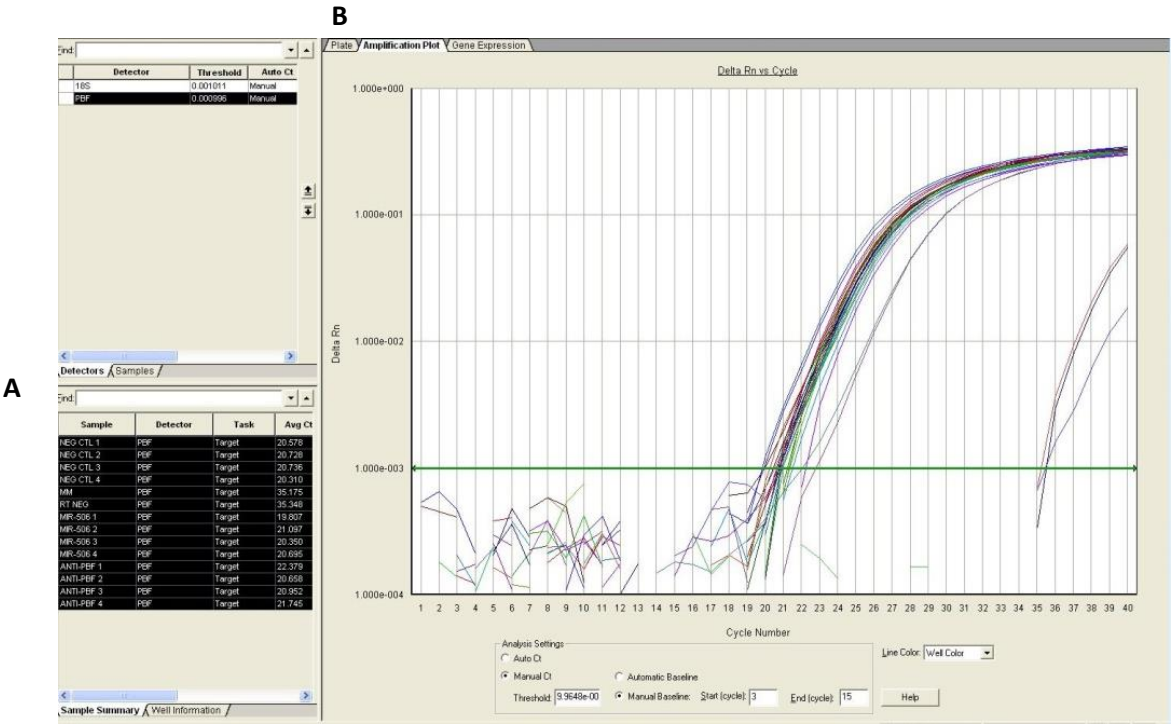

Supplementary figure 2: PBF example plot from 7500 system software

A) Raw data from 7500 system software indicating cDNA and RT negative mastermix controls were at higher average CT values compared to data from samples containing cDNA and RT positive mastermix.

B) Plots for PBF for samples containing cDNA and RT positive mastermix can be seen close together with cDNA and RT negative mastermix control plots at a higher cycle number. The threshold bar can be seen at 1.000e-003 Delta Rn.

RECOGNITION OF PREVIOUSLY UNDESCRIBED RING DOMAIN RESIDUES REQUIRED FOR BRCA1:BARD1 AND RING1B:BMI1 UBIQUITIN LIGASE ACTIVITY

by

ALICE FLETCHER

This project is submitted in partial fulfilment of the requirements for the award of the MRes Biomedical Research 2013/2014.

ABSTRACT

BRCA1:BARD1 and RING1B:BMI1 are type I RING-type E3 ubiquitin ligases required within the final stage of the ubiquitin pathway. Although much is understood about the way RING-type E3 ubiquitin ligases function, the mechanism of E2-ubiquitin binding and locking remains elusive in type I RING-type E3 ubiquitin ligases despite being defined in type II RING-type E3 ubiquitin ligases.

The aim of this investigation was to determine whether a residue conserved throughout type I RING-type E3 ubiquitin ligases was required for the ubiquitin ligase activity of BRCA1:BARD1 and RING1B:BMI1 and if so, whether this is due to a role of the residue in binding and locking of ubiquitin within an E2:ubiquitin conjugate. This was achieved by mutagenesis of the selected residues followed by purification of proteins, which were used in ubiquitin ligase assays.

Results indicated a requirement of the conserved residue in BRCA1:BARD1 and RING1B:BMI1 ubiquitin ligase activity, with further investigations into RING1B:BMI1 ubiquitin sensitivity indicating the importance of a number of residues on ubiquitin's surface for ubiquitin ligase activity. Modelling highlighted residues of interest in RING1B:BMI1 and ubiquitin have the potential to interact via E2-ubiquitin binding and locking however, a more stringent investigation needs to be completed to confirm findings.

ACKNOWLEDGEMENTS

Having had a very insightful and enjoyable experience with the Morris group, I would firstly like to thank Dr Jo Morris for the opportunity to work on this project.

I would also like to thank Dr Ruth Densham for all her help and support throughout as well as all the other members of the Morris group; Dr Jo Strachan, Dr Alex Garvin, Dr Sarah Blair-Reid, James Beesley, Helen Stone, Manolo Daza, Kirsty Lawrence and Thea Konstantinou who not only helped me but created an enjoyable working environment.

CONTENTS

1. INTRODUCTION

1.1. The Ubiquitin Pathway

Protein ubiquitination is a conserved multi-step reaction mediated by three enzymes; E1, E2 and E3, resulting in the covalent attachment of ubiquitin onto a lysine on its relevant substrate within the ubiquitin pathway. This is required for cell-cycle regulation, DNA repair, cell growth and immune function (Nath, D. and Shadan, S., 2009). Protein ubiquitination is initiated by an E1 ubiquitin-activating enzyme requiring ATP to load ubiquitin, which is then transferred onto the active site of an E2-ubiquitin conjugating enzyme (Figure 1). The E2-ubiquitin conjugate is then bound by an E3 ubiquitin ligase, which functions by one of two general mechanisms dependent on the type of E3 ubiquitin ligase. RING-type E3 ubiquitin ligases mediate the transfer of ubiquitin directly from an E2-ubiquitin conjugate onto the substrate whereas HECT-type E3 ubiquitin ligases act as intermediates in substrate ubiquitination (Metzger, M.B., et al., 2014) (Figure 1).

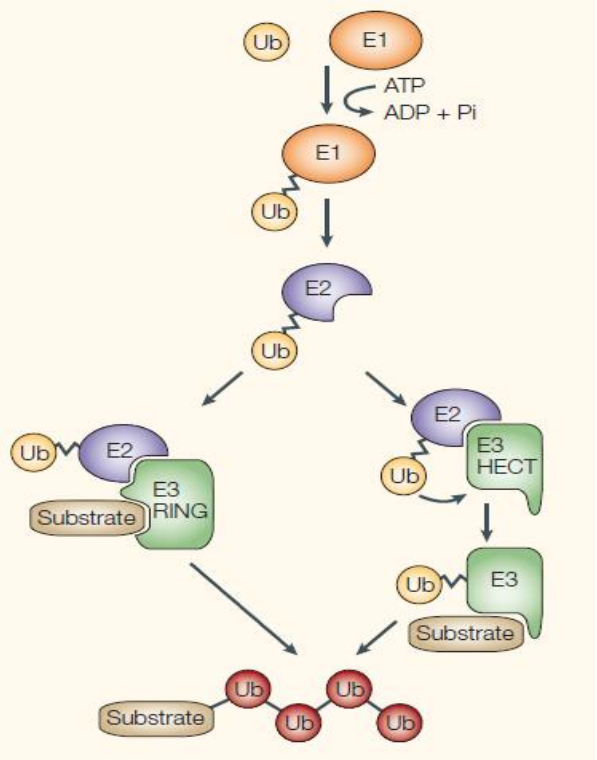

Figure 1: The ubiquitin pathway
The ubiquitin pathway initiated by the E1 ubiquitin-activating enzyme binding to ubiquitin, requiring ATP. This is followed by the transfer of ubiquitin onto the E2 ubiquitin-conjugating enzyme, which can then take one of two pathways. RING-type E3 ubiquitin ligases mediate the transfer of ubiquitin directly from the E2-ubiquitin complex onto the substrate whereas the HECT-type E3 ubiquitin ligases act as an intermediate before transferring the ubiquitin to its respective substrate. (Image from: Paolo Di Fiore, P., et al., 2003. When Ubiquitin Meets Ubiquitin Receptors: A Signalling Connection. Molecular Cell Biology, 4, pp.491-497).

1.2. RING-type E3 Ubiquitin Ligases

There have been over 600 E3 ubiquitin ligases identified in mammals - with most defined as RING-type E3 ubiquitin ligases (Dou, H., et al., 2013), which are found as monomers, dimers and multi-subunit complexes (Metzger, M.B., et al., 2012). Dimeric RING-type E3 ligases can be categorised as either type I or type II complexes with the main difference being the way the protomers interact. Type I RING-type dimers have flat dimerisation interfaces used to 'stick' the two protomers together as the α-helices that flank the central RING combine as a four-helix bundle (Brzovic, P.S., et al., 2001), whereas in type II RING-type dimers each protomer has an 'arm', which 'hugs' the other protomer to hold the dimer together (Figure 2).

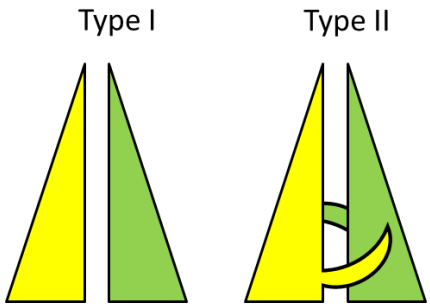

Figure 2: Type I vs. type II RING-type E3 ubiquitin ligases
Type I RING-type E3 ubiquitin ligases have flat dimerisation interfaces, which stick together due to the formation of a four helix bundle to form the functional dimer whereas type II RING-type E3 ubiquitin ligases have 'arms', which hug each other to hold the dimer together.

1.2.1. RING1B:BMI1

RING1B, also known as ring finger protein 2 (RNF2), is 334 residues long; with a 41 residue long N-terminal RING domain (Martínez-Gómez, A.I., et al., 2013) required for its heterodimerisation with B-cell-specific Moloney murine leukaemia virus integration site 1 (BMI1), to form a functional type I RING-type E3 ubiquitin ligase (Figure 3). This dimerisation is essential because the E3 ubiquitin ligase activity of RING1B is enhanced by BMI1 (Buchwald, G., et al., 2006), despite BMI1 not normally displaying any detectable ubiquitin ligase activity itself (Li, Z., et al., 2006).

As RING1B and BMI1 are both polycomb group proteins within the chromatin modulating complex - polycomb repressive complex 1 (PRC1) (Li, Z., et al., 2006) - they are required for histone H2A monoubiquitination and thus transcriptional repression, which is a critical component of the DNA damage response (Leung, J.W., et al., 2014). Consequently, loss of BMI1 results in an impaired repair of DNA double strand breaks by homologous recombination (Ginjala, V., et al., 2011).

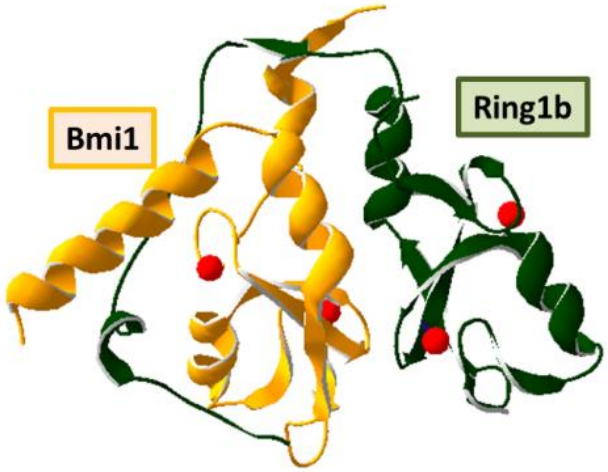

Figure 3: RING1B:BMI1 crystal structure
RING1B and BMI1 in green and orange respectively, with chelated zinc ions in red.
(RCSB Protein Data Bank ID (www.rcsb.org): 2H0D). Image created using SwissPdbViewer (Guex, N. and Peitsch, M.C., (1997)).

Normally BMI1 plays a role in cell cycle, cell immortalisation and senescence (Siddique, H.R. and Saleem, M., 2012) making it important for stem cell self-renewal, resulting in high BMI1 expression in primitive hematopoietic stem cells (HSC), which decreases upon HSC differentiation (Hosen, N., et al., 2007). However, BMI1 has also been observed to be upregulated in a variety of solid tumours, including; breast cancer (Martínez-Romero, C., et al., 2009). This may be due to BMI1 being noted as critical for invasive potential, proliferative capacity (of leukemic stem cells) and cancer stem cell renewal (in glioblastomas multiforme) (Proctor, E., et al., 2013). Furthermore, BMI1 overexpression has been observed to result in the induction of telomerase and thus immortalisaton (in mammary epithelial cells) (Dimri, G.P., et al., 2002).

Consequently, high levels of BMI1 correlate with a poor outcome in a number of human cancers (Guo, B.H., et al., 2011) and it has been described that the effects of BMI1 overexpression are due to BMI1 being a dose-dependent regulator of RING1B's target-specific E3 ubiquitin ligase activity (Buchwald, G., et al., 2006).

1.2.2. BRCA1:BARD1

Breast cancer susceptibility gene 1 (BRCA1) is a nuclear phosphoprotein of 1863 amino acids, which heterodimerises with BRCA1-associated RING domain protein 1 (BARD1) via its RING domain giving rise to an active type I RING-type E3 ubiquitin ligase (Figure 4A), in a manner structurally similar to RING1B:BMI1 heterodimerisation (Figure 4B). This structural similarity has been described to be representative of a general mode of interaction between RING domains (Buchwald, G., et al., 2003, Li, Z., et al., 2006).

BRCA1:BARD1 is described as an 'obligate heterodimer' with BARD1 increasing BRCA1's activity (Hashizume, R., et al 2001) as well as stabilising BRCA1 at sites of DNA damage (Simons, A.M., et al., 2006). BRCA1:BARD1 co-ordinates multiple pathways in response to DNA damage, including; DNA repair, mRNA transcription, cell cycle regulation and protein ubiquitination (Kennedy, R.D., et al., 2004). Out of these roles, the only biochemical activity related to BRCA1 is the E3 ubiquitin ligase activity required for protein ubiquitination, owing to BRCA1's RING domain (Christensen, D.E., et al., 2007).

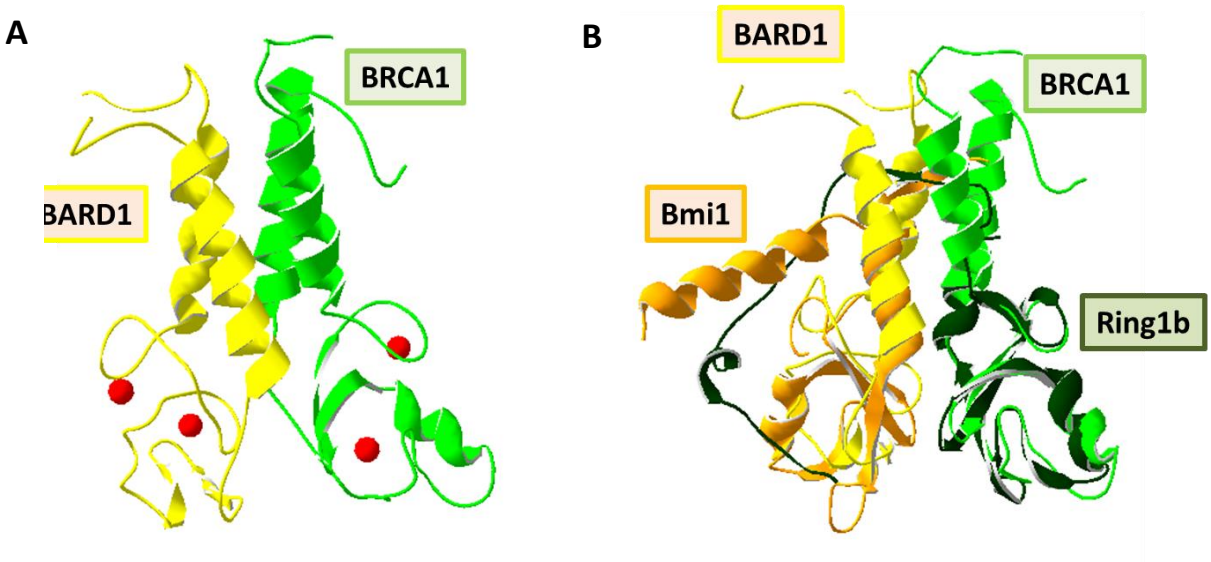

Figure 4: BRCA1:BARD1 crystal structure
A) BRCA1:BARD1 in green and yellow respectively, with chelated zinc ions in red.
(RCSB Protein Data Bank ID (www.rcsb.org): 1JM7).
B) Crystal structure of BRCA1:BARD1 (Figure 4A) and RING1B:BMI1 (Figure 3) aligned, highlighting structural similarity within the RING domains. Image created using SwissPdbViewer (Guex, N. and Peitsch, M.C., (1997)).

Mutations in BRCA1 have been found in families with breast and ovarian cancer (Castilla, L.H., et al., 1994) consequently, resulting in them being responsible for 40% of inherited breast cancers (http://www.genecards.org/cgi-bin/carddisp.pl?gene=BRCA1). Many of these cancer pre-disposing mutations have been identified within the RING domain of BRCA1, which have been shown to abolish the BRCA1:BARD1 ubiquitin ligase activity (Ruffner, H., et al., 2001). However, the exact role of the BRCA1 RING domain still remains unclear, with some debating whether it plays a role in cancer at all due to observations by Shakya, R. et al. of the BRCA1 I26A RING mutant reducing ubiquitin ligase activity but not presenting a cancerous phenotype *in vivo* (2014).

1.3. E2-ubiquitin Conjugate Binding and Locking in Type II RING-type E3 Ubiquitin Ligases

Previously, it has been identified that E2 binding and E3 activity is intrinsic to RING domains (Joazeiro, C.A.P., et al., 1999). However, it has also been described that the degree of E2 binding is not a direct measure of ubiquitin ligase activity (Lorick, K.L., et al., 1999), indicative of another factor being required. Recently, it has been shown that the ubiquitin moiety of an E2-ubiquitin conjugate must contact a RING domain for ubiquitin transfer to successfully take place (Nakatani, Y., et al., 2013) as well as an immobilisation of ubiquitin described to increase the rate of ubiquitin ligase activity (Berndsen, C.E. and Wolberger, C., 2014). Ubiquitin contacts are essential as ubiquitin is able to adopt a wide range of positions (Soss, S.E., et al., 2013) and must be locked into place via 'conformational selection' (Berndsen, C.E. and Wolberger, C., 2014) allowing access to the E2 active site for transfer and activation of the E2-ubiquitin conjugate thioester (Dou, H., et al., 2013).

Three structures of RING-type E3 ubiquitin ligases (Ring finger protein 4 (RNF4), ubiquitination factor E4B and baculoviral IAP repeat containing 7 (BIRC7)) in complex with E2-ubiquitin conjugates from the UbcH5 family have been described in a position ready for ubiquitin transfer (Metzger, M.B., et al., 2014). This has led to a mechanism being defined in RNF4, for preferential E2-ubiquitin conjugate binding and locking, whereby the E2 binds to one protomer and ubiquitin reaches across and binds to the other protomer (Plechanovová, A., et al., 2011). This mechanism is owing to the fact RNF4 is a type II RING-type E3 ubiquitin ligase and thus the protomers each have an 'arm', which does not only play a structural role but also a functional role in E2-ubiquitin binding and locking (Figure 5B). The E2 binds to one RNF4 protomer and the side chain of Y193 on the arm of the other protomer stacks with

the main chain E34 to G35 of ubiquitin, facilitating E2-ubiquitin conjugate binding and ubiquitin transfer (Figure 6). This highlights the importance of both RING domains and dimerisation in the RNF4 E3 ubiquitin ligase activity (Plechanovová, A., et al., 2012).

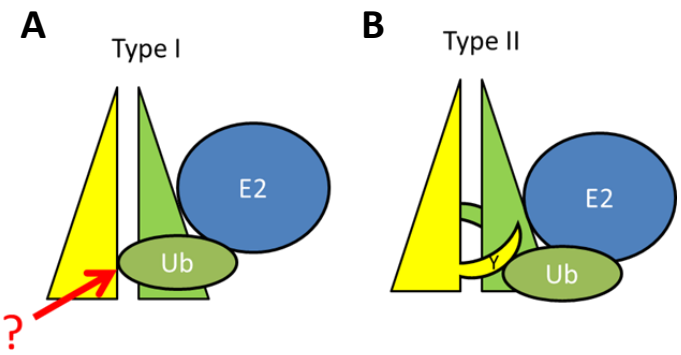

Figure 5: Type I vs. type II RING-type E3 ubiquitin ligases
A) Hypothesised mechanism of E2-ubiquitin conjugate binding by type I RING-type E3 ubiquitin ligases.
B) Type II RING-type ubiquitin ligases bind and lock an E2-ubiquitin conjugate via Y193 on the 'arm' of one of the protomers in the dimeric complex.

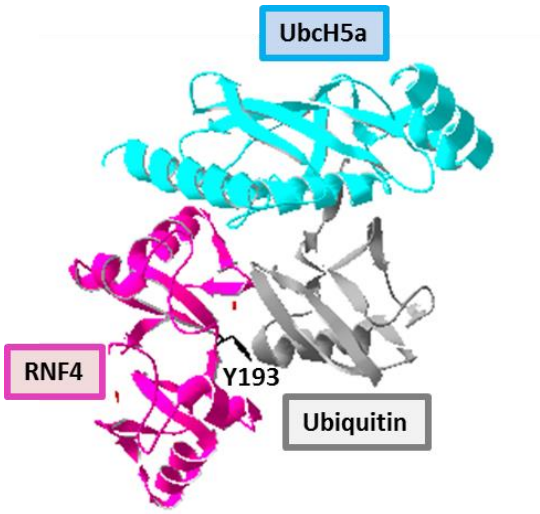

Figure 6: RNF4 and E2-ubiquitin conjugate crystal structure
Crystal structure of RNF4 homodimer in pink with the E2-ubiquitin conjugate in blue and grey respectively, highlighting how E2 binds to one partner and the ubiquitin reaches across to interact with the other partner. The Y193 residue (black) of RNF4 is highlighted as it is known to interact with ubiquitin (RCSB Protein Data Bank ID (www.rcsb.org): 4AP4). Image created using SwissPdbViewer (Guex, N. and Peitsch, M.C., (1997)).

1.4. E2-ubiquitin Conjugate Binding and Locking in Type I RING-type E3 Ubiquitin Ligases

Dou, H., et al. stated that there is an allosteric mechanism for ubiquitin transfer (2013) and consequently, Morris, J., et al. have proposed a mechanism for E2-ubiquitin binding and locking in type I RING-type E3 ubiquitin ligases that is parallel to that observed in RNF4, a type II RING-type E3 ubiquitin ligase. Recognition of this gap in knowledge contributes to

the aims and hypotheses formed within this investigation, whereby a conserved residue on one of the protomers in dimeric type I RING-type E3 ubiquitin ligases, with particular focus on BRCA1:BARD1 and RING1B:BMI1, has been hypothesised to bind and lock ubiquitin in an E2-ubiquitin conjugate for efficient ubiquitin ligase activity (Figure 5A).

Brzovic, P.S., et al. has mapped the E2 (UbcH5) binding site of BRCA1:BARD1 to be on the BRCA1 RING domain (Brzovic, P.S., et al., 2003) due to residues within the Zn^{2+} binding loops of BRCA1 creating a platform for E2 binding (Metzger, M.B., et al., 2014) and subsequently, Morris et al. used a yeast three-hybrid screen to identify residues on BARD1 predicted to be required within the hypothesised mechanism of binding and locking ubiquitin within an E2-ubiquitin conjugate (Unpublished). Following preliminary data, BARD1 R99 in BRCA1:BARD1 was highlighted as essential for BRCA1:BARD1 E3 ubiquitin ligase activity (Unpublished). BARD1 R99 is found at the base of the central helix and modelling has shown it to be externally facing (Figure 7) and thus independent of the dimer binding interface. Subsequently, Morris, J., et al. demonstrated BARD1 R99 was not required for BRCA1 or E2 binding (Unpublished) suggestive of another role in the ubiquitin pathway - potentially in the hypothesised mechanism of E2-ubiquitin conjugate binding and locking (Figure 8).

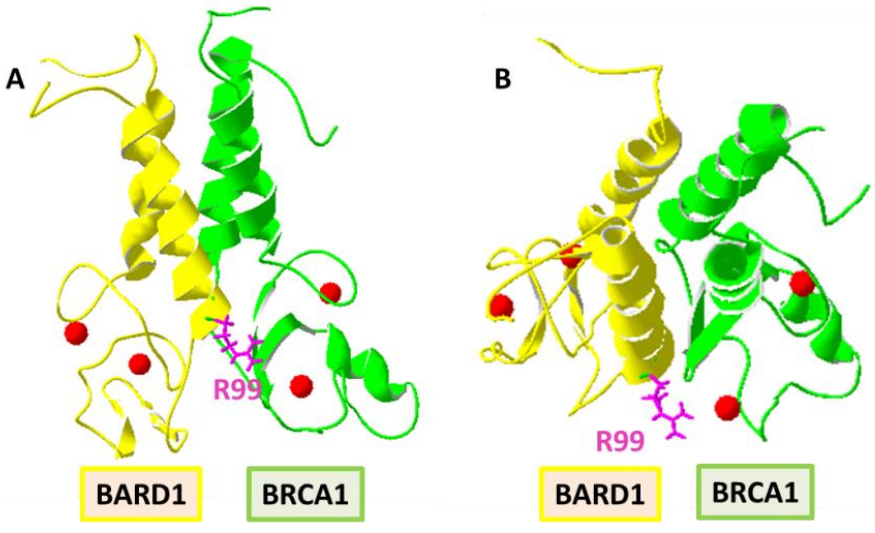

Figure 7: BRCA1:BARD1 R99
Side view **(A)** and top view **(B)** of BRCA1:BARD1 crystal structure in green and yellow respectively with the BARD1 R99 residue in pink, hypothesised to be involved in ubiquitin ligase activity (RCSB Protein Data Bank ID (www.rcsb.org): 1JM7). Image created using SwissPdbViewer (Guex, N. and Peitsch, M.C., (1997)).

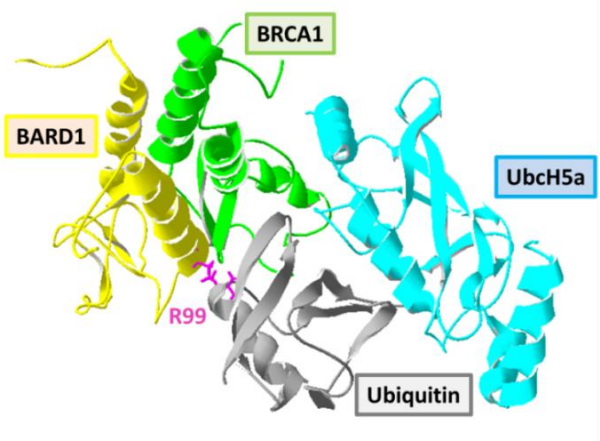

Figure 8: BRCA1:BARD1 modelled with E2-ubiquitin conjugate
BRCA1:BARD1 crystal structure in green and yellow respectively, with the residue of interest, R99, in pink modelled with the E2-ubiquitin conjugate in blue and grey respectively from the crystal structure of RNF4:E2-Ub conjugate (RCSB Protein Data Bank ID (www.rcsb.org): 1JM7 and 4AP4). Image created using SwissPdbViewer (Guex, N. and Peitsch, M.C., (1997)).

The residue of interest in BARD1 has been identified to be conserved across most other type I RING-type E3 ubiquitin ligases with the exception of BRCA1 and RING1B (Figure 9), highlighting the potential of this residue to be required in the ubiquitin ligase activity of all type I RING-type E3 ubiquitin ligases. As RING1B:BMI1 is the only other heterodimeric type I RING-type E3 ubiquitin ligase and in a structurally similar manner to BRCA1LBARD1 the E2-binding site is located on the RING1B RING domain (Bentley, M.L., et al., 2011, Buchwald, G., et al., 2006) it was predicted that the conserved residue of interest on BMI1 would be required for RING1B:BMI1 ubiquitin ligase activity, in a manner similar to BARD1 R99 in BRCA1:BARD1, as the functions of BRCA1:BARD1 have been described to be reminiscent of RING1B:BMI1 (Irminger-Finger, I. and Jefford, C.E., 2006).

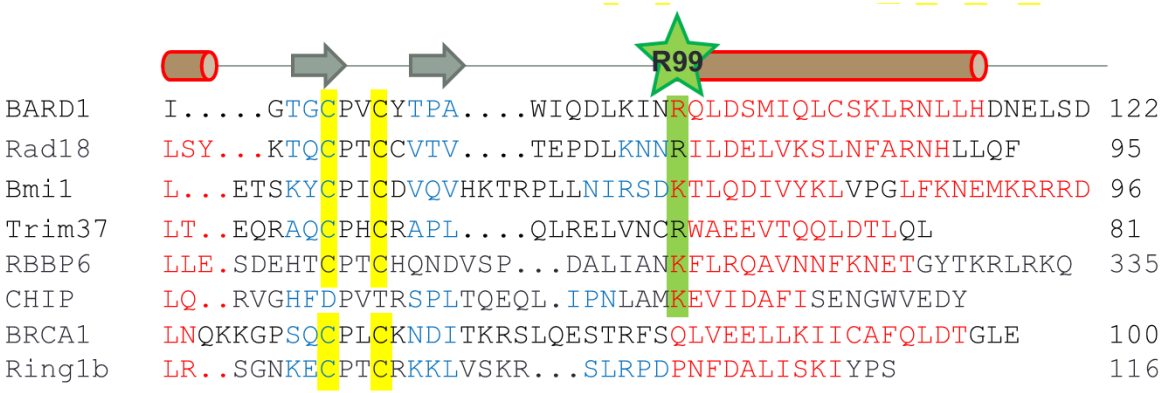

Figure 9: Conservation of residue of interest throughout type I RING-type E3 ubiquitin ligases
The residue hypothesised to play a role in E2-ubiquitin conjugate binding and locking in the type I RING-type E3 ubiquitin ligases can be seen conserved throughout this family suggestive of an important functional role. (Image from: Ruth Densham, Morris lab).

The conserved residue of interest in RING1B:BMI1 is BMI1 K73 (Figure 9), which like BARD1 R99 is found at the base of the central helix and is externally facing (Figure 10), which fits with its hypothesised role in the binding and locking of an E2-ubiquitin conjugate (Figure 11). In RING1B:BMI1 the interaction between an E2-ubiquitin conjugate and the nucleosomal substrate places the activated ubiquitin within a few angstroms of histone H2A (Bentley, M.L., et al., 2011), highlighting the importance of ubiquitin positioning for RING1B:BMI1 ubiquitin ligase activity.

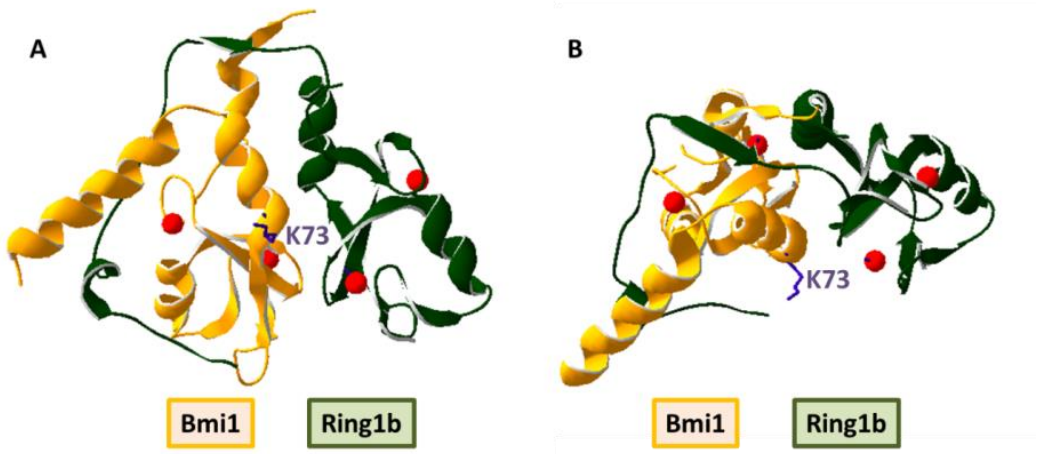

Figure 10: RING1B:BMI1 K73
Side view **(A)** and top view **(B)** of RING1B:BMI1 crystal structure in green and orange respectively with the BMI1 K73 residue in purple, hypothesised to be involved in ubiquitin ligase activity (RCSB Protein Data Bank ID (www.rcsb.org): 2H0D). Image created using SwissPdbViewer (Guex, N. and Peitsch, M.C., (1997)).

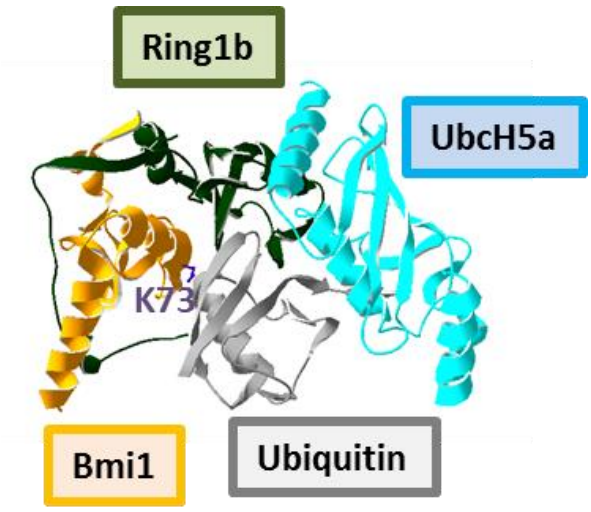

Figure 11: RING1B:BMI1 modelled with E2-ubiquitin conjugate
RING1B:BMI1 crystal structure in green and orange respectively, with the residue of interest, K73, in purple modelled with the E2-ubiquitin conjugate in blue and grey respectively from the crystal structure of RNF4:E2-Ub conjugate (RCSB Protein Data Bank ID (www.rcsb.org): 2H0D and 4AP4). Image created using SwissPdbViewer (Guex, N. and Peitsch, M.C., (1997)).

In line with the aforementioned hypothesis of E2-ubiquitin conjugate binding and locking, previous evidence has described that in BRCA1:BARD1 and RING1B:BMI1 one E3 RING binds the E2 and the other RING facilitates efficient ubiquitination of selective substrates (Woodsmith, J., et al., 2012). Subsequently, this means ubiquitin may fold back onto the E2 to form contacts with both RING protomers in BRCA1:BARD1 and RING1B:BMI1 respectively, in a similar mechanism to that observed by Plechanovová, A., et al. in RNF4 (2012). On the contrary, this hypothesis challenges the views of Metzger, M.B., et al. who have stated that in BRCA1:BARD1 and RING1B:BMI1 the second 'inactive' RING domain (e.g. BARD1 or BMI1) is not predicted to be involved in E2-ubiquitin binding and locking (2014).

1.5. Aims

The aims of this investigation were to determine whether BARD1 R99 and BMI1 K73 play a role in the E3 ubiquitin ligase activity of BRCA1:BARD1 and RING1B:BMI1 respectively, due to the hypothesised role of these residues in the binding and locking of ubiquitin in an E2-ubiquitin conjugate. To determine whether BARD1 R99 and BMI1 K73 play a role in the BRCA1:BARD1 and RING1B:BMI1 ubiquitin ligase activity respectively, BRCA1:BARD1 and RING1B:BMI1 WT and mutant (BARD1 R99E, BMI1 K73A and BMI1 K73E) proteins were purified alongside known E2-binding mutants (BRCA1 I26A (Brzovic, P.S., et al., 2003) and RING1B D56K (Bentley, M.L., et al., 2012)). Subsequently, ubiquitin ligase assays were carried out to assess the ubiquitin ligase activity of WT versus novel mutant proteins compared to known E2-binding mutants.

It was hypothesised that by mutating BARD1 R99 and BMI1 K73 in BRCA1:BARD1 and RING1B:BMI1 respectively, the ubiquitin ligase activity would subsequently be reduced or

abrogated. Further investigations may determine whether this is due to the hypothesised role of BARD1 and BMI1 in E2-ubiquitin conjugate binding, which may consequently aid determination of a common mechanism by which type I RING-type E3 ubiquitin ligases bind and lock an E2-ubiquitin conjugate.

2. MATERIALS & METHODS

2.1. BRCA1:BARD1 Ubiquitin Ligase Activity Analysis

	BRCA1:	**BARD1:**
WT	WT	WT
BRCA1 I26A	I26A Mutant	WT
BRCA1 C61G	C61G Mutant	WT
BARD1 R99E	WT	R99E Mutant

Table 1: BRCA1:BARD1 WT and mutant abbreviations

2.1.1. His-tagged Protein Preparations

WT and mutant His-BRCA1 (1-300):BARD1 (26-119) plasmids were obtained from the Morris lab. 1µl plasmid DNA for WT and mutant BRCA1:BARD1 (BRCA1 I26A, BRCA1 C61G and BARD1 R99E) was added to 6µl BL21-DE3 competent cells (Bioline) respectively and left on ice for 30 minutes, heat shocked at 42^{o}C for 45 seconds, then 200µl LB broth was added to each and incubated at 37^{o}C for 1 hour. Mixtures were spread on LB agar plates containing ampicillin (0.1mg/ml) and incubated for 16 hours at 37 ^{o}C.

Following this a colony from each plate was picked and grown in 5ml LB broth containing ampicillin (0.1mg/ml) at 37^{o}C and 200rpm for 16 hours. The next day each culture was added to 500ml LB broth containing ampicillin (0.1mg/ml), before being induced with 0.2mM IPTG and grown for 16 hours at 25^{o}C and 200rpm.

The following day bacteria were centrifuged at 3,000rpm, supernatant removed and 2ml lysis buffer (50mM sodium phosphate pH7, 300mM NaCl, 5% glycerol and 10mM β-mercaptoethanol) + 1 protease inhibitor cOmplete ULTRA tablet (Roche)/50ml lysis buffer)

was added to each pellet and incubated for 20 minutes. Lysates were sonicated by pulsing on ice for 3 x 30 seconds at 20% intensity with the Microson Ultrasonic Cell Disrupter, centrifuged at 4^{o}C at 3,700 rpm for 20 minutes, then supernatant was made to 10ml with lysis buffer. 500µl Nickel beads (Sigma) were added and incubated with rotation at 4^{o}C for 24 hours.

Beads were washed with wash buffer (50mM sodium phosphate pH7, 300mM NaCl, 5% glycerol, 10mM β-mercaptoethanol and 50mM imidazole) and proteins were eluted with 400µl ice cold lysis buffer + 300mM imidazole on ice for 20 minutes. Dialysis was carried out overnight at 4^{o}C in dialysis buffer (25mM Tris-HCl pH7.5, 10% glycerol, 2mM DTT and 150mM KCl) to remove the imidazole.

2.1.2. Determining Protein Concentrations

Antibody	Company	Dilution
Mouse anti-BRCA1 MS110	Abcam	1:1,000 (In 5% non-fat milk)
Mouse anti-ubiquitin P4D1	Santa Cruz	1:1,000 (In 5% BSA)
Rabbit anti-mouse	Dako	1:20,000 (In 5% non-fat milk)

Table 2: Antibodies for BRCA1:BARD1 ubiquitin ligase activity analysis
All antibodies used within this part of the investigation listed at the dilution used and the company antibodies were purchased from.

A range of protein volumes for WT and mutant BRCA1:BARD1 preparations were each made to a total volume of 10µl with dH_2O and resolved on a 12% SDS-polyacrylamide gel. Proteins were transferred onto PVDF membrane (Immobilon) and probed with a mouse anti-BRCA1 antibody at room temperature for 1 hour, washed in PBST and probed with rabbit-anti-mouse antibody at room temperature for 1 hour. Membranes were incubated with homemade ECL reagent (10ml 0.1M Tris pH8.5, 50µl luminol, 22µl coumaric acid and 6µl

hydrogen peroxide) placed into a light-excluding cassette and exposed to x-ray film, which was developed by the Xograph Compact X4 film processor.

2.1.3. In vitro Ubiquitin Ligase Assay

WT and mutant BRCA1:BARD1 concentrations were normalised from the Western blot and 10µl of each was made in duplicate along with an E3 negative control of 10µl dH_2O for the ubiquitin ligase assay. Ubiquitin ligase activity was measured by ubiquitin chain formation. Reactions were carried out by adding 10µl ubiquitin mix (1µl ATP (100mM), 1µl E1 (1:8 dilution from 800µg/ml stock), 1µl UbcH5a (1:4 dilution from 1µg/ml), 0.5µl ubiquitin (1:10 dilution from 25mg/ml stock), 1µl 10x ubiquitin ligase buffer (0.5M Tris-HCl pH7.5, 50mM $MgCl_2$, 5m DTT) and 5.5µl dH_2O) or 10µl 1x ubiquitin ligase buffer to each 10µl WT and mutant BRCA1:BARD1 duplicates, and incubating at 37^{o}C and 400rpm for 30 minutes. Reactions were stopped with 10µl protein sample loading buffer.

2.1.4. Western Blotting

Two 10µl samples of each reaction mix were resolved on separate precast 4-20% tris-glycine gradient gels (Novex), then transferred onto PVDF membranes. One membrane was probed with a mouse anti-ubiquitin antibody and the other with a mouse anti-BRCA1 antibody – both at room temperature for 1 hour. Membranes were washed in PBST and probed with their respective secondary antibodies at room temperature for 1 hour, then developed using ECL, as described in 2.1.2.

2.2. RING1B:BMI1 Ubiquitin Ligase Activity Analysis

	RING1B:	**BMI1:**
WT	WT	WT
BMI1 K73A	WT	K73A Mutant
BMI1 K73E	WT	K73E Mutant
RING1B D56K	D56K Mutant	WT

Table 3: RING1B:BMI1 WT and mutant abbreviations

2.2.1. WT Plasmid Preparation

GST-RING1B (1-159):BMI1 (1-109) in a pGEX6P-3 vector was obtained from the Sixma lab, as described in Buchwald, G., et al., 2006. 1µl WT RING1B:BMI1plasmid DNA was added to 6µl α-select gold competent cells (Bioline) and the transformation protocol followed as in 2.1.1. The next day a colony was picked and grown in 5ml LB broth containing ampicillin (0.1mg/ml) at 37^{o}C and 200rpm overnight. The next day the 5ml culture was added to 500ml LB broth containing ampicillin (0.1mg/ml) and grown at 37^{o}C and 200rpm. 16 hours later, the culture was centrifuged at 3,000rpm for 10 minutes and using a NucleoBond Xtra Maxi kit (Machery-Nagel) high-copy number plasmid DNA was obtained, which was confirmed by DNA sequencing.

2.2.2. Mutant Plasmid Preparations

2.2.2.2. Site-directed Mutagenesis

Forward and reverse primers were designed for BMI1 K73A, BMI1 K73E and RING1B D56K in the RING1B:BMI1 plasmid (Table 2). Reaction mixtures for site-directed mutagenesis for each mutant contained: 1µl forward primer (10µM), 1µl reverse primer

(10µM), 5µl Pfu DNA Polymerase 10X Reaction Buffer (ProMega), 1µl polymerase Pfu (ProMega), 5µl dNTPs, 1µl template DNA (100ng) and 36µl nuclease free water. A control reaction was made the same, besides substituting primers for nuclease free water. Reaction mixtures underwent the following PCR programme: 98°C for 1 minute, 25 cycles of 98°C for 1 minute, 50°C for 30 seconds and 68°C for 20 minutes, then 1 cycle of 68°C for 20 minutes. Following this, 1µl DpnI was added to each reaction mixture for 3 hours at 37°C.

Primer	Forward Sequence	Reverse Sequence
BMI1 K73A	CTACTGAATATAAGGTCAGAT GCAACTCTCCAAGATATTG	CAATATCTTGGAGAGTTGCATCT GACCTTATATTCAGTAG
BMI1 K73E	CTACTGAATATAAGGTCAGATG AAACTCTCCAAGATATTG	CAATATCTTGGAGAGTTTCATCTG ACCTTATATTCAGTAG
RING1B D56K	GTGCCCAATTTGTTTGAAAATG TTGAAGAACACCATGAC	GTCATGGTGTTCTTCAACATTTTC AAACAAATTGGGCAC

Table 4: Primer design
RING1B:BMI1 primer designs for BMI1 K73A, BMI1 K73E and RING1B D56k mutants, with designed sites for mutagenesis highlighted in yellow.

1µl plasmid DNA for mutant RING1B:BMI1 (BMI1 K73A, BMI1 K73E and RING1B D56K RING1B:BMI1) was added to 6µl α-select gold competent cells respectively and the transformation protocol followed as in 2.1.1. The next day, a colony from each plate was picked and grown in 5ml LB broth containing ampicillin (0.1mg/ml) at 37°C and 200rpm overnight. The following day each culture was centrifuged at 1,300rpm and using the GeneJET Plasmid Mini-prep Kit (Thermo Scientific) plasmid DNA was obtained, which was confirmed by DNA sequencing.

2.2.3. GST-tagged Protein Preparations

1µl plasmid DNA for WT and mutant RING1B:BMI1 (BMI1 K73A, BMI1 K73E and RING1B D56K) was added to 6µl BL21 competent cells (Bioline) respectively and the transformation protocol followed, as in 2.1.1. The next day a colony from each plate was

picked and grown in 100ml LB broth containing ampicillin (0.1mg/ml) overnight at 37^{o}C and 200rpm. The following day each culture was added to 900ml LB broth containing ampicillin (0.1mg/ml) at 37^{o}C for 1 hour before being induced with 0.5mM IPTG and grown at 20^{o}C and 200rpm for 16 hours.

Bacteria were centrifuged at 3,000rpm, supernatant removed and 2ml buffer A (50mM Tris-HCl pH7.5, 100mM NaCl, 1µM $ZnCl_2$ and 2mM DTT) + 1 protease inhibitor cOmplete ULTRA tablet (Roche)/50ml buffer A + 40µl lysozyme (125mg/ml)/ml buffer A) was added to each pellet and incubated for 20 minutes. Lysates were sonicated by pulsing on ice for 6 x 30 seconds at 20% intensity with the Microson Ultrasonic Cell Disrupter, centrifuged at 4^{o}C at 3,700 rpm for 20 minutes, then supernatant was made to 10ml with buffer A. 500µl glutathione sepharose 4B beads (GE Healthcare) were added and incubated with rotation at 4^{o}C for 24 hours.

Beads were washed with buffer A and buffer B (50mM Tris-HCl pH7.5, 100mM NaCl, 1µM $ZnCl_2$, 2mM DTT, 50mM KCl, 10mM $MgCl_2$ and 2mM ATP), then each protein sample was eluted in 300µl elution buffer (50mM Tris-HCl pH7.5, 50mM glutathione) on ice for 30 minutes. Proteins were dialysed at 4^{o}C overnight in PreScission protease cleavage buffer (50mM Tris-HCl pH7, 150mM NaCl, 1mM EDTA and 1mM DTT) to remove the glutathione. Half of each sample was stored at -80^{o}C and to the other half of each sample, 1 unit of PreScission Protease (GE Healthcare) was added and incubated for 6 hours at 4^{o}C. 100µl glutathione sepharose 4B beads were incubated with each sample at 4^{o}C with rotation overnight before supernatants were collected and stored at -80^{o}C.

2.2.4. Confirmation of Protein Preparations

Antibody	Company	Dilution
Rabbit anti-BMI1 ab137416	Abcam	1:1,000 (In 5% non-fat milk)
Rabbit anti-GST	Sigma	1:500 (In 5% non-fat milk)
Mouse anti-ubiquitin P4D1	Santa Cruz	1:1,000 (In 5% BSA)
Mouse anti-ubiquityl-H2A	Millipore	1:1,000 (In 5% BSA)
Rabbit anti-mouse	Dako	1:20,000 (In 5% non-fat milk)
Swine anti-rabbit	Dako	1:20,000 (In 5% non-fat milk)

Table 5: Antibodies for RING1B:BMI1 ubiquitin ligase activity analysis
All antibodies used within this part of the investigation listed at the dilution used and the company antibodies were purchased from.

20µl protein samples for WT and mutant RING1B:BMI1 preparations were made in triplicate and resolved on three separate 12% SDS-polyacrylamide gels. One gel was placed in coomassie stain (0.12% Brilliant Blue R-250 (Sigma)) for 30 minutes then transferred into destain (10% methanol and 10% acetic glacial acid) and the other two were transferred onto PVDF membrane and probed with a rabbit anti-GST antibody or a rabbit anti-BMI1 antibody – both at room temperature for 1 hour, washed in PBST, then probed with a swine anti-rabbit antibody at room temperature for 1 hour and developed using ECL, as in 2.1.2.

2.2.5. In vitro Ubiquitin Ligase Assay

Ubiquitin ligase activity was measured by autoubiquitination or H2A monoubiquitination. For autoubiquitination, the ubiquitin ligase assay was completed as in 2.1.3. however, GST-tagged WT and mutant RING1B:BMI1 proteins were used, instead of BRCA1:BARD1

proteins, and 10x ubiquitin buffer was replaced with a RING1B:BMI1 10x ubiquitin ligase buffer (0.5M Tris-HCl pH 7.5, 1M NaCl, 10µM $ZnCl_2$ and 1mM DTT). In addition, conditions were changed so samples were incubated at 30^{o}C and 400rpm for 1 hour. For H2A monoubiquitination, the ubiquitin ligase assay was completed as in 2.1.3. however, untagged WT and mutant RING1B:BMI1 proteins were used, instead of BRCA1:BARD1 proteins, and 1µl dH_2O was replaced with 1µl nucleosomes (HeLa Oligo) (1.7µg/ul) (Reaction Biology Corporation)/10µl reaction mixture and the RING1B:BMI1 10x ubiquitin ligase buffer and conditions were used as for autoubiquitination above.

2.2.6. Western Blotting

For autoubiquitination, one 10µl sample of reaction mix was resolved on a precast 4-20% tris-glycine gradient gel and another 10µl sample was resolved on a 12% SDS-polyacrylamide gel, then both were transferred onto PVDF membranes. The membrane from the precast gel was probed with a mouse anti-ubiquitin P4D1 antibody and the other membrane was probed with a rabbit anti-BMI1 antibody, which was followed by the respective secondary antibodies and developed using ECL, as in 2.1.2.

For H2A monoubiquitination, two 10µl samples of reaction mix were resolved on separate 12% SDS-polyacrylamide gels, then transferred onto PVDF membranes. One membrane was probed with a mouse anti-ubiquityl-H2A antibody in 5% BSA and the other with a rabbit anti-BMI1 antibody, followed by the respective secondary antibodies, then developed using ECL, as in 2.1.2.

2.3. RING1B:BMI1 Ubiquitin Sensitivity Analysis

Reactions were carried out by incubating 10µl WT or mutant ubiquitin (2.5mg/ml) (Morris lab) with 10µl ubiquitin mix (1µl ATP (100mM), 1µl E1 (1:8 dilution from 800µg/ml stock),

1µl UbcH5a (1:4 dilution from 1µg/ml), 5µl 10x RING1B:BMI1 ubiquitin ligase buffer and 2µl WT or mutant GST-RING1B:BMI1 (diluted as required)) at 30^{o}C and 400rpm for 1 hour or 37^{o}C and 400rpm for 2 hours. Reactions were stopped with 10µl protein sample loading buffer.

2.3.1. Western Blotting

Antibody	Company	Dilution
Rabbit anti-BMI1 ab137416	Abcam	1:1,000 (In 5% non-fat milk)
Rabbit anti-ubiquitin	Viva Bioscience	1:1,000 (In 5% BSA)
Swine anti-rabbit	Dako	1:20,000 (In 5% non-fat milk)

Table 6: Antibodies for RING1B:BMI1 ubiquitin ligase sensitivity analysis
All antibodies used within this part of the investigation listed at the dilution used and the company antibodies were purchased from.

One 10µl sample of reaction mix was resolved on a precast 4-20% tris-glycine gradient gel and another 10µl sample was resolved on a 12% SDS-polyacrylamide gel, both were then transferred onto PVDF membranes. The membrane from the precast gel was probed with rabbit anti-ubiquitin and the other membrane was probed with a rabbit anti-BMI1 antibody – both for 1 hour at room temperature, washed in PBST followed by a swine anti-rabbit antibody and developed using ECL, as described in 2.1.2.

3. RESULTS

3.1. Effect of BARD1 R99 Mutant on BRCA1:BARD1 Ubiquitin Ligase Activity

3.1.1. His-tagged Protein Preparations

Before the ubiquitin ligase assay was completed for BRCA1:BARD1 a Western blot was used to determine WT and mutant BRCA1:BARD1 protein concentrations. Figure 11A indicates that the protein concentrations of the BRCA1:BARD1 WT and mutants vary and this was therefore adjusted for in the ubiquitin ligase assay, with; 4µl WT + 6µl 1x ubiquitin ligase buffer, 5µl BRCA1 I26A + 5µl 1x ubiquitin ligase buffer, 10µl C61G BRCA1 and 10µl BARD1 R99E BRCA1:BARD1 used. This ensured subsequent loading of BRCA1:BARD1 in the ubiquitin ligase assay was equal, allowing a fair comparison of the effect of the mutations on BRCA1:BARD1 ubiquitin ligase activity to be determined.

3.1.2. In vitro Ubiquitin Ligase Assay

Figure 12C shows that upon addition of the ubiquitin mix in the absence of BRCA1:BARD1 no ubiquitination takes place and only two bands can be seen, the lower indicating free ubiquitin and the higher indicating the E2-ubiquitin conjugate (Lane 1), highlighting the requirement of BRCA1:BARD1 for ubiquitin chain formation. However, upon addition of the ubiquitin mix to WT BRCA1:BARD1 a long ‘smear’ of ubiquitin was observed (Figure 11C, Lane 3), representing long polyubiquitin chains due to ubiquitination taking place. In addition, the bands representing free ubiquitin and an E2-ubiquitin conjugate, as seen previously (Figure 12C, Lane 1), were observed to be shifted up the gel due to the formation of ubiquitin chains on these as well (Figure 12C, Lane 3).

When observing the effect of the BRCA1 126A mutant on ubiquitin ligase activity, upon addition of the ubiquitin mix only a very faint ‘smear’ of ubiquitin was observed (Figure 12C, Lane 5), indicating that ubiquitin ligase activity had been reduced, as was predicted due to this being a known BRCA1 E2-binding mutant (Brzovic, P.S., et al., 2003) at the E2-E3 interface (Figure 12B). Furthermore, when observing the effect of the BRCA1 C61G mutant no ‘smear’ of ubiquitin was observed upon addition of the ubiquitin mix (Figure 12C, Lane 7), indicating a complete abrogation of ubiquitin ligase activity as was expected due to BRCA1 C61G preventing BARD1 and E2 binding to BRCA1 (Brzovic, P.S., et al., 2003). Due to BRCA1 I26A and C61G resulting in defective BRCA1:BARD1 ubiquitin ligase activity as expected, it confirmed this assay was representative of BRCA1:BARD1 ubiquitin ligase activity and would act as an accurate assay to determine the effect of the BARD1 R99E mutant on BRCA1:BARD1 ubiquitin ligase activity.

Figure 12C shows that upon addition of ubiquitin mix to the BARD1 R99E mutant a large reduction in ubiquitin ligase activity was observed, as indicated by the light ‘smear’ of ubiquitin representing ubiquitin chains (Figure 12C, Lane 9), which was almost as severe as the decrease in ubiquitin ligase activity observed with the BRCA1 I26A mutant. Furthermore, it is important to note that BRCA1:BARD1 loading between the WT and mutant proteins, denoted by use of an anti-BRCA1 antibody, is approximately equal between all the samples (Figure 12C) indicating this result is not due to uneven BRCA1:BARD1 loading but owing to the effect of the mutant itself on ubiquitin ligase activity. In addition, in the case of all three mutants the bands representing the free ubiquitin and E2-ubiquitin conjugate can be seen in the same place as in the absence of BRCA1:BARD1. This indicates the effect on ubiquitin ligase activity is owing to a defective BRCA1:BARD1, as the E2 is successfully loaded with ubiquitin.

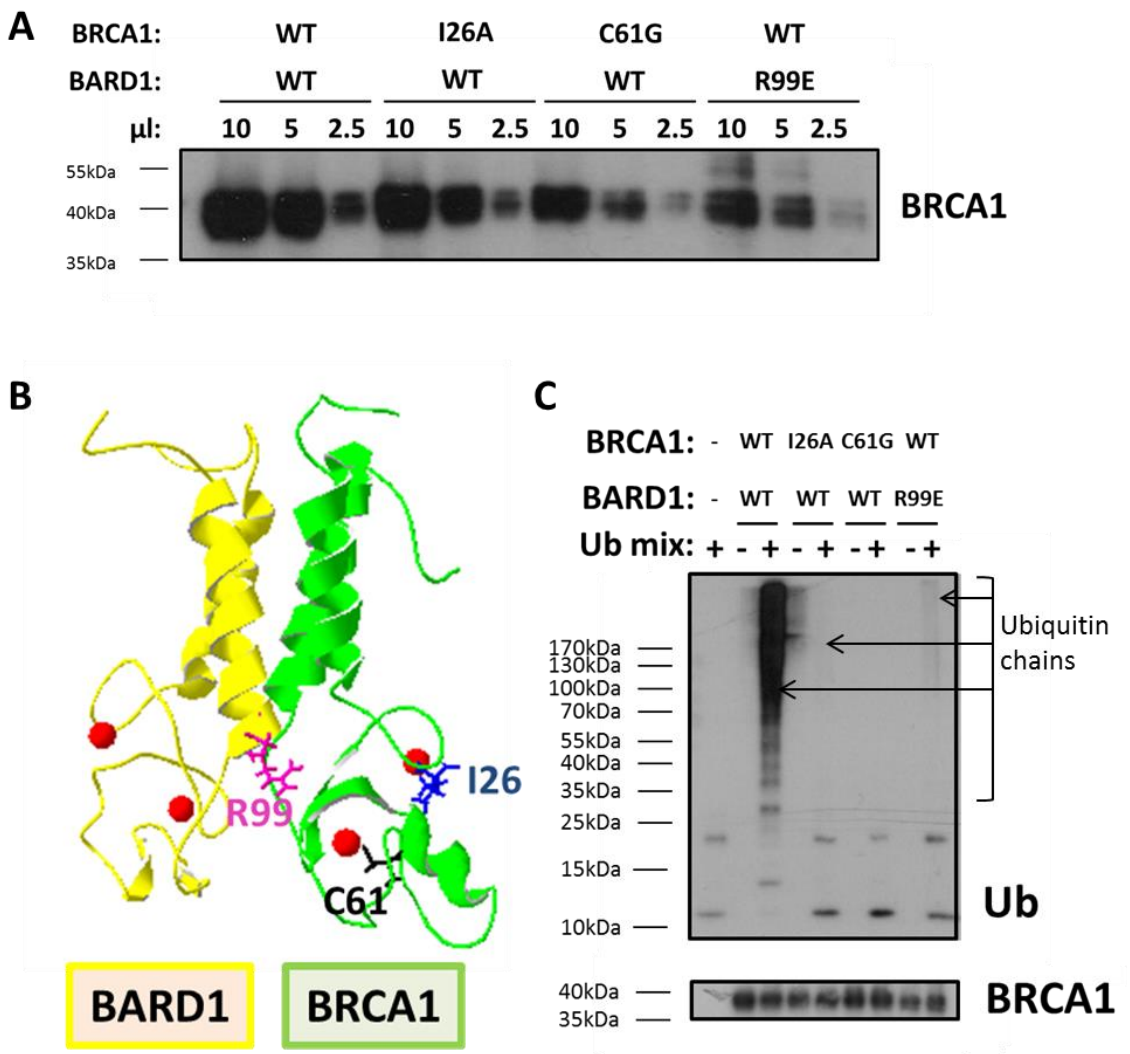

Figure 12: BRCA1:BARD1 ubiquitin ligase activity

A) Western blot of BRCA1:BARD1 WT and mutants (BRCA1 I26A, BRCA1 C61G and BARD1 R99E) at different volumes; 10µl, 5µl and 2.5µl required for normalisation of protein concentration in the ubiquitin ligase assay.

B) BRCA1:BARD1 crystal structure in green and yellow respectively, highlighting the BRCA1 I26 (blue), BRCA1 C61 (black) and BARD1 R99 (pink) residues (RCSB Protein Data Bank ID (www.rcsb.org): 1JM7). Image created using SwissPdbViewer (Guex, N. and Peitsch, M.C., (1997)).

C) WT and mutant BRCA1:BARD1 ubiquitin ligase activity was assessed by incubating these E3 ubiquitin ligases with a ubiquitin mix in ligase buffer containing ubiquitin, E1, ATP and E2 at 37^{o}C for 30 minutes. Samples were analysed for ubiquitination by SDS-PAGE and Western blot. BRCA1 I26A, BRCA1 C61G and BARD1 R99 all caused a decrease in ubiquitination compared to WT BRCA1:BARD1.

3.2. Effect of BMI1 K73 Mutant on RING1B:BMI1 Ubiquitin Ligase Activity

3.2.1. WT Plasmid Sequence Confirmation

The RING1B:BMI1 in a pGEX6P-3 plasmid from the Sixma lab was sequenced by Source BioScience LifeSciences and the sequence alignment was completed on Multalin (Corpet, F., 1988) (Supplementary figure 1), confirming it contained GST-RING1B (Reisudes 1-159) followed by a linker attaching this to mouse BMI1 (Residues 1-109) (Figure 13), with no mutations introduced (Supplementary figure 1). Furthermore, between the GST-tag and RING1B there was a PreScission protease cleavage site (Figure 13).

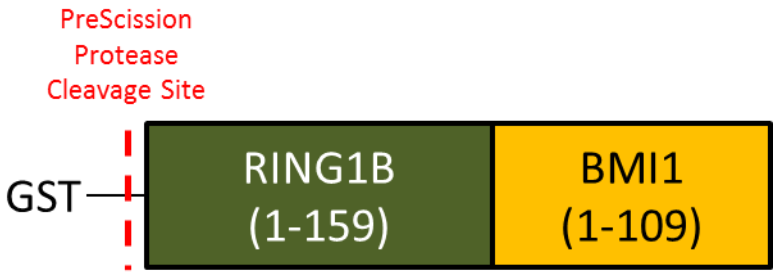

Figure 13: GST-RING1B:BMI1 schematic
Schematic of GST-tagged RING1B:BMI1 construct received from Buchwald, G., et al. (2006) RING1B (1-159) has a GST-tag with a PreScission protease cleavage site for removal upon purification. In addition, RING1B (1-159) is linked to BMI1 (1-109).

However, as the RING1B:BMI1 construct was, unexpectedly, of mouse origin the conservation with the human RING1B and BMI1 was assessed. Supplementary figure 2 indicates that at the peptide level no differences were observed between mouse and human RING1B between amino acids 1-159 or mouse and human BMI1 between amino acids 1-109. Furthermore, polycomb group proteins have been described to be evolutionarily conserved transcriptional repressors (Li, Z. et al., 2006).

3.2.2. Mutant Plasmid Sequence Confirmation.

Following site-directed mutagenesis of BMI1 K73A, BMI1 K73E and RING1B D56K in RING1B:BMI1 (Figure 14G), plasmid samples were sent for sequencing and results were aligned on Multalin (Supplementary figure 3). Figures 14A and 14B indicate that the site-directed mutagenesis for BMI1 K73A was successful with AAA being mutated to GCA. However, two extra mutations were also introduced either side of this mutation due to the primer, which was designed for human BMI1 albeit the construct was mouse RING1B:BMI1. However, this was not a problem as these were silent mutations and caused no change at the amino acid level. Figures 14C and 14D indicate that the site-directed mutagenesis for BMI1 K73E was also successful with AAA being mutated to GAA. However, as seen previously with BMI1 K73A, two extra silent mutations were also introduced either side of this mutation due to the primer design. Figures 14E and 14F indicate that the site-directed mutagenesis for RING1B D56K was also successful with GAT being mutated to AAA. However, as before, a silent mutation was also introduced due to primer design.

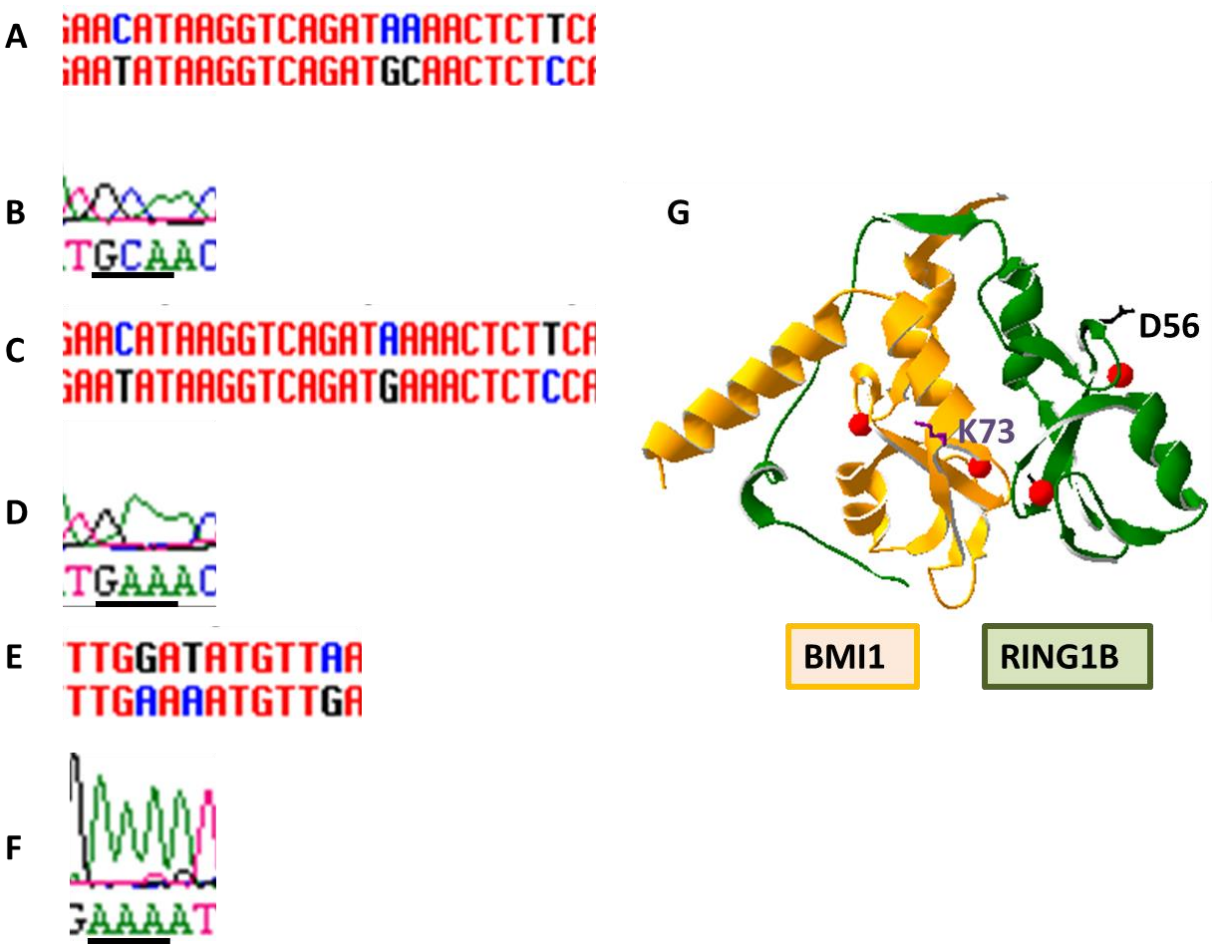

Figure 14: RING1B:BMI1 mutant sequence alignments and electopherograms
A) Sequence alignment on mutalin (Corpet, F., 1988) of RING1B:BMI1, with successful site-directed mutagenesis of BMI1 K73A (AAA → GCA).
B) Electropherogram indicating clear sequencing of mutation from AAA → GCA for BMI1 K73A.
C) Sequence alignment on mutalin (Corpet, F., 1988) of RING1B:BMI1, with successful site-directed mutagenesis of BMI1 K73E (AAA → GAA).
D) Electropherogram indicating clear sequencing of mutation from AAA → GAA for BMI1 K73E.
E) Sequence alignment on mutalin (Corpet, F., 1988) of RING1B:BMI1, with successful site-directed mutagenesis of RING1B D56K (GAT → AAA).
F) Electropherogram indicating clear sequencing of mutation from GAT → AAA for RING1B D56K.
G) RING1B:BMI1 crystal structure in green and orange respectively with the BMI1 K73 residue in purple, hypothesised to be involved in ubiquitin ligase activity and RING1B D56K in black, which is the designed E2-binding mutant (RCSB Protein Data Bank ID (www.rcsb.org): 2H0D). Image created using SwissPdbViewer (Guex, N. and Peitsch, M.C., (1997)).

3.2.3. GST-tagged Protein Preparations

To determine whether protein preparations of WT and mutant RING1B:BMI1 were successful, eluted pre-cleavage protein samples were resolved by SDS-PAGE and coomassie stained. Figure 15B indicates the predicted presence of GST-tagged RING1B at approximately 40kDa, some products between 40kDa and 26kDa predicted to be due to degradation of the GST-tag and BMI1 at approximately 13kDa (Figure 15B).

Following overnight cleavage of WT and mutant RING1B:BMI1protein preparations with PreScission protease, cleaved protein samples were resolved and coomassie stained as before. Figure 15C indicates the GST-tag was successfully cleaved, observed by a band at 26kDa. In addition, a band at approximately 15kDa was observed; predicted to be RING1B cleaved from the GST-tag and another band at approximately 13kDa (Figure 15C), believed to be BMI1, as seen previously pre-cleavage (Figure 15B).

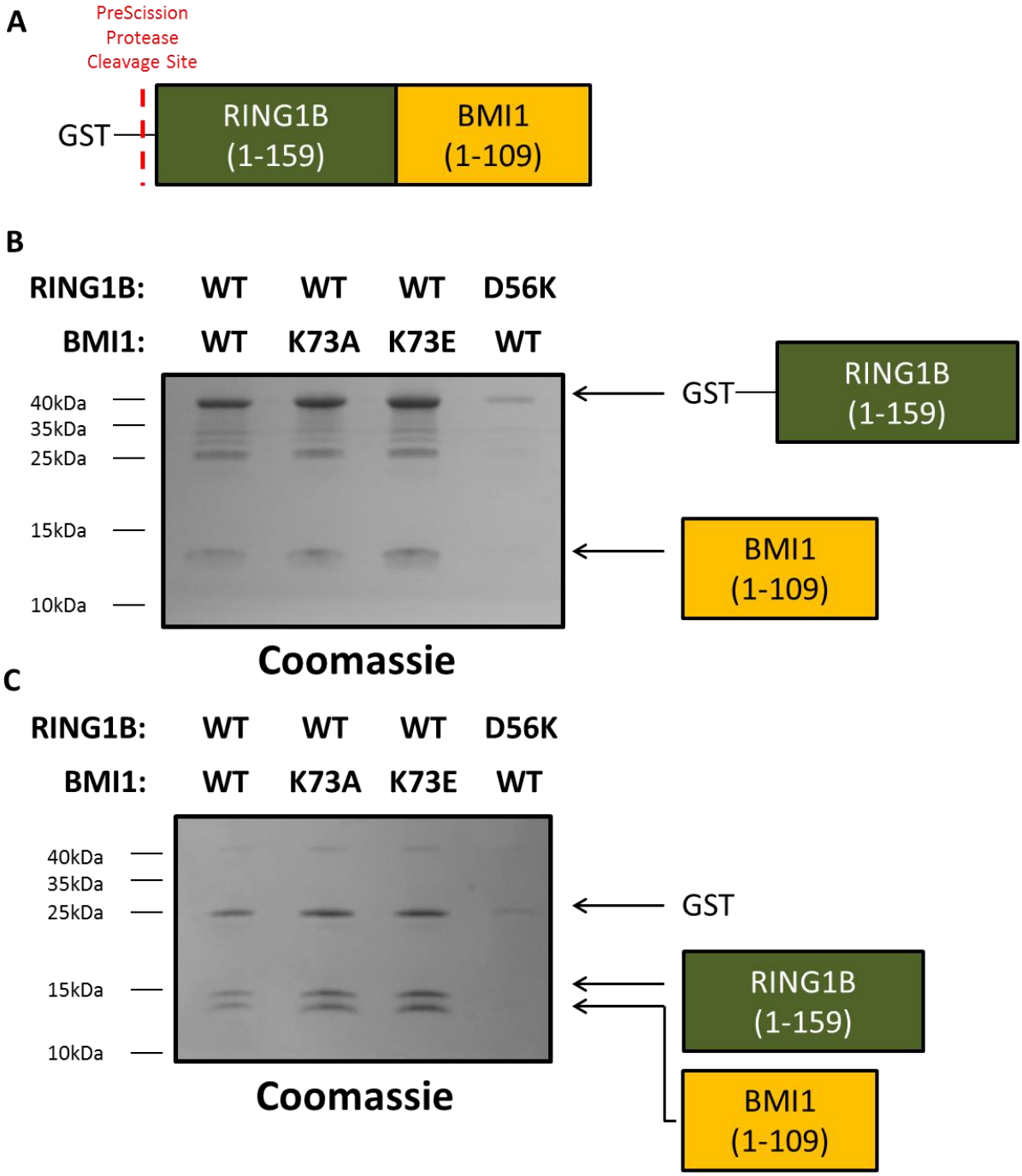

Figure 15: Prediction of RING1B and BMI1 in protein preparation
A) Schematic of GST-tagged RING1B:BMI1 construct received from Buchwald, G. et al. (2006).
B) Eluted pre-cleavage proteins were resolved by SDS-PAGE and the gel was coomassie stained. GST-RING1B is predicted to be at 40kDa and BMI1 at 13kDa in the WT, BMI1 K73A, BMI1 K73E and RING1B D56K RING1B:BMI1 protein preparations.
B) Eluted post-cleavage proteins were resolved by SDS-PAGE and the gel was coomassie stained. Free GST-tag is predicted to be at 26kDa, RING1B at 15kDa and BMI1 at 13kDa in the WT, BMI1 K73A, BMI1 K73E and RING1B D56K RING1B:BMI1 protein preparations.

To confirm the bands shown on the coomassie were what they were predicted to be, the cleaved protein samples were resolved by SDS-PAGE and a Western blot was completed. Figure 16 shows the GST-tag at approximately 26kDa – the correct molecular weight for a GST-tag - due to the tag being cleaved from RING1B, and BMI1 at approximately 13kDa, confirming what was predicted from the coomassie stain. Although it was not possible to confirm the presence of RING1B, as an anti-RING1B antibody recognising the RING1B amino acid region 1-159 was not available, due to the change in the banding patterns pre- and post-PreScission protease cleavage (Figure 15) it was confirmed that all four protein preparations contained RING1B:BMI1. However, it is important to note, that due to the concentration of the RING1B:BMI1 D56K protein preparation being considerably lower than the WT, BMI1 K73A and BMI1 K73E RING1B:BMI1 protein preparations this was taken into consideration and normalised for the subsequent ubiquitin ligase assays.

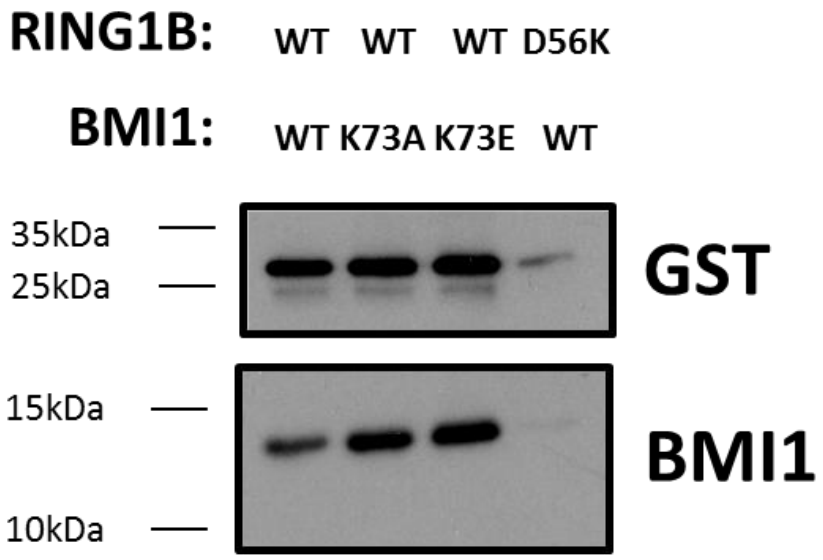

Figure 16: Confirmation of RING1B and BMI1 in protein preparation
Eluted post-cleavage proteins were resolved by SDS-PAGE and Western blot. Free GST-tag is observed at 26kDa and BMI1 at 13kDa in the WT, BMI1 K73A, BMI1 K73E and RING1B D56K RING1B:BMI1 protein preparations indicative of successful purification of RING1B:BMI1.

3.2.4. In vitro Ubiquitin Ligase Assay

Following confirmation of successful RING1B:BMI1 protein preparations, a ubiquitin ligase assay was completed with nucleosomes using WT RING1B:BMI1 and the RING1B D56K mutant (Figure 17A), which was selected as a control for RING1B:BMI1 ubiquitin ligase. Despite the anti-ubiquityl-H2A antibody being slightly non-specific, identifying free ubiquitin and E2-ubiquitin conjugate, Figure 17B (Lane 3) indicates that WT RING1B:BMI1 monoubiquitinated H2A, its substrate, in the presence of the ubiquitin ligase mix whereas the RING1B D56K mutant did not (Figure 17B, Lane 5), indicating abrogated ubiquitin ligase activity. It is important to note the anti-BMI1 antibody denotes approximately equal RING1B:BMI1 loading between each sample (Figure 17B), indicating that the change in ubiquitin ligase activity is not due to uneven RING1B:BMI1 loading.

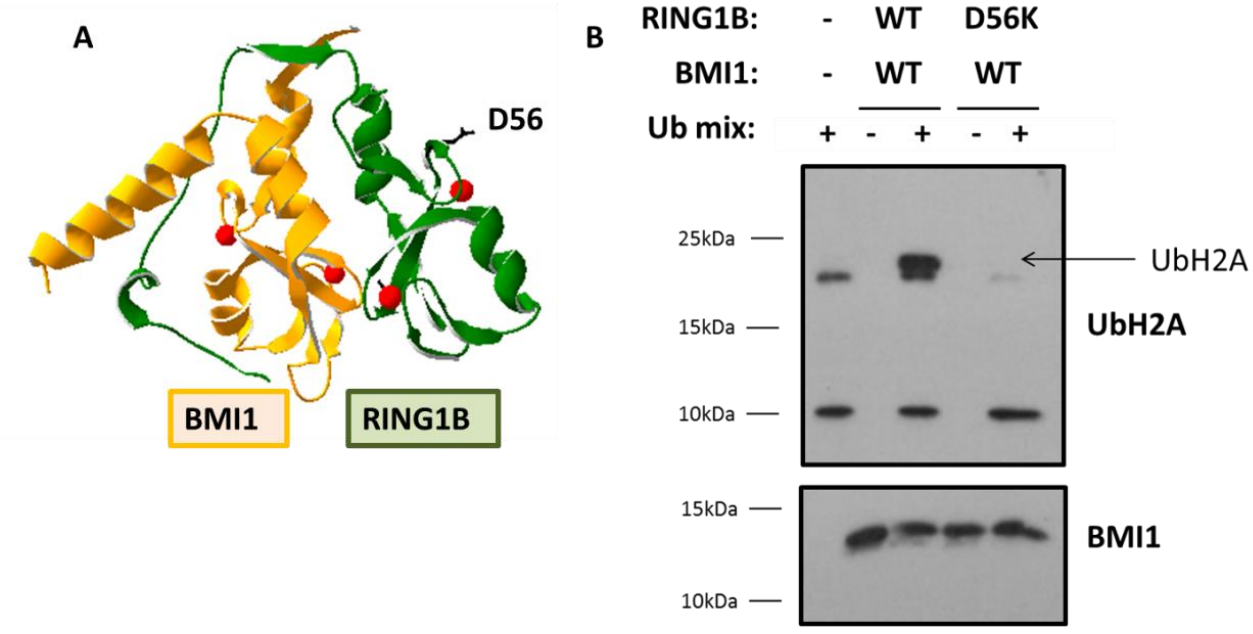

Figure 17: RING1B:BMI1 ubiquitin ligase activity
A) RING1B:BMI1 crystal structure in green and orange respectively, highlighting the RING1B D56 residue (black) (RCSB Protein Data Bank ID (www.rcsb.org): 2H0D). Image created using SwissPdbViewer (Guex, N. and Peitsch, M.C., (1997)).
B) WT RING1B:BMI1 and RING1B D56K mutant ubiquitin ligase activity was assessed by incubating these E3 ubiquitin ligases with a ubiquitin mix in ligase buffer containing ubiquitin, E1, ATP, E2 and nucleosomes at 30°C for 1 hour. Samples were analysed for ubiquitination by SDS-PAGE and Western blot. RING1B D56K caused an abrogation in ubiquitination, as observed by no H2A ubiquitination taking place compared to WT RING1B:BMI1.

Following confirmation of RING1B D56K lacking ubiquitin ligase activity it was planned this same assay would be completed for BMI1 K73A and BMI1 K73E, however no nucleosomes were available. Therefore, GST-tagged WT RING1B:BMI1 and BMI1 K73 RING1B:BMI1 mutants were used in a ubiquitin ligase assay in the absence of nucleosomes. Upon the addition of ubiquitin mix in the absence of RING1B:BMI1 no ubiquitin chains were observed however, upon addition of ubiquitin mix to WT RING1B:BMI1 a 'smear' of ubiquitin was observed representing ubiquitin chain formation (Figure 18B, Lane 3), indicating WT RING1B:BMI1's ubiquitin ligase activity. In addition, a similar effect, if not greater, was also observed with the BMI1 K73A mutant (Figure 18B, Lane 5). Whereas, upon addition of the ubiquitin mix to the BMI1 K73E mutant less of a 'smear' of ubiquitin was observed (Figure 18B, Lane 7), highlighting a decrease in ubiquitin ligase activity compared to the WT, despite approximately equal BMI1 loading (Figure 18B).

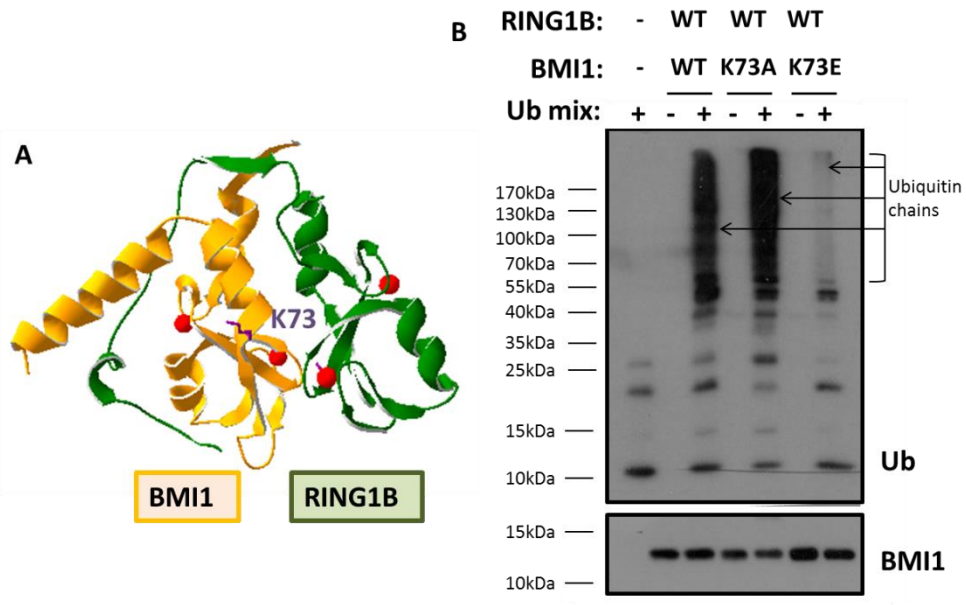

Figure 18: RING1B:BMI1 ubiquitin ligase activity

A) RING1B:BMI1 crystal structure in green and orange respectively, highlighting the BMI1 K73 residue (purple) (RCSB Protein Data Bank ID (www.rcsb.org): 2H0D). Image created using SwissPdbViewer (Guex, N. and Peitsch, M.C., (1997)).

B) GST-tagged WT RING1B:BMI1 and BMI1 K73A and BMI1 K73E mutants ubiquitin ligase activity was assessed by incubating these E3 ubiquitin ligases with a ubiquitin mix in ligase buffer containing ubiquitin, E1, ATP and E2 at 30^{o}C for 1 hour. Samples were analysed for ubiquitination by SDS-PAGE and Western blot. BMI1 K73E caused a decrease in ubiquitination compared to WT RING1B:BMI1.

3.3. RING1B:BMI1Ubiquitin Sensitivity

3.3.1. WT RING1B:BMI1

A ubiquitin ligase assay was completed using WT RING1B:BMI1 in the presence of WT and mutant ubiquitin constructs to determine the ubiquitin sensitivity of RING1B:BMI1. By mutating lysine residues on ubiquitin, RING1B:BMI1 ubiquitin ligase activity was altered significantly, with the most striking results indicating that a ubiquitin K6R mutation caused a complete loss of WT RING1B:BMI1 ubiquitin ligase activity as seen by no 'smear' of ubiquitin (Figure 19B). Furthermore, ubiquitin mutants; K27R, K48R and K63R also caused a reduction in ubiquitin ligase activity compared to WT ubiquitin (Figure 19B). However, the ubiquitin K33R mutation caused an increase in WT RING1B:BMI1 ubiquitin ligase with a 'smear' of ubiquitin, representing ubiquitin chain formation, considerably greater than that observed with WT ubiquitin (Figure 19B).

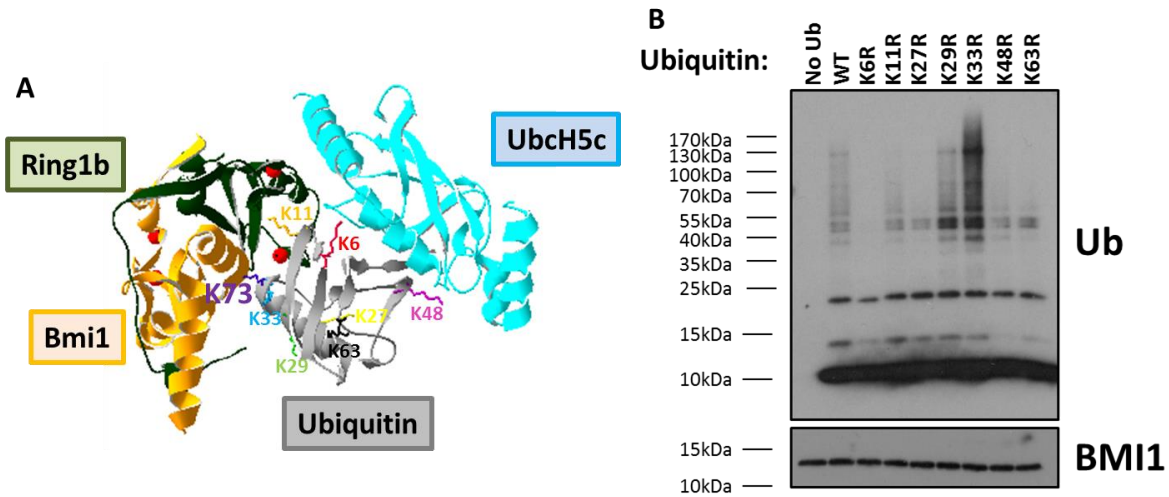

Figure 19: WT RING1B:BMI1 ubiquitin sensitivity
A) RING1B:BMI1 crystal structure in green and orange respectively, highlighting the BMI1 K73 residue (purple) modelled with the E2-ubiquitin conjugate in blue and grey respectively from the crystal structure of RNF4:E2-Ub conjugate, with ubiquitin mutants marked in a range of colours (RCSB Protein Data Bank ID (www.rcsb.org): 2H0D and 4AP4). Image created using SwissPdbViewer (Guex, N. and Peitsch, M.C., (1997)).
B) Ubiquitin sensitivity with GST-tagged WT RING1B:BMI1 was assessed by ubiquitin ligase activity by incubating WT and ubiquitin mutants with a ubiquitin mix in ligase buffer containing E1, ATP, E2 and GST-RING1B:BMI1 at 30^{o}C for 1 hour. Samples were analysed for ubiquitination by SDS-PAGE and Western blot.

In addition, the effect of mutating other ubiquitin residues at various patches on ubiquitin (Figure 20A and Figure 20B) was also observed with respect to WT RING1B:BMI1. Results indicate the requirement of a number of residues from a variety of different patches on ubiquitin, with the most striking observation due to mutating ubiquitin E34 (Figures 20B and 20C). When ubiquitin E34 was mutated to a glycine a reduction in ubiquitin ligase activity was observed whereas, mutation to an arginine caused an increase in ubiquitin ligase activity with respect to WT ubiquitin (Figure 20C). In addition ubiquitin F4A, I36A and I44A all independently caused a decrease in RING1B:BMI1 ubiquitin ligase activity compared to WT ubiquitin (Figure 20C).

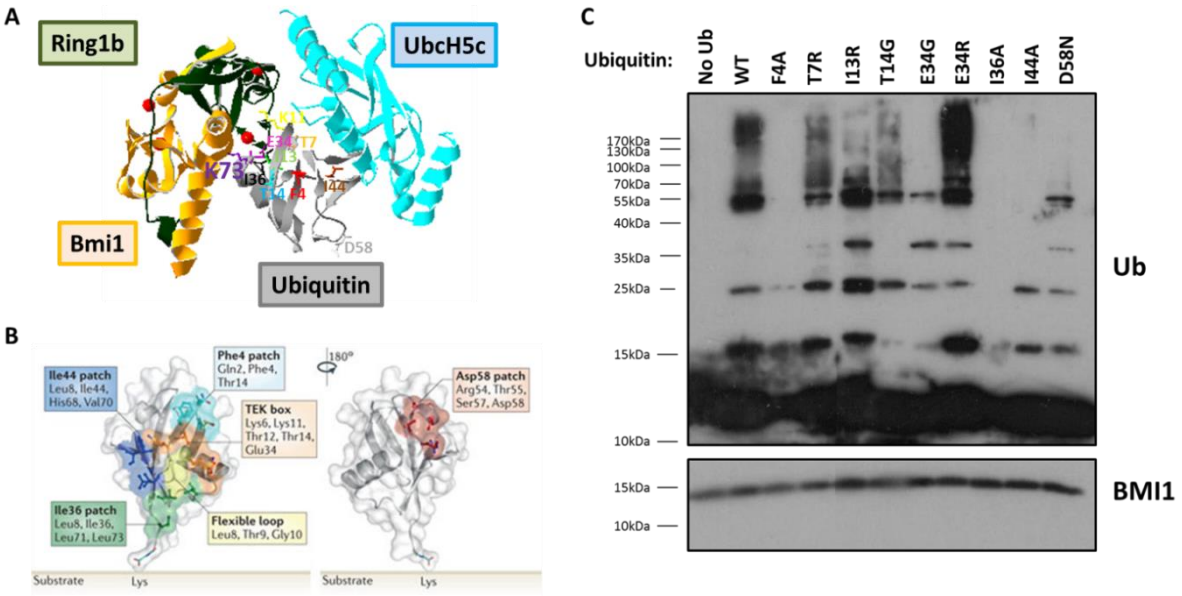

Figure 20: WT RING1B:BMI1 ubiquitin sensitivity

A) RING1B:BMI1 crystal structure in green and orange respectively, highlighting the BMI1 K73 residue (purple) modelled with the E2-ubiquitin conjugate in blue and grey respectively from the crystal structure of RNF4:E2-Ub conjugate, with ubiquitin mutants marked in a range of colours (RCSB Protein Data Bank ID (www.rcsb.org): 2H0D and 4AP4). Image created using SwissPdbViewer (Guex, N. and Peitsch, M.C., (1997)).

B) Model of ubiquitin indicating different patches and the TEK box where some of the ubiquitin mutants used in the ubiquitin sensitivity assay have been derived from (Image from: Kulathu, Y. and Komander, D., 2012. Atypical Ubiquitylation – the Unexplored World of Polyubiquitin Beyond Lys46 and Lys63 Linkages. Nature Reviews Molecular Cell Biology, 13, pp.508-523.).

C) Ubiquitin sensitivity with GST-tagged WT RING1B:BMI1 was assessed by ubiquitin ligase activity by incubating WT and ubiquitin mutants with a ubiquitin mix in ligase buffer containing E1, ATP, E2 and GST-RING1B:BMI1 at 30^{o}C for 1 hour. Samples were analysed for ubiquitination by SDS-PAGE and Western blot.

3.3.2. Mutant RING1B:BMI1

Ubiquitin ligase assays to determine ubiquitin sensitivity were completed for RING1B:BMI1 mutants; BMI1 K73A and BMI1 K73E in the presence of WT and mutant lysine ubiquitin constructs. Figures 21B and 21C indicate a similar pattern of ubiquitination for BMI1 K73A and BMI1 K73E to that observed with WT RING1B:BMI1 in the presence of WT and mutant ubiquitin constructs (Figure 19B), including the most striking loss of ubiquitin ligase activity due to the K6R mutant (Figure 21B and Figure 21C). Furthermore, as seen previously with WT RING1B:BMI1, the ubiquitin K33R mutant caused a greater 'smear' of ubiquitin compared to WT ubiquitin with BMI1 K73A, indicating an increase in ubiquitin ligase activity (Figure 21B). However, a slight decrease in ubiquitin chain formation as observed by a decrease in the ubiquitin 'smear' was observed with ubiquitin K33R compared to WT ubiquitin with BMI1 K73E (Figure 21C).

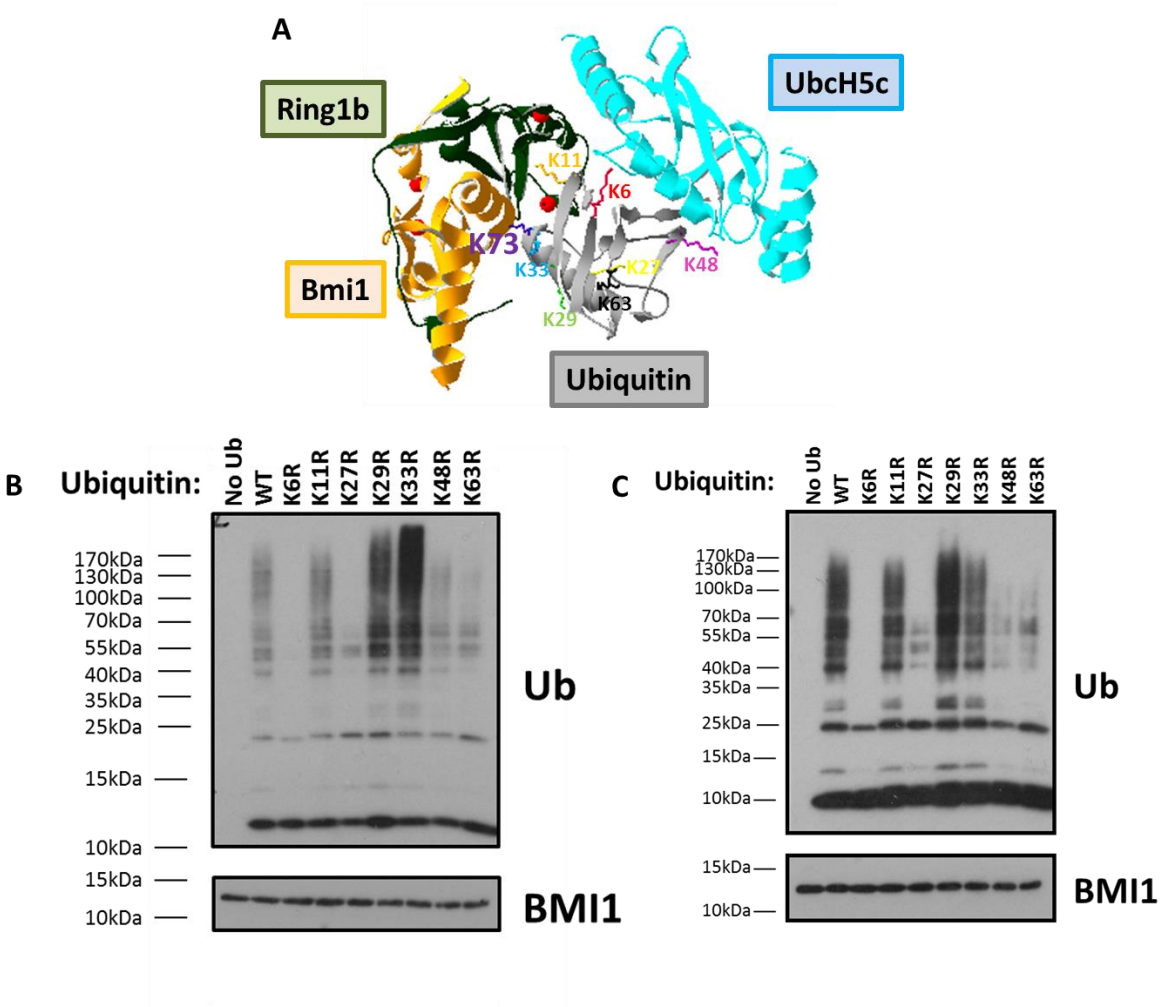

Figure 21: Mutant RING1B:BMI1 ubiquitin sensitivity

A) RING1B:BMI1 crystal structure in green and orange respectively, highlighting the BMI1 K73 residue (purple) modelled with the E2-ubiquitin conjugate in blue and grey respectively from the crystal structure of RNF4:E2-Ub conjugate, with ubiquitin mutants marked in a range of colours (RCSB Protein Data Bank ID (www.rcsb.org): 2H0D and 4AP4). Image created using SwissPdbViewer (Guex, N. and Peitsch, M.C., (1997)).

B) Ubiquitin sensitivity with GST-tagged mutant RING1B:BMI1 (BMI1 K73A) was assessed by ubiquitin ligase activity by incubating WT and ubiquitin mutants with a ubiquitin mix in ligase buffer containing E1, ATP, E2 and GST-RING1B:BMI1 at 30^{o}C for 1 hour. Samples were analysed for ubiquitination by SDS-PAGE and Western blot.

C) Ubiquitin sensitivity with GST-tagged mutant RING1B:BMI1 (BMI1 K73E) was assessed by ubiquitin ligase activity by incubating WT and ubiquitin mutants with a ubiquitin mix in ligase buffer containing E1, ATP, E2 and GST-RING1B:BMI1 at 37^{o}C for 2 hours. Samples were analysed for ubiquitination by SDS-PAGE and Western blot.

4. DISCUSSION

Type I RING-type E3 ubiquitin ligases are fundamental to ubiquitin ligase activity and consequently mutation or upregulation of these E3s, including BRCA1:BARD1 and RING1B:BMI1, has been observed in cancer (Ruffner, H., et al., 2001, Buchwald, G., et al., 2007, Martínez-Romero, C., et al., 2009). This investigation focused on trying to determine the mechanism by which the type I RING-type E3 ubiquitin ligases bind and lock an E2-ubiquitin conjugate based on previous observations in RNF4; a type II RING-type E3 ubiquitin ligases (Plechanovová, A., et al., 2011). Consequently, it was shown that BARD1 R99 and BMI1 K73 play a role in BRCA1:BARD1 and RING1B:BMI1 ubiquitin ligase activity respectively, which may be due to their involvement in the binding and locking of ubiquitin in an E2-ubiqutin conjugate - challenging the opinion of Metzger, M.B., et al. who suggested BARD1 and BMI1 are not involved in E2-ubiquitin binding and locking (2014).

4.1. BARD1 R99E Reduced BRCA1:BARD1 Ubiquitin Ligase Activity

The BARD1 R99E mutation in BRCA1:BARD1 was observed to cause a reduction in ubiquitin ligase activity compared to WT BRCA1:BARD1, almost equivalent to the designed BRCA1 E2-binding mutant; BRCA1 I26A (Figure 12C), which is known to reduce BRCA1:BARD1 ubiquitin ligase activity. This is suggestive of BARD1 R99 playing an important role within the ubiquitin pathway. Subsequently, Morris, J., et al. have extended this work and observed that BARD1 R99E was unable to promote the transfer of ubiquitin from a loaded E2-ubiquitin conjugate during autoubiquitination of BRCA1:BARD1 (Morris, J., et al., Unpublished). This highlighted the requirement of BARD1 R99 to bind and lock ubiquitin in an E2-ubiquitin conjugate into place for ubiquitin transfer to successfully take place, in a mechanism similar to that described for RNF4 and BIRC7 where both RING

protomers ensure essential ubiquitin contacts are made for optimal ubiquitin transfer and thus ubiquitin ligase activity (Plechanovová, A., et al., 2012, Dou, H., et al., 2012).

These findings of BARD1's role in the ubiquitin ligase activity of BRCA1:BARD1 are interesting as not only do they offer a mechanistic insight but may also bear clinical relevance due to BRCA1:BARD1 ubiquitin ligase activity being described to be important in the prevention of breast and ovarian cancer development (Hashizume, R., et al., 2001). Previously, BARD1 has been shown to be mutated in breast cancer patients (Karppinen, S-M., et al., 2004, Thai, T.H., et al., 1997) providing evidence that BARD1 mutations do take place in cancer, however future investigations could extend studies on BARD1 mutants to observe whether deleterious BARD1 R99 mutants are present in breast and ovarian cancer patients, particularly in genetic testing when breast cancer patients are known to be negative for harmful BRCA1 mutants. Analysis of DNA samples from individuals with a personal and/or family history of cancer could be taken, then by using PCR and next generation sequencing techniques it could be assessed whether these patients carry BARD1 R99 mutations, in particular a BARD1 R99E mutation.

4.2. BMI1 K73E Reduced RING1B:BMI1 Ubiquitin Ligase Activity

The results from the ubiquitin ligase assays with RING1B:BMI1 indicated that the BMI1 K73E mutant caused a reduction in RING1B:BMI1 ubiquitin ligase activity compared to WT RING1B:BMI1, suggestive of this residue having an important role within the ubiquitin pathway. Despite this, BMI1 K73A caused an increase in RING1B:BMI1 ubiquitin ligase activity (Figure 18C). However, it is important to note that these observations were made in the context of GST-tagged RING1B:BMI1 constructs and in the absence of nucleosomes, the substrate for RING1B:BMI1, due to a lack of nucleosomes being available and untagged

proteins not creating ubiquitin chains in the absence of nucleosomes. Consequently, this raises some concern over whether BMI1 K73E does have a deleterious effect on RING1B:BMI1's ubiquitin ligase activity as this assay may not be an accurate representation.

Although, in support of this observation, it has previously been described that RING1B can self-ubiquitinate (Ben-Saadon, R., et al., 2006), highlighting that substrate may not be required to determine ubiquitin ligase activity. Furthermore, the ubiquitin chains produced with the GST-tagged RING1B:BMI1 constructs compared to no chains when using the untagged RING1B:BMI1, in the absence of nucleosomes, is predicted to be due to an amplification of ubiquitin ligase activity owing to GST-tag dimerisation resulting in heterotetrameric RING1B:BMI1 complexes, which have previously been shown by Buchwald, G., et al. to create long polyubiquitin chains (2006). However, in any case as all proteins used were GST-tagged the effect the tag has would be global for WT and mutant RING1B:BMI1 constructs alike indicating the assay should still be representative of the respective constructs ubiquitin ligase activity.

Nevertheless, with more time, it would be crucial to observe the ubiquitin ligase activity of untagged WT and mutant RING1B:BMI1 constructs in the presence of nucleosomes to confirm whether BMI1 K73E has a deleterious effect and BMI1 K73A does increase ubiquitin ligase activity compared to WT RING1B:BMI1 respectively. If this was the case, one explanation for the difference observed between the BMI1 K73 mutants may be that a lysine to alanine mutation causes a positive to neutral charge change and subsequently less deleterious impact on ubiquitin ligase activity however, a lysine to glutamic acid results in a positive to negative charge change, which is more likely to negatively impact ubiquitin ligase activity.

4.3. RING1B:BMI1 Ubiquitin Sensitivity

By mutating residues in ubiquitin it was possible to begin to determine the ubiquitin sensitivity of RING1B:BMI1. Firstly, due to the observation of K6, K27, K48 and K63 in ubiquitin being required for WT as well as mutant (BMI K73A and BMI1 K73E) RING1B:BMI1's ability to form polyubiquitin chains (Figures 19B, 21B and 21C) it was predicted this was due to the ability of branched ubiquitin chains involving K6, K27 and K48 linkages to form on RING1B (Ben-Saadon, R., et al., 2006), which was not affected by the BMI1 K73 mutation. Another interesting effect observed upon mutating lysine residues in ubiquitin was that of ubiquitin K33R, which caused an increase in ubiquitin ligase activity with WT and BMI1 K73A RING1B:BMI1 (Figure 19B and 21B) compared to a slight decrease in ubiquitin ligase activity with BMI1 K73E RING1B:BMI1 (Figure 21C). This may be suggestive of a potential interaction between ubiquitin K33 and BMI1 K73 for ubiquitin ligase activity, particularly due to the correlation with previous findings of BMI1 K73A not having a deleterious effect on RING1B:BMI1 ubiquitin ligase activity when BMI1 K73E did (Figure 18C).

Further investigations indicated the importance of a number of other ubiquitin residues for WT RING1B:BMI1 ubiquitin ligase activity (Figure 20C). One of the most striking observations was that of mutating ubiquitin I36, which resulted in completely abrogated WT RING1B:BMI1 ubiquitin ligase activity (Figure 20C), which is in line with observations by Dou, H., et al. who identified ubiquitin I36 to be required for contacting the BIRC7 dimer interface for correct ubiquitin positioning required during ubiquitin transfer (2012). This was described to be due to a requirement of both BIRC7 protomers for recruiting the E2-ubiquitin conjugate (Dou, H., et al., 2012), in a manner similar to the binding and locking mechanism for the E2-ubiquitin conjugate hypothesised in RING1B:BMI1.

Furthermore, it was observed that the mutation of ubiquitin E34 altered WT RING1B:BMI1 ubiquitin ligase activity, with ubiquitin E34R causing an increase in activity compared to ubiquitin E34G, which caused a decrease in activity (Figure 20C). This was a similar pattern to that observed for WT RNF4's ubiquitin ligase activity whereby ubiquitin E34G saw a decrease in activity and ubiquitin E34R resulted in no change in activity (Morris, J., et al., Unpublished). Consequently, this may suggest BMI1 K73 acts in a similar way to RNF4 Y193 with regard to ubiquitin binding, as the side chain of Y193 on the RNF4 RING domain has been shown to stack with the main chain E34 to G35 of ubiquitin (Plechanovová, A., et al., 2012),

Altogether, these observations highlight the potential of BMI1 K73 to interact with ubiquitin in a manner to that previously identified in other RING-type E3 ubiquitin ligases. Modelling completed on SwissPdbViewer with RING1B:BMI1 and an E2-ubiquitin conjugate highlighted ubiquitin K33 and E34 (within an E2-ubiquitin conjugate) to be in close proximity to BMI1 K73 (Figure 22), supporting the hypothesis of BMI1 K73 being involved in a mechanism of binding and locking of an E2-ubiquitin conjugate. However, it is important to note a full conclusion cannot be drawn from these ubiquitin sensitivity assays as they are not specific enough in determining how the ubiquitin mutants alter ubiquitin ligase activity.

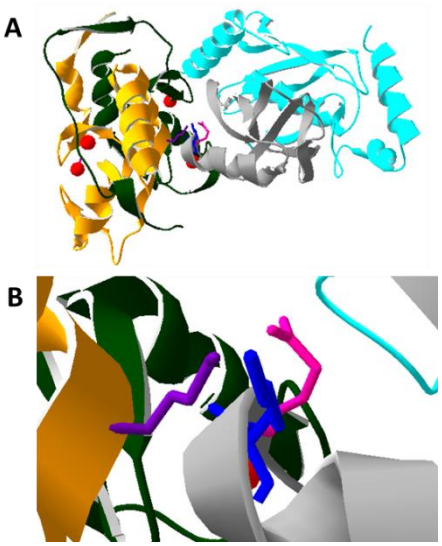

Figure 22: RING1B:BMI1 and E2-ubiquitin conjugate modelling
A) RING1B:BMI1 crystal structure in green and orange respectively, highlighting the BMI1 K73 residue (purple) modelled with the E2-ubiquitin conjugate in blue and grey respectively from the crystal structure of RNF4:E2-Ub conjugate, with ubiquitin K33 and E34 marked in blue and pink respectively
(RCSB Protein Data Bank ID (www.rcsb.org): 2H0D and 4AP4). Image created using SwissPdbViewer (Guex, N. and Peitsch, M.C., (1997)).
B) Zoomed view of residues of interest in Figure 22A.

4.4. Limitations

Due to time restrictions it was unfortunate that there were some initial issues in purifying RING1B:BMI1, whereby following the first protein preparation only GST-RING1B was purified and no BMI1 was present. Therefore, the protocol was altered by analysing how other groups had purified this protein, resulting in new wash buffers to be used in conjunction with Buchwald, G., et al. (2006), which resulted in a successful purification of both GST-RING1B and BMI1. Furthermore, during protein preparations despite having an anti-BMI1 antibody to confirm the purification of BMI1 (1-109), which was untagged there was no antibody available against RING1B (1-159). When identifying GST-RING1B this was not a problem as an anti-GST antibody was available, however upon cleavage of this tag it was not possible to detect RING1B via Western blot. Therefore, if a suitable antibody against the region of RING1B within this investigation became available in the future it would be useful to use this to confirm the purification of RING1B.

Another limitation within this investigation was the use of modelling, albeit useful as a guideline it is not 100% accurate. The structure of an E2-ubiquitin conjugate with RNF4 was used to model the hypothesised E2-ubiqutin conjugate interaction with BRCA1:BARD1 and RING1B:BMI1, however it is known that RING:E2 contacts vary (Deshaies, R.J. and Joazeiro, C.A.P., 2009) and in the case of RING1B:BMI1, which sits on a nucleosome (Bentley, M.L., et al., 2011) contacts are likely to be altered further. In addition, as the structure of RNF4 in complex with an E2-ubiquitin conjugate was determined by crystal structure the residues are detected as static whereas in reality they are flexible, resulting in the true interactions of residues not being truly determined. However, as ubiquitin adopts a wide variety of positions (Soss, S.E., et al., 2013) and structural similarities have been observed between RING domains (Buchwald, G., et al., 2003, Li, Z., et al., 2006) it was predicted that

by modelling the E2-ubiquitin conjugate from RNF4 with BRCA1:BARD1 or RING1B:BMI1 this would allow a fair representation of interactions.

4.5. Future Research

These preliminary findings offer huge potential and Morris, J., et al. have already completed further research on BARD1 R99 in BRCA1:BARD1, as described previously, meaning the majority of the future work would need to be focused on RING1B:BMI1. Firstly, it would be essential to complete the aforementioned ubiquitin ligase assay with nucleosomes for untagged WT RING1B:BMI1 and BMI1 K73A and BMI1 K73E mutants to ensure BMI1 K73E decreases RING1B:BMI1 ubiquitin ligase activity compared to WT.

Following confirmation of BMI1 K73E being deleterious to RING1B:BMI1 ubiquitin ligase activity it would then be important to determine why BMI1 K73E has this effect. Firstly, a yeast three-hybrid system could be used to determine whether BMI1 K73E affects RING1B and E2 binding, which if it did would result in defective ubiquitin ligase activity. However, if BMI1 K73E does not affect RING1B and E2 binding, it would then need to be determined whether BMI1 K73E affects ubiquitin transfer during autoubiquitination of RING1B:BMI1, as previously observed for BARD1 R99 in BRCA1:BARD1. This could be achieved by loading an E2 with lysine free ubiquitin, to prevent chain formation, then adding WT or mutant RING1B:BMI1 respectively and following autoubiquitination over a period of time. Due to the previous observations in BRCA1:BARD1, it would be predicted that BMI1 K73E is unable to transfer ubiquitin, due to defective E2-ubiquitin conjugate binding.

Subsequently, if the aforementioned assay did confirm BMI1 K73E in RING1B:BMI1 plays a role in E2-ubiquitin conjugate binding and locking in a manner identical to that of BARD1 R99 in BRCA1:BARD1 this may highlight a generic mechanism in type I RING-type E3

ubiquitin ligases. Furthermore, these findings may not only offer a mechanistic insight but may also bear clinical relevance. Therefore, it would be essential to extend studies to *in vivo* work by creating BARD1 R99E and BMI1 K73E mice to see if they display a cancerous phenotype. Previously, BRCA1:BARD1 RING mutants, which reduce ubiquitin ligase activity have been described to play a role in cancer pre-disposition (Ruffner, H., et al., 2001) however, it has also recently been observed that the BRCA1 I26A RING mutant, despite reducing ubiquitin ligase activity, does not cause cancer in a mouse model (Shakya, R., et al., 2014).

4.6. Conclusions

BARD1 R99 and BMI1 K73 appear to play a role in the ubiquitin ligase activity of BRCA1:BARD1 and RING1B:BMI1 respectively. Morris, J., et al. have highlighted that BARD1 R99 in BRCA1:BARD1 plays a role in the binding and locking of an E2-ubiquitin conjugate however, due to time limitations further investigations are required to determine whether BMI1 K73 plays a similar role in RING1B:BMI1.

If both BARD1 R99 and BMI1 K73 were shown to play a role in the binding and locking of an E2-ubiquitin conjugate it would be interesting to extend studies to observe whether this is a generic mechanism across all type I RING-type E3 ubiquitin ligases and furthermore, whether these mutants bear any clinical relevance.

5. REFERENCES

Ben-Saadon, R., et al., 2006. The Polycomb Protein RING1B Generates Self Atypical Mixed Ubiquitin Chains Required for its in vitro Histone H2A Ligase Activity. Molecular Cell, 24, pp.701-711.

Bentley, M.L., et al., 2011. Recognition of UbcH5c and the Nucleosome by the BMI1/RING1B Ubiquitin Ligase Complex. EMBO Journal, 30, pp.3285-3297.

Berndsen, C.E. and Wolberger, C., 2014. New Insights into Ubiquitin E3 Ligase Mechanism. Nature Structural and Molecular Biology, 21, pp.301-307.

Brzovic, P.S., et al., 2001. Structure of a BRCA1:BARD1 Heterodimeric RING-RING Complex. Nature Structural Biology, 8, pp.833-837.

Brzovic, P.S., et al., 2003. Binding and Recognition in the Assembly of an Active BRCA1:BARD1 Ubiquitin-Ligase Complex. PNAS, 100, pp.5646-5651.

Buchwald, G., et al., 2006. Structure and E3-ligase Activity of the Ring-Ring Complex of Polycomb Proteins BMI1 and RING1B. The EMBO Journal, 25, pp.2465-2474.

Castilla, L.H., et al., 1994. Mutations in the BRCA1 Gene in Families with Early-onset Breast and Ovarian Cancer. Nature Genetics, 8, pp.387-391.

Christensen, D.E., et al., 2007. E2-BRCA1 RING Interactions Dictate Synthesis of Mono- or Specific Polyubiqutin Chain Linkages. Nature Structural & Molecular Biology, pp.1-8.

Corpet, F., 1988. Multiple Sequence Alignment with Hierachical Clustering. Nucleic Acids Research, 16, pp.10881-10890. (Mutalin website: http://multalin.toulouse.inra.fr/multalin/ Accessed on 01/02/14).

Deshaies, R.J. and Joazeiro, C.A.P., 2009. RING Domain E3 Ubiquitin Ligases. Annual Review of Biochemistry, 78, pp.399-434.

Dimri, G.P., et al., 2002. The BMI1 Oncogene Induces Telomerase Activity and Immortalises Human Mammary Epithelial Cells. The Journal of Cancer Research, 62, pp.4736-4745.

Dou, H., et al., 2012. Structure of BIRC7-E2 Ubiquitin Conjugate Reveals the Mechanism of Ubiquitin Transfer by a RING Dimer. Nature Structural and Molecular Biology, 19, pp.1-21.

Dou, H., et al., 2013. Essentiality of a Non-RING Element in Priming Donor Ubiquitin for Catalysis by a Monomeric E3. Nature Structural and Molecular Biology, 20, pp.982-987.

Ginjala, V., et al., 2011. BMI1 is Recruited to DNA Breaks and Contributes to DNA Damage-induced H2A Ubiquitination and Repair. Molecular and Cellular Biology, 31, pp.1972-1982.

Guex, N. and Peitsch, M.C., (1997). SWISS-MODEL and the Swiss-Pdb Viewer: An Envrionment for Comparative Protein Modelling. Electrophoresis, 18, pp.2714-2723.

Guo, B.H., et al., 2011. BMI1 Promotes Invasion and Metastasis, and its Elevated Expression is Correlated with an Advanced Stage of Breast Cancer. Molecular Cancer, 10, pp.1-23.

Hashizume, R., et al 2001. The RING Heterodimer BRCA1:BARD1 is a Ubiquitin Ligase Inactivated by a Breast Cancer-derived Mutation. The Journal of Biological Chemistry, 276, pp.14537-14540.

Hosen, N., et al., 2007. BMI1-green Fluorescent Protein-knock-in Mice Reveal the Dynamic Regulation of BMI1 Expression in Normal and Leukemic Hematopoietic Cells. Stem Cells, 25, pp.1635-1644.

Irminger-Finger, I. And Jefford, C.E., 2006. Is there more to BARD1 than BRCA1? Nature, 6, pp.382-391.

Joazeiro, C.A.P., et al., 1999. The Tyrosine Kinase Negative Regulator c-Cbl as a RING-type E2-dependent Ubiquitin-protein Ligase. Science, 286, pp.309-312

Karppinen, S-M., et al., 2004. Mutation Screening of the BARD1 Gene: Evidence for Involvement of the Cys557Ser Allele in Hereditary Susceptibility to Breast Cancer. Journal of Medical Genetics, 41, pp.1-5.

Kennedy, R.D., et al., 2004. The Role of BRCA1 in the Cellular Response to Chemotherapy. Journal of the National Cancer Institute, 96, pp.1659-1668.

Leung, J.W., et al., 2014. Nucleosome Acidic Patch Promotes RNF168- and RING1B/BMI1-dependent H2AX and H2A Ubiquitination and DNA Damage Signalling. PLoS, 10, pp.1-14.

Li, Z., et al., 2006. Structure of a BMI1-RING1B Polycomb Group Ubiquitin Ligase Complex. The Journal of Biological Chemistry, 281, pp.20643-20649.

Lorick, K.L., et al., 1999. RING Fingers Mediate Ubiquitin-conjugating Enzyme (E2)-dependent Ubiquitination. Proceedings of the National Academy of Sciences, 96, pp.11364-11369.

Martínez-Gómez, A.I., et al., 2013. The Isolated N-terminus of RING1B is a Well-folded Monomeric Fragment with Native-like Structure. Protein Engineering, Design and Selction, pp.1-11.

Martínez-Romero, C., et al., 2009. The Epigenetic Regulators BMI1 and RING1B are Differentially Regulated in Pancreatitis and Pancreatic Ductal Adenocarcinoma. Journal of Pathology, 219, pp.205-213.

Metzger, M.B., et al., 2012. HECT and RING Finger Families of E3 Ubiquitin Ligases at a Glance. Journal of Cell Science, 125, pp.531-537.

Metzger, M.B., et al., 2014. RING-type E3 Ligases: Master Manipulators of E2-ubiquitin Conjugating Enzymes and Ubiquitination. Biochimica et Biophysica Acta, 1843, pp.47-60.

Morris, J., et al., Unpublished.

Nakatani, Y., et al., 2013. Regulation of Ubiquitin Transfer by XIAP, a Dimeric RING E3 Ligase. Biochemical Journal, 450, pp.629-638.

Nath, D. and Shadan, S., 2009. The Ubiquitin System. Nature, 458, p.421.

Plechanovová, A., et al., 2011. Mechanism of Ubiquitylation by Dimeric RING Ligase RNF4. Nature Structural and Molecular Biology, 18, pp.1052-1058.

Plechanovová, A., et al., 2012. Structure of a RING E3 Ligase and Ubiquitin-loaded E2 Primed for Catalysis. Nature, 489, pp.115-120.

Proctor, E., et al., 2013. BMI1 Enhances Tumorigenicity and Cancer Stem Cell Function in Pancreatic Adenocarcinoma. PLoS One, 8, pp.1-12.

Ruffner, H., et al., 2001. Cancer-predisposing Mutations within the RING Domain of BRCA1: Loss of Ubiquitin Protein Ligase Activity and Protection from Radiation Hypersensitivity. Proceedings of the Natural Academy of Sciences, 98, pp.51345-5139.

Shakya, R., et al., 2014. BRCA1 Tumor Suppression Depends on BRCT Phosphoprotein Binding, But Not its E3 Ligase Activity. Science, 334, pp.525-528.

Siddique H.R. and Saleem M., 2012. Role of BMI1, a Stem Cell Factor, in Cancer Recurrence and Chemoresistance: Preclinical and Clinical Evidences. Stem Cells, 30, pp.372-378.

Simons, A.M., et al., 2006. BRCA1 DNA-binding Activity is Stimulated by BARD1. American Association for Cancer Research, 66, pp.2012-2018.

Soss, S.E., et al., 2013. Activation of UbcH5c-Ub is the Result of a Shift in Interdomain Motions of the Conjugate Bound to U-Box E3 Ligase E4B. American Chemical Society, 52, pp.2991-2999.

Thai, T.H., et al., 1997. Mutations in the BRCA1-associated RING Domain (BARD1) Gene in Primary Breast, Ovarian and Uterine Cancers. Human Molecular Genetics, 7, pp.195-202.

Woodsmith, J., et al., 2012. Systematic Analysis of Dimeric E3-RING Interactions Reveals Increased Combinatorial Complexity in Human Ubiquitination Networks. Molecular and Cellular Proteomics, 11, ePUB:M111.016162.

http://www.genecards.org/cgi-bin/carddisp.pl?gene=BRCA1. Accessed on 09/02/14.

6. APPENDIX

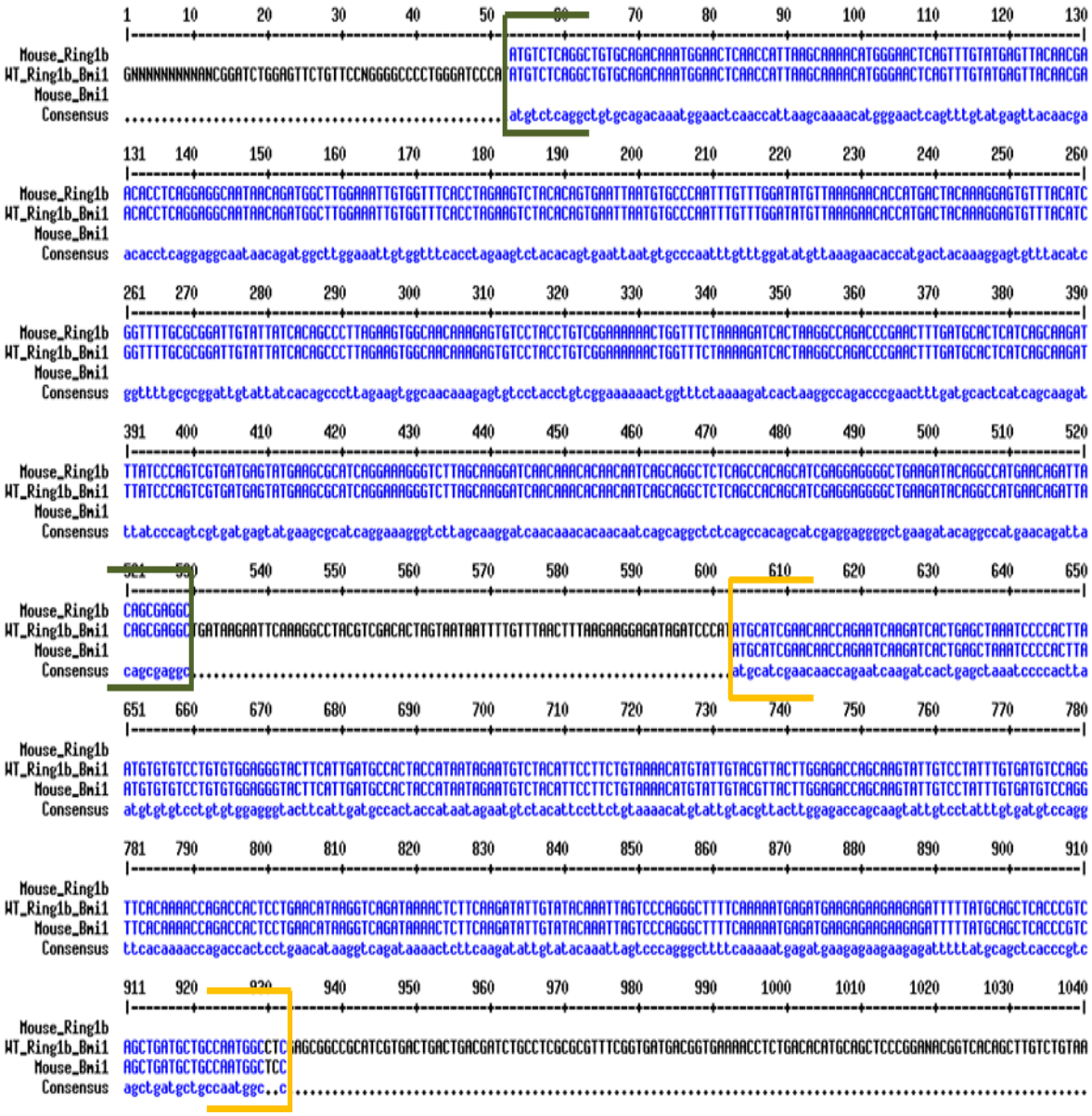

Supplementary figure 1: WT RING1B:BMI1 sequence alignment
Sequence alignment on mutalin (Corpet, F., 1988) of WT RING1B:BMI1, with RING1B highlighted in a green bracket followed by a linker attaching this to BMI1 in an orange bracket.

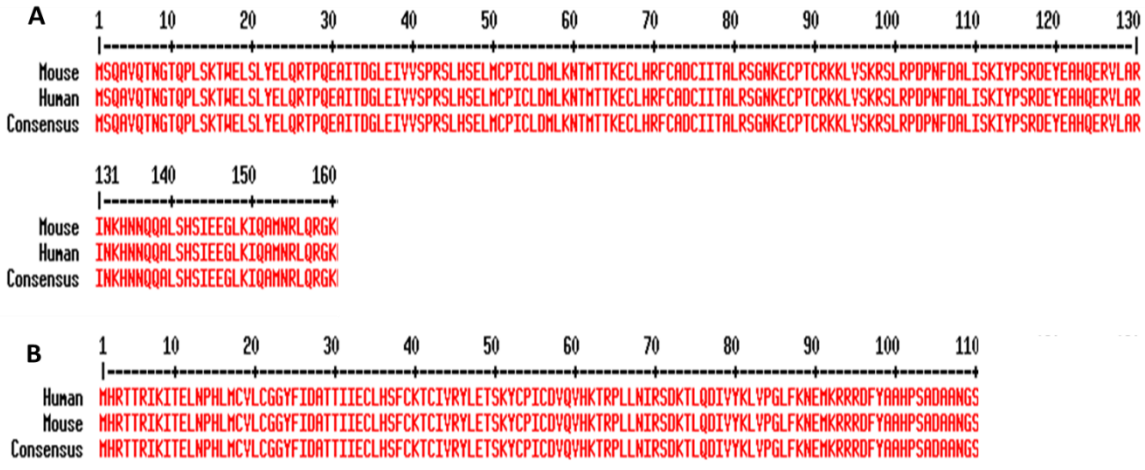

Supplementary figure 2: RING1B and BMI1 amino acid conservation between mouse and human

A) Sequence alignment on mutalin (Corpet, F., 1988) of human and mouse WT RING1B (1-159) indicating 100% conservation.

B) Sequence alignment on mutalin (Corpet, F., 1988) of human and mouse WT BMI1 (1-109) indicating 100% conservation.

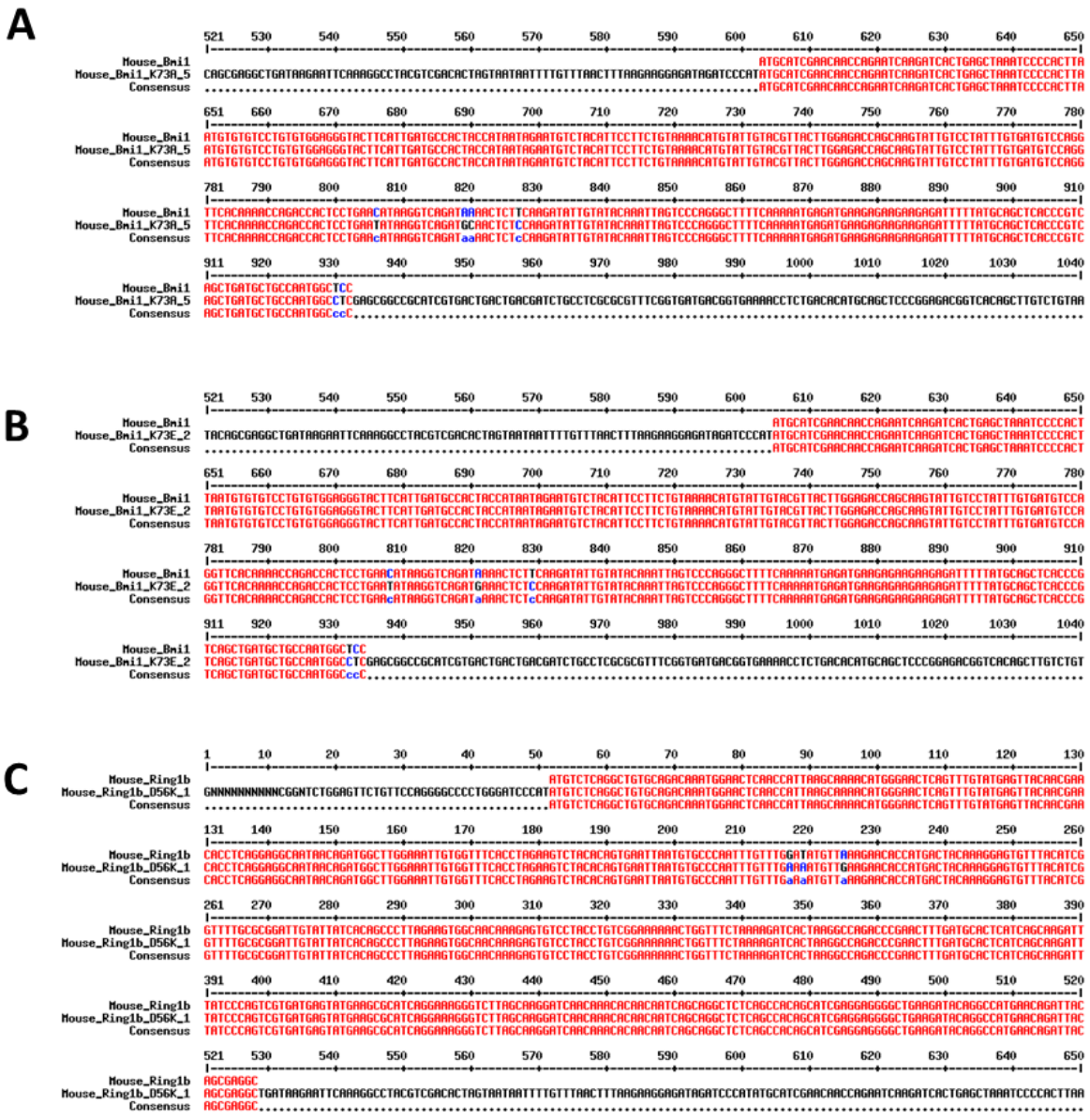

Supplementary figure 3: RING1B:BMI1 mutant sequence alignment

A) Sequence alignment on mutalin (Corpet, F., 1988) of RING1B:BMI1, with successful site-directed mutagenesis of BMI1 K73A (AAA → GCA). In addition, some additional mutations can be seen introduced either side of this mutation, due to primer design.

B) Sequence alignment on mutalin (Corpet, F., 1988) of RING1B:BMI1, with successful site-directed mutagenesis of BMI1 K73E (AAA → GAA). In addition, some additional mutations can be seen introduced either side of this mutation, due to primer design.

C) Sequence alignment on mutalin (Corpet, F., 1988) of RING1B:BMI1, with successful site-directed mutagenesis of RING1B D56K (GAT → AAA). In addition, some additional mutations can be seen introduced either side of this mutation, due to primer design